



Wind turbine power performance measurement with the use of spinner anemometry

Demurtas, Giorgio; Friis Pedersen, Troels; Wagner, Rozenn

Publication date:
2016

Document Version
Publisher's PDF, also known as Version of record

[Link back to DTU Orbit](#)

Citation (APA):
Demurtas, G., Friis Pedersen, T., & Wagner, R. (2016). Wind turbine power performance measurement with the use of spinner anemometry. DTU Wind Energy. (DTU Wind Energy PhD; No. 0063(EN)).

DTU Library

Technical Information Center of Denmark

General rights

Copyright and moral rights for the publications made accessible in the public portal are retained by the authors and/or other copyright owners and it is a condition of accessing publications that users recognise and abide by the legal requirements associated with these rights.

- Users may download and print one copy of any publication from the public portal for the purpose of private study or research.
- You may not further distribute the material or use it for any profit-making activity or commercial gain
- You may freely distribute the URL identifying the publication in the public portal

If you believe that this document breaches copyright please contact us providing details, and we will remove access to the work immediately and investigate your claim.

Wind turbine power performance measurement with the use of spinner anemometry

Department of
Wind Energy
PhD Report 2016

Giorgio Demurtas

DTU Wind Energy PhD-0063(EN)

August 2016



Authors: Giorgio Demurtas

Title: Wind turbine power performance measurement with the use of spinner anemometry

Department: Wind Energy

Summary (max 2000 characters):

The spinner anemometer was patented by DTU in 2004 and licenced to ROMO Wind in 2011. By 2015 the spinner anemometer was installed on several hundred wind turbines for yaw misalignment measurements. The goal of this PhD project was to investigate the feasibility of use of spinner anemometry for power performance measurements. First development of spinner anemometer was related to calibration of yaw misalignment measurements. Here the first innovation was made in the spinner anemometer mathematical model, introducing a new calibration constant, $k\alpha = k1/k2$. This constant was found to be directly related to measurements of inflow angle (yaw misalignment and flow inclination). The calibration of the constant was based on yawing the stopped turbine several times in and out of the wind comparing the varying inflow angle measurement with the yaw position sensor. The calibration for inflow angle measurements was further improved with an innovation step to calibrate without use of the yaw position sensor, saving cost and time of installing the additional yaw sensor. The so called "wind speed response method" was validated by comparing 27 different calibration tests to the fist methods. This method is now used as default in commercial calibrations. To evaluate the power performance of a wind turbine with the use of spinner anemometry, an experiment was organized in collaboration with Romo Wind and Vattenfall. A met-mast was installed close to two wind turbines equipped with spinner anemometers at a flat wind farm site. A procedure to calibrate the spinner anemometer for wind speed measurements was developed to determine the k1 calibration constant, and the IEC61400-12-2 standard was used to measure the nacelle transfer function (NTF). The power curves of the two wind turbines with use of met-mast and spinner anemometer were then compared. Application of the NTF from one turbine to the other was made with a difference of only 0.38% in AEP. Different methods of analysis of fast sampled measurements such as the Langevin power curve were tested, concluding that the method of bins (IEC61400-12-1) was the most simple and robust method, and could also be applied directly to fast sampled measurements. The probability distribution of wind speed was playing a major role in being able to complete a power curve measurement in short time.

2016

Project Period:

2013-09-15 to 2016-08-15

Education:

PhD

Field:

Wind Energy

Supervisor:

Troels Friis Pedersen

Co-supervisor:

Rozenn Wagner

Remarks:

Contract no.:

J.nr. 64012-0107

Project no.:

iSpin EUDP-2012-I

Sponsorship:

1/3 EUDP iSpin and FastWind

1/3 DTU

1/3 Romo Wind

Front page:

Nørrekær Enge wind farm
(credit: Giorgio Demurtas)

Pages: 135

Tables: 9

References: 28

Danmarks Tekniske Universitet

DTU Vindenergi
Niels Koppels Allé
Bygning 403
2800 Kgs. Lyngby
Telephone

www.vindenergi.dtu.dk

Foreword

I started this PhD in September 2013, after one year as research assistant at DTU on the same topic. Now that I am about to complete the PhD, when I look back to the past 3 years I see that I made some important advances regarding spinner anemometry. I gained new knowledge and a lot of experience in business start-up, I become better at writing and at oral presentations. Considering that I am 30 years old, so far I invested more than 10% of my life in spinner anemometry. As of my personality I am very curious of many aspects of energy technology and I need to do more things at the same time to keep the motivation up. So, in this foreword I will tell about most of the side projects I ran along the academic part of the research.

During the first year of PhD I attended at DTU three courses related to entrepreneurship: Patent course, Knowledge based entrepreneurship, Innovation in product development. The final assignment of the last course was a business plan to commercialize a DTU invention about a gas turbine. Together with some class mates we submitted the business plan to a Danish business plan competition (Venture CUP) and we made it to the final.

In 2014 I founded a new startup to make controllers for solar trackers (Startak IVS) and we were finalists again at Venture CUP, and awarded twice a grant from FFE-YE (Fonden for entreprenørskab).

Between February and August 2014 I was responsible for the installation of a 80 m met-mast in the Nørrekær Enge wind farm to evaluate power performance with the use of spinner anemometry. I acted as a project manager, preparing the documentation and coordinating all the people involved: my DTU managers, local authorities, Romo Wind, Vattenfal (owner of the wind farm), suppliers, installation crew. How is a met-mast installed and who are the possible suppliers? Ask me.

In September 2015 I went to visit the Poul La Cour museum in Askov (Denmark). I went to Husum Wind exhibition in Germany and to the conference "Wind Energy Denmark" in Herning where I won an i-pad for best presentation and poster.

In October and November 2015 I took a leave from the PhD to work as consultant for a small wind turbine manufacturer located in Italy. I reviewed the schematics of their 20-30 kW direct drive, pitch regulated wind turbine, developed the control strategy and implemented it in the PLC (Programmable Logic Controller). Quite rewarding to see seven wind turbines running with my software and several other turbines under construction in the factory!

This pause and change of topic was like a breath of fresh air. I learned many new things regarding wind turbine control, and I had to deal with many practical details (of which unfortunately books does not talk about). When I came back to the PhD I was full of energy, and I could see that I was able to get more work done.

I completed the development of the calibration methods in January 2016, and Romo Wind had used my method on more than one hundred spinner anemometers by then. Romo Wind engineers noted a relation between wind speed and yaw misalignment for a non calibrated spinner anemometer, which was very accentuate for a flat spinner. There was a strong need to communicate with Romo Wind's engineers. Therefore in February 2016 I spent one month at their office in Aarhus, and I developed a new method to calibrate a spinner anemometer for yaw misalignment measurements without using a yaw position sensor. This innovative method allowed Romo Wind to save the cost connected with installing the yaw positions sensor.

In March 2016 I decided to start up my own small wind turbine factory. I composed a team with DTU engineers and DTU master students, we wrote a business plan and got accepted in the incubator program of Climate KIC (a European fund aiming at developing green businesses). We received a small grant from both climate KIC and FFE-YE, and we are moving forward with the turbine design. While I was in Aarhus I took the opportunity to visit a blade manufacturer nearby, which will probably make our blades. For the business plan competitions I had to make several times a pitch on the stage, or in front of a jury, or in front of a camera. I can see a clear improvement in my oral presentation skills thanks to this constant exercise and thanks to the course "Presentation techniques" which I had the chance to attend thanks to the PhD.

During the PhD study I also came up with two invention disclosures. The first one was a cup anemometer which didn't work as expected when I tested it in the wind tunnel. The second one (a passive yaw wind turbine topology that can prevent cable twist) went a bit more forward, but the patent agent found an existing patent very close to my idea. However, it was useful to be in the patenting process.

One thing that disappointed me during the PhD is that most of the time is spent reporting research results and only a small time is spent to generate new results.

I am looking forward for a work in industry with more focus on results than on reporting, and on having a huge impact on the global economy.

You can now continue to read this PhD thesis to find out the challenges and opportunities that a spinner anemometer can offer.

Acknowledgements

I would like to thank my supervisor Troels Friis Pedersen and co-supervisor Rozenn Wagner of the Technical University of Denmark for their great supervision, help and patience.

I acknowledge Romo Wind A/S for financing one third of my PhD project and provide opportunity for a stay at RomoWind to develop the "wind speed response" method in cooperation with Nick G. C. Janssen. I am very grateful to my colleagues and DTU managers for making DTU such a great, informal, collaborative and efficient work place. For any errors or inadequacies that may remain in this work, of course, the responsibility is entirely my own.

Giorgio Demurtas

August 11, 2016

Roskilde, Denmark

Summary in Danish

Spinner anemometret blev patenteret af DTU i 2004 og licenseret til ROMO Wind i 2011. I 2015 var spinner anemometret installeret på flere hundrede vindmøller til måling af krøje-fejl. Målet med dette PhD projekt var at undersøge anvendelsen af spinner anemometret til effektkurvemålinger. Første undersøgelse af spinner anemometret var relateret til kalibrering af flow vinkel målinger. Her blev den første innovation gjort med hensyn til den matematiske model for spinner anemometret med introduktion af en ny kalibreringskonstant . Denne konstant viste sig at være direkte relateret til måling af flow vinklen (krøjefejl og flow hældning). Kalibrering af konstanten var baseret på krøjning af den stoppede vindmølle adskillige gange ind og ud af vinden, hvor måling af den varierende krøjefejl blev sammenlignet med krøjefejlen. Kalibrering af flow vinkel målingen blev yderligere forbedret med et innovativt step til kalibrering uden brug af krøjepositionssensor, hvormed omkostninger og tid ved installation af krøjesensor kan spares. Den såkaldte "Wind speed response method" blev valideret ved 27 forskellige kalibreringstests i forhold til den første metode. Denne metode har erstattet den første metode ved kommercielle målinger.

For at evaluere en vindmølles effektkurve ved brug af spinner anemometri blev der etableret et eksperiment i samarbejde med ROMO Wind og Vattenfall. En mast blev installeret tæt på to vindmøller hvorpå der var monteret spinner anemometre. Der blev udviklet en procedure til kalibrering af spinner anemometre til vindhastighedsmålinger i henhold til IEC61400-12-2 standarden til bestemmelse af konstanten og nacelle overføringsfunktionen, NTF. Effektkurverne på de to vindmøller blev derefter sammenlignet. Anvendelse af nacelle overføringsfunktionen fra en vindmølle til den anden kunne gøres med en difference på kun 0.38% i AEP.

Forskellige metoder til analyse af hurtigt samplede data, som for eksempel Langevin metoden, blev undersøgt. Konklusionen var at "method of bins" metoden var den mest simple og robuste metode, og den kunne også anvendes til hurtigt samplede data. Sandsynlighedsfordelingen af vindhastigheden viste sig at spille den største rolle i fuldførelsen af en effektkurve på kort tid.

Contents

1	Introduction	1
1.1	Thesis objectives	2
1.2	Approach	2
1.3	Structure of the thesis	4
2	Spinner anemometer basics and calibration	5
3	Innovative method for calibration of flow angle measurements	26
4	Calibration for wind speed measurements	43
5	Power performance measurements and uncertainty analysis	63
6	Power curve with Dynamic Data Analysis	95
6.1	Introduction	96
6.2	Reference power curve from 126 h of measurements and the method of bins .	96
6.3	Method of bins applied to 4 hours of spinner anemometer measurements . . .	97
6.4	The Langevin method	100
6.5	Langevin method applied to 4 hours of spinner anemometer measurements . .	102
6.6	Comparison of DDA methods	103
6.7	Conclusion on DDA methods	105
7	Conclusions	106
7.1	Specific conclusion	106
7.2	Recommendations for future work	109
8	Appendix	111
8.1	Appendix A - Wind speed measurement by sonic means	112
8.2	Appendix B - Calibration of a spinner anemometer for angular measurements on a Siemens 2.3 MW wind turbine	113
8.3	Appendix C - Calibration of a spinner anemometer for wind speed measure- ments on a Siemens 2.3 MW wind turbine	118
8.4	Appendix D - Drift curves for a Siemens 2.3 MW wind turbine	120

List of articles

- Paper A: Calibration of a spinner anemometer for yaw misalignment measurements.
T. F. Pedersen, G. Demurtas, F. Zahle.
Wiley, Wind Energy, 2014.
- Paper B: An innovative method to calibrate a spinner anemometer without use of yaw position sensor. G. Demurtas. N. G. Janssen.
Submitted to Wind Energy Science in May 2016.
- Paper C: Calibration of a spinner anemometer for wind speed measurements.
G. Demurtas, T. F. Pedersen, F. Zahle.
Wiley, Wind Energy, 2015.
- Paper D: Nacelle power curve measurement with spinner anemometer and uncertainty evaluation. G. Demurtas, T. F. Pedersen, R. Wagner.
Submitted to Wind Energy Science in August 2016.

Chapter 1

Introduction

The measurement of power performance of wind turbines requires measurement of the wind speed experienced by the wind turbine and the electric power output. While the second one is easy to measure being it already in electrical form, the challenge is to measure the wind.

One way of measuring the wind is to place a cup anemometer on a meteorological tower at a certain distance from the wind turbine, as described in the standard IEC61400-12-1, [1]. This solution is expensive due to the cost of the met-mast tower, therefore an alternative method was developed in the standard IEC61400-12-2 [2] where the wind speed sensor is placed on the wind turbine itself. A cup anemometer or a sonic anemometer mounted on the rear part of the nacelle rooftop are well known solutions, however they present some drawbacks [3] because they measure the wind where it is disturbed by the wake of the blade roots and nacelle.

Another option to measure the wind experienced by the wind turbine, allowed by the standard, is to use a spinner anemometer. A spinner anemometer consist of three one dimensional sonic wind speed sensors mounted on the spinner of a wind turbine. The spinner anemometer was invented in 2004 by Troels Friis Pedersen and the international patent [4] was granted in 2007. The patent was licenced to the company Romo Wind in 2011 which now offers the spinner anemometer commercially. While the spinner anemometer is a known option to measure yaw misalignment, there is very little experience in its use for measuring flow inclination and horizontal wind speed.

Work done previous to commencement of this PhD tested the spinner anemometer concept using a small spinner in a large open jet wind tunnel [5]. The measurements were used to identify a suitable mathematical model [6] to describe the wind speed measured by each of the three sonic sensors as a function of the inflow speed, direction, and rotor azimuth position. A conversion algorithm was then developed [7] based on the wind tunnel test to convert the sonic sensor wind speeds to horizontal wind speed, flow inclination and yaw misalignment. An installation procedure was described in the spinner anemometer manual by Metek [8]. The spinner anemometer was tested on a 3.6 MW wind turbine at Høvsøre [9,10]. Procedures for calibration used in [9–11] were based on a simple linear model comparing the spinner anemometer with a met-mast wind vane.

The spinner anemometer was tested in a wind farm environment in [7] to measure flow inclination, yaw misalignment and power curves with the contribution of the author. This PhD project started in 2013 to examine in depth and demonstrate the use of spinner anemometer for power performance measurements.

1.1 Thesis objectives

The aim of this PhD were to investigate the advantages and limitations of the instrument, in relation to wind turbine power performance measurments. The research project tried to answer the following research questions:

1. How to calibrate a spinner anemometer?
2. How to ensure traceability?
3. How to use a spinner anemometer for power performance measurements?
4. How is the uncertainty of spinner anemometer measurements evaluated?
5. Is it possible to avoid individual calibration of spinner anemometers?
6. What are the impacts of mounting imperfections of the sonic sensors, and how can this be documented?
7. Is there any advantage in using short time averages to measure a power curve?
8. What minimum time is required to measure a power curve?

1.2 Approach

The research activities aiming at answering the research questions were mostly based on analysis of wind measurements collected in the field with dedicated experiments. During the three years of research, the work proceeded in the following order:

1. **Calibration of the spinner anemometer and traceability.** This topic was addressed first, as it is the basis for accurate measurements. The calibration procedures were developed for yaw misalignment calibration in chapters 2 and 3, and for wind speed calibration in chapter 4. The spinner anemometer can be used to simply measure the yaw misalignment or to measure power performance. This two uses have different calibration requirements, which were explained in chapter 4.
2. **Evaluation of uncertainties.** This is somewhat more complicated compared to a normal 3D sonic anemometer. In fact, while a 3D sonic can be calibrated in a wind tunnel in one piece, the three sensor paths of a spinner anemometer have to be calibrated independently and then mounted on the spinner, since the spinner of a MW size turbine is too large to fit in a wind tunnel, and it is not feasible to remove the spinner from a turbine to undergo the calibration. The three velocities measured by the three sonic sensors (rotating with the spinner) are combined with a conversion algorithm to calculate the horizontal wind speed, yaw misalignment and flow inclination. The uncertainties are also combined trough the conversion algorithm. The general concepts described in the GUM (Guide for expression of Uncertainties in Measurements) were applied, and several considerations regarding combination of uncertainties were made in chapter 5.

3. Application of spinner anemometry for power performance measurements.

Chapter 5 describes an experiment where the power curves of two identical wind turbines was measured with both met-mast and spinner anemometer.

The aim of the project was to investigate the feasibility of measuring the power curve of several wind turbines with the NTF (Nacelle Transfer Function) and calibration determined on one reference wind turbine.

4. Evaluation of fast sampled measurements. The spinner anemometer wind speed has a very good correlation with the wind turbine power compared to the met-mast anemometer or with the nacelle anemometer, which suggests that: 1) a shorter averaging time could be used (shorter than the typical 10 min.), 2) a shorter time of observation is sufficient to evaluate the wind turbine power performance.

Fast sampled (10 Hz) measurements of pitch regulated and stall regulated wind turbines were analysed with the Langevin method and other methods. Results of this were published in the Fastwind project report E-0082 [12]. The relevant parts of that report are presented in chapter 6.

5. Innovative applications. One of the issues with the calibration of a spinner anemometer for inflow angle measurements was the necessity to install an additional yaw sensor, as the signal of the one present for control purposes was not always available. In collaboration with Romo Wind a new method was developed, based on the non linearity of the spinner anemometer conversion algorithm. While the method is pretty simple, it is based on a long experience on spinner anemometry. The innovative method is presented in chapter 2 and is now used for commercial calibrations by Romo Wind A/S.

1.3 Structure of the thesis

This thesis is written as a collection of four journal articles and a portion of a report. Two of the articles have been published while the last two have been submitted for publication. The articles are included inside the main body of the thesis and the reader should read them for a full understanding of the thesis.

The articles were based on measurements taken on

- a Nordtank 500 kW stall regulated wind turbine (chapter 2 and 4),
- a Neg-Micon 2 MW wind turbine (chapter 3),
- a Siemens 2.3 MW wind turbine (chapter 5 and 6).

For completeness within this PhD thesis, the methods presented in the chapters 2, 3 and 4 were also applied on a Siemens 2.3 MW and the results are presented in Appendix B and C. The following chapter 2 will describe the spinner anemometer basic assumptions and mathematical model. The calibration methods are presented in chapter 2, 3 and 4. The power performance measurement and uncertainty analysis are presented in chapter 5. Chapter 6 presents the use of spinner anemometer for calculation of a power curve with a method of dynamic data analysis. Conclusions are made in chapter 7.

Chapter 2

Spinner anemometer basics and calibration

The spinner anemometer measurement principle is based on the flow distortion caused by the spinner of the wind turbine [5, 13]. Three sonic sensors measure the wind speed near the spinner at three locations. The measurement principle of the sonic wind speed sensor is explained in Appendix A. The rotor position is measured thanks to accelerometers embedded in the root of the sonic sensor. The conversion algorithm described in this chapter converts the velocities V_1 , V_2 , V_3 measured by the three sonic sensors and the rotor position ϕ into horizontal wind speed U_{hor} , flow inclination angle β and yaw misalignment γ .

Two constants are part of the conversion algorithm to take into account the shape of the spinner. k_1 mainly related to wind speed measurements, k_α entirely related to flow angle measurements. When a spinner anemometer is mounted on a spinner of a new wind turbine type the spinner anemometer constants are normally not known. Meanwhile, data can be acquired with default spinner anemometer constants (for example $k_{1,d} = k_{2,d} = 1$, or use of a good guess from a similarly shaped spinner), and later be corrected when calibration correction factors F_α and F_1 have been determined. The subscript d refers to values measured with default value.

The following article

- describes the coordinate system
- describes the conversion algorithm
- derives the expression of the correction factors
- describe five methods for the calibration of a spinner anemometer for flow angle measurements and apply them on a 500 kW stall regulated wind turbine.

RESEARCH ARTICLE

Calibration of a spinner anemometer for yaw misalignment measurements

T. F. Pedersen, G. Demurtas and F. Zahle

Technical University of Denmark, Frederiksborgvej 399, PO Box 49, 4000 Roskilde, Denmark

ABSTRACT

The spinner anemometer is an instrument for yaw misalignment measurements without the drawbacks of instruments mounted on the nacelle top. The spinner anemometer uses a non-linear conversion algorithm that converts the measured wind speeds by three sonic sensors on the spinner to horizontal wind speed, yaw misalignment and flow inclination angle. The conversion algorithm utilizes two constants that are specific to the spinner and blade root design and to the mounting positions of the sonic sensors on the spinner. One constant, k_2 , mainly affects the measurement of flow angles, while the other constant, k_1 , mainly affects the measurement of wind speed. The ratio between the two constants, $k_\alpha = k_2/k_1$, however, only affects the measurement of flow angles. The calibration of k_α is thus a basic calibration of the spinner anemometer.

Theoretical background for the non-linear calibration is derived from the generic spinner anemometer conversion algorithm. Five different methods were evaluated for calibration of a spinner anemometer on a 500 kW wind turbine. The first three methods used rotor yaw direction as reference angular, while the wind turbine, was yawed in and out of the wind. The fourth method used a hub height met-mast wind vane as reference. The fifth method used computational fluid dynamics simulations. Method 1 utilizing yawing of the wind turbine in and out of the wind in stopped condition was the preferred method for calibration of k_α . The uncertainty of the yaw misalignment calibration was found to be 10%, giving an uncertainty of 1° at a yaw misalignment of 10° . © 2014 The Authors. *Wind Energy* published by John Wiley & Sons, Ltd.

KEYWORDS

anemometer; yaw misalignment; yaw error; flow inclination angle; nacelle anemometer; spinner anemometer; calibration

Correspondence

T. F. Pedersen, Wind Energy Department, DTU, Building 118, Frederiksborgvej 399, PO Box 49, 4000 Roskilde, Denmark.
E-mail: trpe@dtu.dk

This is an open access article under the terms of the Creative Commons Attribution License, which permits use, distribution and reproduction in any medium, provided the original work is properly cited.

Received 14 June 2013; Revised 7 May 2014; Accepted 25 July 2014

LIST OF SYMBOLS

F_1	calibration factor converting $k_{1,d}$ to k_1
F_2	calibration factor converting $k_{1,d}$ to k_1
F_α	calibration factor converting $k_{\alpha,d}$ to k_α
k_1	algorithm and calibration constant mainly related to wind speed measurements
$k_{1,d}$	default algorithm constant mainly related to wind speed measurements
k_2	algorithm constant mainly related to angular measurements
$k_{2,d}$	default algorithm constant mainly related to angular measurements
k_α	angular measurement calibration constant equal to k_2/k_1
$k_{\alpha,d}$	default angular measurement calibration constant equal to $k_{2,d}/k_{1,d}$
U	wind speed vector modulus
U_{hor}	horizontal wind speed (calibrated)
$U_{hor,d}$	horizontal wind speed (measured with $k_{1,d}$ and $k_{2,d}$)
$U_{hor,d,c}$	horizontal wind speed (calibrated with correct k_α but not correct k_1)

$U_{x,n}$	horizontal wind speed component along nacelle x -axis
$U_{y,n}$	horizontal wind speed component transversal to shaft axis
$U_{z,n}$	vertical wind speed component
V_1	wind speed along sonic sensor path 1
V_2	wind speed along sonic sensor path 2
V_3	wind speed along sonic sensor path 3
V_{ave}	average wind speed of sonic sensors
α	wind inflow angle relative to the shaft axis
β	flow inclination angle relative to horizontal (positive when upwards)
γ	yaw misalignment defined as wind direction minus turbine yaw direction
γ_{ref}	reference yaw misalignment (calculated as mast wind direction minus wind turbine yaw direction)
δ	shaft tilt angle
ϕ	rotor azimuth position (equal to zero when sonic sensor 1 is at top position, positive clockwise seen from the front of the wind turbine)
θ	spinner azimuth position of flow stagnation point (relative to sonic sensor 1)
θ_{dir}	wind direction measured at the met mast, referred to geographical north
$\theta_{dir,10}$	10 min average of θ_{dir}
θ_{yaw}	yaw direction of the wind turbine nacelle, measured by the yaw position sensor
$\theta_{yaw,10}$	10 min average of θ_{yaw} .
$\overline{\theta_{dir}}$	mean wind direction during the calibration test, referred to the yaw position sensor

1. INTRODUCTION

A challenge in wind turbine design is how to achieve an accurate and cheap measurement of the wind that flows into the wind turbine rotor. An accurate knowledge of the incoming wind is important in order to regulate yaw and pitch for optimized power, without being jeopardized by higher rotor loads or noise. Nacelle anemometry is used in wind turbine yaw control to measure wind speed and wind direction by cup anemometers and wind vanes or 2D sonic anemometers, mounted on top of the nacelle. Nacelle-mounted sensors are, however, influenced significantly by flow distortion from blade root sections and by a range of other sources, see the work of Frandsen *et al.*¹ Computational fluid dynamics (CFD) calculations confirm the sensitivity to flow distortion on the turbine nacelles.² The flow distortion is normally corrected for in the control systems, often based on a wind speed dependent function. However, mounting and adjustments of the wind sensors might introduce large yaw misalignments if not made with high precision in mounting, adjustment and calibration. Variations in the flow inclination angle due to terrain slope or swirl of wakes of other wind turbines may also influence on the efficiency of nacelle-based wind direction sensors. Inefficient yaw misalignment measurements lead to loss of energy.³

An alternative to nacelle anemometry is spinner anemometry,⁴ which measures yaw misalignment without offset or mounting and alignment errors. This type of wind sensor utilizes sonic sensor technology; the same technology used on 2D sonic anemometers on nacelles today. The spinner anemometer integrates three surface mounted 1D sonic sensors (Figure 1) with the spinner of a wind turbine and utilizes the flow over the spinner. The three 1D sonic sensors detect direc-



Figure 1. A 1D sonic sensor normally mounted from the inside of the spinner.

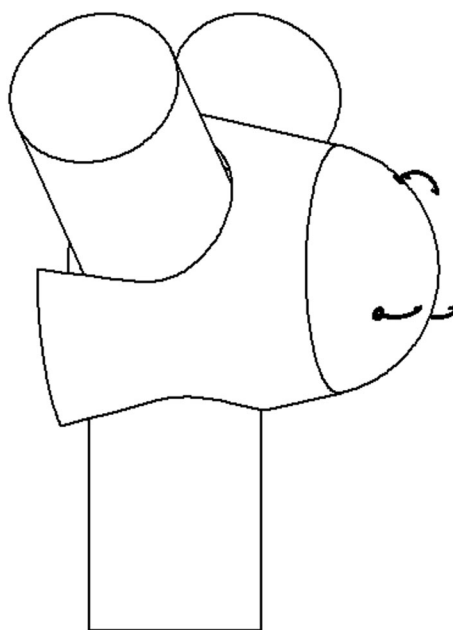


Figure 2. A spinner anemometer with three sonic sensors.

tional wind speeds in three positions over the spinner surface, while the wind component due to rotation is out-compensated as the sonic sensor paths are perpendicular to the velocity component due to rotation (Figure 2).

In axial flow with the flow stagnation point directly on the nose centre, all sonic sensors measure the same wind speed. In skew air flow, the stagnation point moves away from the nose. A sonic sensor closer to the stagnation point experiences reduced wind speed, while a sensor further away experiences increased wind speed. This results in a sinusoidal variation in wind speed seen by each sonic sensor during rotation.

The spinner anemometer includes an algorithm to transform the wind speeds measured by the three sonic sensors to horizontal wind speed, yaw misalignment and flow inclination angle.⁵ The algorithm utilizes two spinner anemometer constants, k_1 and k_2 . These are specific to the design of the spinner and blade roots and the mounting of the sonic sensors on the spinner. The two constants must be calibrated in order to measure the wind accurately at the spinner. The constants are considered to represent free wind speed measurements when the wind turbine is stopped and the rotor is pointing into the wind. During operation, the measurements represent the wind at the spinner as it is disturbed by the induced wind speed due to the rotor, and this will cause measurements at the spinner to deviate from free wind measurements. If the induced wind speed is known, then corrections can be made to convert wind conditions at the spinner to free wind conditions.

When default constants, $k_{1,d}$ and $k_{2,d}$, are inserted in the spinner anemometer box, the spinner anemometer can still measure wind speed, yaw misalignment and flow inclination angle in the same way a cup anemometer can measure wind speed without applying the calibration constants on beforehand. In this case, the measurements must be corrected with the right calibration constants after measurements have been made. For a spinner anemometer with a non-linear conversion algorithm, this correction is more complicated than for a cup anemometer. However, if the spinner anemometer is calibrated in the sequence—internal calibration, calibration for angular measurements, calibration of wind speed—then measured wind speeds can be converted linearly, like for cup anemometers. Calibration for angular measurements is thus an important calibration in the calibration chain, not just for yaw misalignment and flow inclination angle measurements but also for wind speed measurements. This article will focus on the correct calibration for angular measurements when the influence of the non-linear conversion algorithm is taken into account. A practical example that includes and evaluates different methods is provided.

2. THE SPINNER ANEMOMETER CONVERSION ALGORITHM

The spinner anemometer conversion algorithm⁵ transforms the measured wind speeds of the three sonic sensors to the horizontal wind speed, the yaw misalignment and the flow inclination angle. The algorithm is revisited here for the overall understanding of the measurement principle and for clarification of the transformations back and forth, which are used in the calibration data analysis to derive the correct calibration factor. We first set up a coordinate system.

2.1. Coordinate systems

The coordinate systems for transforming the spinner anemometer parameters from the rotating spinner to the fixed nacelle are shown in Figure 3. The inflow angle α , which is not directly shown, is the angle between the shaft axis and the vector of the inflow wind speed U . The yaw misalignment γ is defined as the wind direction minus the yaw direction (equation (1)).

$$\gamma = \theta_{dir} - \theta_{yaw} \tag{1}$$

2.2. Generic spinner anemometer wind speed relations

The basic spinner anemometer measurements consist of the three sonic sensor wind speeds V_1, V_2 and V_3 , and the rotor azimuth position ϕ . The azimuth position is derived from accelerometers, mounted in each foot of the sonic sensors. The generic equations that relate these measurements to the vector wind speed U , the inflow angle relative to the shaft axis α and the azimuth position of the flow stagnation point on the spinner θ are, as derived in the work of Pedersen,⁴ as follows:

$$V_1 = U(k_1 \cos \alpha - k_2 \sin \alpha \cos \theta) \tag{2}$$

$$V_2 = U \left(k_1 \cos \alpha - k_2 \sin \alpha \cos \left(\theta - \frac{2\pi}{3} \right) \right) \tag{3}$$

$$V_3 = U \left(k_1 \cos \alpha - k_2 \sin \alpha \cos \left(\theta - \frac{4\pi}{3} \right) \right) \tag{4}$$

The generic equations include the two spinner anemometer algorithm constants k_1 and k_2 .

2.3. Transformation from sonic sensor measurements to spinner anemometer parameters

The sonic sensor wind speeds V_1, V_2 and V_3 and the rotor azimuth position ϕ measurements are converted (Figure 4) to the spinner anemometer output parameters, horizontal wind speed U_{hor} , yaw misalignment γ and flow inclination angle β , in a number of steps.

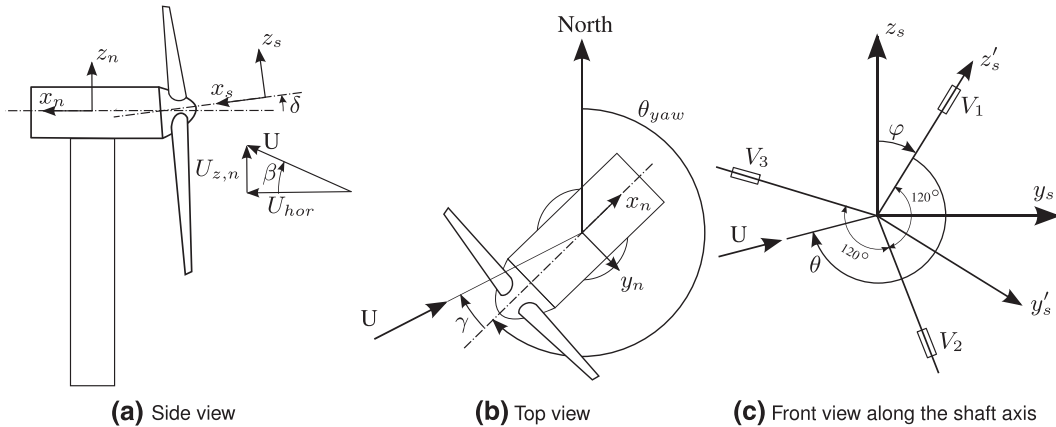


Figure 3. Coordinate systems and definition of angles: rotating spinner coordinate system (x'_s, y'_s, z'_s) , non-rotating shaft coordinate system (x_s, y_s, z_s) , fixed nacelle coordinate system (x_n, y_n, z_n) , yaw direction θ_{yaw} , yaw misalignment γ , flow inclination angle β , tilt angle δ , azimuth position of flow stagnation point on spinner θ (relative to sonic sensor 1), rotor azimuth position ϕ (position of sonic sensor 1 relative to vertical). (a) Side view, (b) top view and (c) front view along the shaft axis.

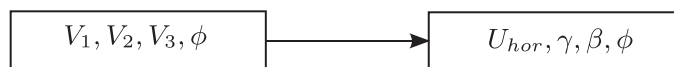


Figure 4. Direct transformation from sonic sensor wind speed to spinner anemometer parameters.

The first step in the transformation relates the sonic sensor wind speeds to the vector wind speed U , the inflow angle relative to the shaft axis α and the azimuth position of the flow stagnation point θ in the rotating spinner coordinate system of Figure 3. The inflow angle relative to the rotor axis is

$$\alpha = \arctan\left(\frac{k_1 \sqrt{3(V_1 - V_{ave})^2 + (V_2 - V_3)^2}}{\sqrt{3}k_2 V_{ave}}\right) \quad (5)$$

where the average of the sonic sensor wind speeds is

$$V_{ave} = \frac{1}{3}(V_1 + V_2 + V_3) \quad (6)$$

The module of the vector wind speed is

$$U = \frac{V_{ave}}{k_1 \cos \alpha} \quad (7)$$

And the flow stagnation azimuth position is*

$$\theta = \arctan\left(\frac{V_2 - V_3}{\sqrt{3}(V_1 - V_{ave})}\right) + \pi \quad (8)$$

The second step transforms the parameters in the spinner coordinate system to three wind speed components in the non-rotating shaft coordinate system. The wind speed component along the x_s -axis is

$$U_{x,s} = U \cos \alpha \quad (9)$$

The combined wind speed component perpendicular to the x_s -axis is

$$U_\alpha = U \sin \alpha \quad (10)$$

The wind speed component along the y_s -axis is

$$U_{y,s} = -U_\alpha \sin(\phi + \theta) \quad (11)$$

where ϕ is the measured rotor azimuth position. The wind speed component along the z_s -axis is

$$U_{z,s} = -U_\alpha \cos(\phi + \theta) \quad (12)$$

The third step transforms the three wind components in the non-rotating shaft coordinate system to three wind speed components in a fixed nacelle coordinate system, where the y_n -axis is horizontal and parallel with the y_s -axis, the x_n -axis is horizontal and the z_n -axis is vertical, and δ is the shaft tilt angle.

$$U_x = U_{x,s} \cos \delta + U_{z,s} \sin \delta \quad (13)$$

$$U_y = U_{y,s} \quad (14)$$

$$U_z = U_{z,s} \cos \delta - U_{x,s} \sin \delta \quad (15)$$

With the fourth and last step, these wind speed components, similar to a standard 3D sonic anemometer, are transformed to the spinner anemometer output parameters. The horizontal wind speed is

$$U_{hor} = \sqrt{U_x^2 + U_y^2} \quad (16)$$

The yaw misalignment:

$$\gamma = \arctan\left(\frac{U_y}{U_x}\right) \quad (17)$$

And the flow inclination angle:

$$\beta = \arctan\left(\frac{U_z}{U_{hor}}\right) \quad (18)$$

*Because of the properties of the arctangent function (which is the inverse of the tangent only in the first and fourth quadrant), we use the computed function 'atan2', which is available in most programming languages, in all equations. This function takes all quadrants into account, including the singularity where the denominator is equal to zero. The $+\pi$ is necessary to make the position of the stagnation point consistent with the sign of the velocity components along the axis y_s and z_s .

2.4. Transformation from spinner anemometer parameters back to sonic sensor wind speeds

In order to correct measured spinner anemometer data with calibrated spinner anemometer constants, it is necessary to reverse the spinner anemometer algorithm. This inverse transformation to the sensor path speeds is presented in Figure 5. A special consideration of the rotor position ϕ has to be given because the rotor position is not an output parameter of the spinner anemometer.

The first step of the inverse transformation transforms the spinner anemometer output parameters U_{hor} , γ and β to the sonic sensor wind speed components U_x , U_y and U_z in the nacelle coordinate system:

$$U_x = U_{hor} \cos \gamma \quad (19)$$

$$U_y = U_{hor} \sin \gamma \quad (20)$$

$$U_z = U_{hor} \tan \beta \quad (21)$$

The second inverse step transforms the wind speed components in the nacelle coordinate system to wind speed components in the shaft coordinate system:

$$U_{x,s} = U_x \cos \delta - U_z \sin \delta \quad (22)$$

$$U_{y,s} = U_y \quad (23)$$

$$U_{z,s} = U_x \sin \delta + U_z \cos \delta \quad (24)$$

The third inverse step transforms the wind speed components in the shaft coordinate system to wind parameters in the spinner coordinate system. The rotor azimuth position is not important for transformations back and forth and can be set equal to zero. The vector wind speed and the inflow angle to the shaft are:

$$U = \sqrt{U_{x,s}^2 + U_{y,s}^2 + U_{z,s}^2} \quad (25)$$

$$U_\alpha = \sqrt{U_{y,s}^2 + U_{z,s}^2} \quad (26)$$

$$\alpha = \arctan \left(\frac{U_\alpha}{U_{x,s}} \right) \quad (27)$$

And now, using the rotor azimuth position to find the flow stagnation azimuth position,

$$\theta = \arctan \left(\frac{U_{y,s}}{U_{z,s}} \right) - \phi + \pi \quad (28)$$

Finally, the fourth inverse step transforms the wind parameters in the spinner coordinate system to the sonic sensor wind speeds:

$$V_1 = U (k_1 \cos \alpha - k_2 \sin \alpha \cos \theta) \quad (29)$$

$$V_2 = U \left(k_1 \cos \alpha - k_2 \sin \alpha \cos \left(\theta - \frac{2\pi}{3} \right) \right) \quad (30)$$

$$V_3 = U \left(k_1 \cos \alpha - k_2 \sin \alpha \cos \left(\theta - \frac{4\pi}{3} \right) \right) \quad (31)$$

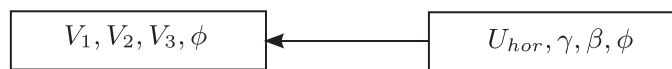


Figure 5. Inverse transformation, from spinner anemometer parameters to sonic sensors wind speeds.

3. CORRECTION FACTORS FOR CORRECTION OF SPINNER ANEMOMETER CONSTANTS

In the calibration process, correction factors (denoted by F) are multiplied to the default constants $k_{1,d}$ and $k_{2,d}$ that are inserted into the spinner anemometer box before calibration to obtain the calibrated k_1 and k_2 constants:

$$k_1 = F_1 k_{1,d} \quad (32)$$

$$k_2 = F_2 k_{2,d} \quad (33)$$

In calibration for angular measurements, the calibration factor $F_\alpha = F_2/F_1$ is determined. F_α is used to set k_2 equal to

$$k_2 = F_\alpha k_{2,d} \quad (34)$$

while $k_1 = k_{1,d}$ is kept constant. The k_2 value shall be set in the spinner anemometer box as soon as the calibration for angular measurements have been made. The spinner anemometer should be operated with default calibration constants only for a minimum of time required to collect measurements needed for determination of F_α .

The correction factors are derived by combining the generic spinner anemometer wind speed relations. Firstly, equations (2) and (3) are rewritten with respect to U and equalled, and α is extracted:

$$\tan \alpha = \frac{\sin \alpha}{\cos \alpha} = \frac{k_1}{k_2} \frac{V_2 - V_1}{V_2 \cos \theta - V_1 \cos \left(\theta - \frac{2\pi}{3} \right)} \quad (35)$$

As seen, the measured inflow angle depends on the position of the stagnation point θ , the wind speed at the sonic sensor paths (V_1 and V_2), and the ratio between the two spinner anemometer constants, which is now, for convenience, defined as

$$k_\alpha = \frac{k_2}{k_1} \quad (36)$$

Then,

$$\alpha = \arctan \left(\frac{V_2 - V_1}{k_\alpha \left(V_2 \cos \theta - V_1 \cos \left(\theta - \frac{2\pi}{3} \right) \right)} \right) \quad (37)$$

It is now clear that the angular measurement is only dependent on k_α . It is thus only necessary to calibrate this value for correct measurements of yaw misalignment and flow inclination angle. We can now introduce the correction factor that relates the constants to the situations before and after the calibration. Some of the variables are not affected by the calibration, while others are. For those affected by the calibration, the subscript d is used to reference default conditions before calibration. The measurements of wind speed in the sensor paths are not affected by a calibration. Therefore, V_1, V_2, V_3 before and after calibration are unchanged, and the position of the stagnation point θ is unchanged (equation (8)).

The inflow angle α , calculated by the spinner anemometer algorithm, is affected by the calibration. Using equation (37) and extracting k_α for conditions before and after calibration, we get before calibration,

$$k_{\alpha,d} = \frac{V_2 - V_1}{\tan \alpha_d \left(V_2 \cos \theta - V_1 \cos \left(\theta - \frac{2\pi}{3} \right) \right)} \quad (38)$$

after calibration,

$$k_\alpha = \frac{V_2 - V_1}{\tan \alpha \left(V_2 \cos \theta - V_1 \cos \left(\theta - \frac{2\pi}{3} \right) \right)} \quad (39)$$

The correction factor for angular calibration is then

$$F_\alpha = \frac{k_\alpha}{k_{\alpha,d}} = \frac{\tan \alpha_d}{\tan \alpha} = \frac{F_2}{F_1} = \frac{k_{1,d} k_2}{k_1 k_{2,d}} \quad (40)$$

F_α is seen to be independent of wind speeds. It is possible to determine F_α by angular relations alone and then derive the correct inflow angle α relative to the shaft axis. When this angle is correct, the derived yaw misalignment and flow inclination angles will also be calculated correctly.

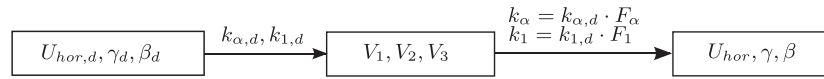


Figure 6. Application of correction factors to data measured with default calibration constants. For calibration for angular measurements, only F_1 is set equal to 1.

The calibration of k_1 can be determined by considering the wind speed U_d , calculated by the spinner anemometer algorithm before calibration, and the wind speed U after calibration. By rewriting the difference between equations (2) and (3), we can isolate k_2 :

before calibration,

$$k_{2,d} = \frac{V_1 - V_2}{U_d \sin \alpha_d \left(\cos \left(\theta - \frac{2\pi}{3} \right) - \cos \theta \right)} \quad (41)$$

after calibration,

$$k_2 = \frac{V_1 - V_2}{U_d \sin \alpha \left(\cos \left(\theta - \frac{2\pi}{3} \right) - \cos \theta \right)} \quad (42)$$

The correction factor F_2 is then

$$F_2 = \frac{k_2}{k_{2,d}} = \frac{U_d \sin \alpha_d}{U \sin \alpha} \quad (43)$$

The correction factor F_1 is obtained by combining equation (36) with (43):

$$F_1 = \frac{F_2}{F_{\alpha}} = \frac{U_d \sin \alpha_d \tan \alpha}{U \sin \alpha \tan \alpha_d} = \frac{U_d \cos \alpha_d}{U \cos \alpha} \quad (44)$$

It is seen that the correction factor F_1 becomes a clean wind speed correction factor when $\alpha = \alpha_d$. This is the case when angular calibration and insertion of the calibrated value into the spinner anemometer box ($k_2 = F_{\alpha} k_{2,d}$ while $k_1 = k_{1,d}$) has been made prior to wind speed calibration. When calibration of wind speed is made, then we can insert the new corrections in the spinner anemometer box: $k_1 = F_1 k_{1,d}$ and $k_2 = F_1 k_{2,d}$.*

4. APPLICATION OF CORRECTION FACTORS ON MEASUREMENTS MADE WITH DEFAULT SPINNER ANEMOMETER CONSTANTS

When a spinner anemometer is mounted on a spinner of a new wind turbine type, the spinner anemometer constants are set as default constants (for example, $k_{\alpha} = 1$ and $k_1 = 1$). When data are acquired with default spinner anemometer constants, then data must be converted with the inverse and forward transformations described in Sections 2.4 and 2.3, respectively, in that order to avoid conversion errors. This is the case for the analysis of the calibration data in order to determine the correction factor F_{α} and F_1 to correct the default constants. This is also the case when measured data without applied calibration spinner anemometer constants have to be converted to calibrated data.† The measured data are corrected completely without conversion errors by the procedure in Figure 6, which uses the conversion procedures developed in Section 3.

For the second step, right of Figure 6, the rotor azimuth position ϕ is not known from the spinner anemometer output when the output mode is in ‘normal mode’ (see the manual of the Spinner anemometer⁶). For the further correction, the rotor azimuth position is set equal to a constant value, for example, zero. This is only reasonable as long as the spinner anemometer has had an internal calibration to take account of all geometric deviations in spinner and sensor paths.⁶ This internal calibration assures that all three sonic sensors measure the same wind speeds during rotation, keeping the average wind speed of the three sensors the same. In this way, we do not derive the actual measured sonic sensor wind speeds for the actual rotor azimuth position, but the ones we derive are equivalent to the measured sonic sensor wind speeds with respect to the conversion to calibrated spinner anemometer data. The flow stagnation azimuth position on the spinner is under these assumptions determined from equation (28) and is correct.

*Note the suffix d is here used for conditions before wind speed calibration but after angular measurement calibration.

†It is always preferred to calibrate F_{α} first and correct k_2 and then calibrate F_1 and correct k_1 and k_2 in the second step before actual measurements are made in order to minimize linearization effects.

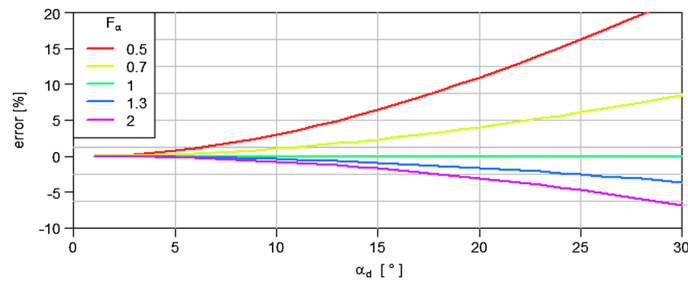


Figure 7. Error due to linearization of the conversion function, equation (46).

4.1. Errors due to linearization effects

The conversion in Figure 6 should be applied to the raw fast scanned data and will give correct results, also when data are afterwards averaged over time. However, if we consider 10 min averaged data where the F_α correction factor has not been applied, the non-linearity of the conversion algorithm results in deviations. To get an estimate of this deviation, we consider a simple case. We neglect the tilt angle (setting $\delta = 0$) and assume the flow inclination angle equal to zero (setting $\beta = 0$). Then, we can derive an expression of the calibrated yaw misalignment as function of the default yaw misalignment:

$$\alpha = \arctan\left(\frac{1}{F_\alpha} \tan \alpha_d\right) \quad (45)$$

The expression of equation (45) is non-linear, which means that averaged values introduce a deviation. As an example, the deviation of a converted default measured yaw misalignment of 10° and a standard deviation of 5° , and with a conversion factor F_α of 0.7 is -0.7% (converted value 14.04° instead of 14.14°), while the deviation is $+0.3\%$ for an F_α value of 1.3 (converted value 7.748° instead of 7.724°). The deviation seems rather constant for different yaw misalignment angles but is reduced for smaller standard deviations. The deviation increases almost exponentially with the distance of F_α from 1.0. For many cases, this deviation is small enough to be neglected, but it should be emphasized that the deviations are eliminated if the calibration of F_α is made before angular measurements are made.

In case we also linearize the conversion of raw fast scanned data to reduce computational and implementation efforts, we introduce another linearization error. When we linearize equation (45), we get

$$\alpha_{lin} = \frac{\alpha_d}{F_\alpha} \quad (46)$$

The error in estimation of F_α by linearization is shown in percentage in Figure 7. The error is seen to be small for correction factors close to 1.0 and also for small yaw misalignments, while for larger yaw misalignments, the error becomes significant.

5. CALIBRATION OF THE CORRECTION FACTOR F_α FOR A SPINNER ANEMOMETER ON A STALL-REGULATED 500 KW WIND TURBINE

The following example of calibration of F_α for angular measurements uses the inverse and forward transformations from Sections 2.4 and 2.3. A spinner anemometer is mounted on a 500 kW stall-regulated wind turbine, described by Paulsen⁷ (Figure 8). Two of the three sonic sensors are seen on the spinner; the one on the top indicating the sonic sensor path in which the wind speed is measured.* After mounting of the spinner anemometer sonic sensors and the conversion box on the spinner, the tilt angle of the rotor shaft and the default spinner anemometer constants $k_{1,d} = k_{2,d} = 1.0$ were set in the spinner anemometer box. An internal calibration was then made according to the operation manual.⁶ The internal calibration was activated and made during operation and was made in less than an hour. The internal calibration must be made prior to the F_α calibration to avoid uncertainties due to the rotor azimuth position and also to avoid 1P variations in the measurements. The internal calibration is made under the precondition that all three sonic sensors measure the same average wind speed over time.

The calibration of F_α consists in finding the value where the yaw misalignment indicated by the spinner anemometer effectively corresponds to the yaw misalignment of the wind turbine as defined in equation (1). The calibration can be

*Note the backwards tilting of the sonic sensor path relative to the local flow in order to avoid sensor head flow distortion.

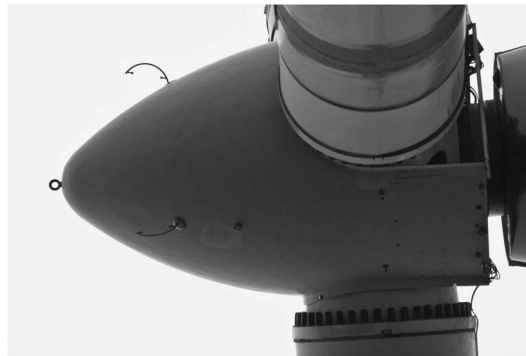


Figure 8. The spinner anemometer on a Nordtank 500 kW wind turbine.

made in several ways. Five methods were considered. Four of them were based on measurements, while the fifth was based on CFD calculations. The calibrations based on measurements used the natural wind for application of a reference wind direction. The first three methods use yawing of the stopped rotor for application of wind direction changes, while the fourth method referenced a met-mast mounted wind vane during operation.

5.1. Calibration of F_{α} method 1: forced yawing of wind turbine in stopped condition and use of tangent relation

Calibration method 1 use data acquired during a measurement campaign where the wind turbine rotor was stopped, and the rotor was yawed in and out of the wind (approximately $\pm 60^\circ$) several times in order to gather a robust statistical database. The rotor azimuth position was assumed not to be important because of the internal calibration. However, it is

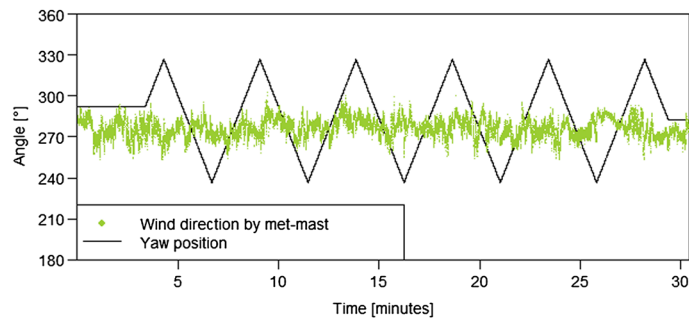


Figure 9. Wind direction at the met mast and yaw position during calibration.

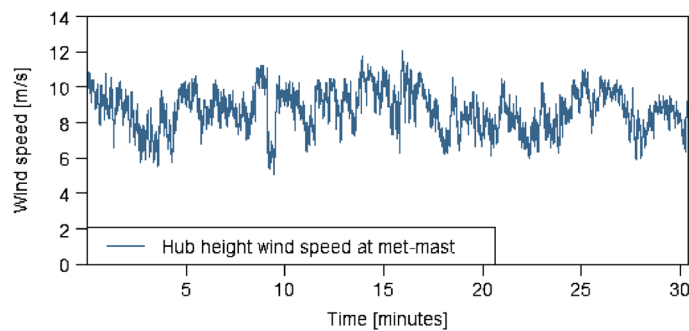


Figure 10. Wind speed at the met mast at hub height during calibration.

found appropriate that the rotor has a vertical symmetry (one blade pointing upwards or downwards) so that one spinner anemometer sonic sensor experiences constant wind while the other two experience variations in opposite directions.

During the calibration measurements, it is important that the wind direction is sufficiently stable (Figure 9). This is achieved by performing the measurements at wind speeds above 6 m s^{-1} to avoid high turbulence at low wind speeds,

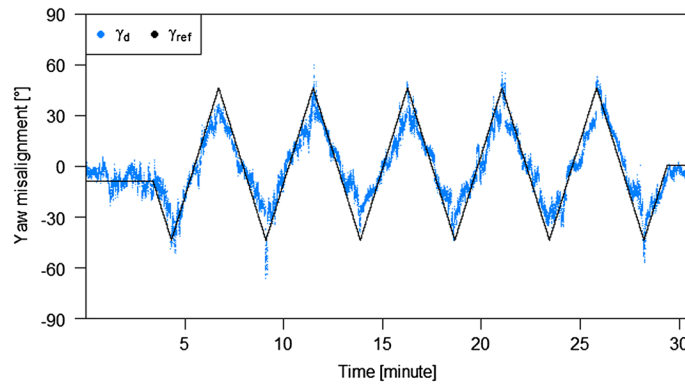


Figure 11. Non-calibrated time series of spinner anemometer and reference (corrected for average wind direction) yaw misalignment.

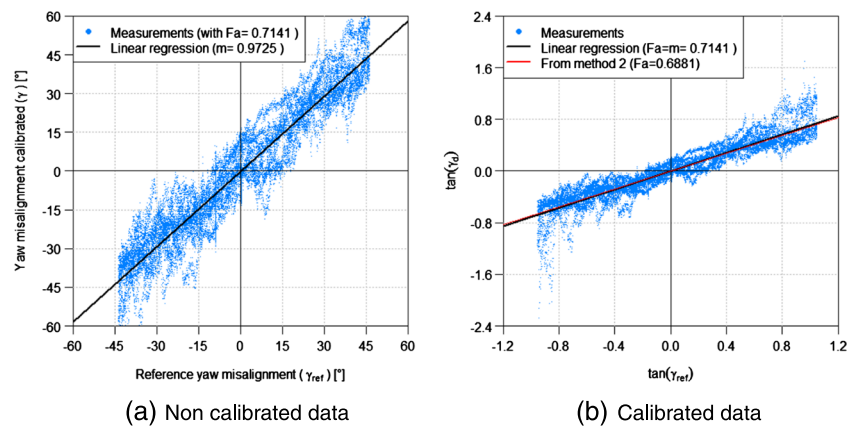


Figure 12. Reference and spinner anemometer data before and after calibration with method 1. (a) Non-calibrated data and (b) calibrated data.

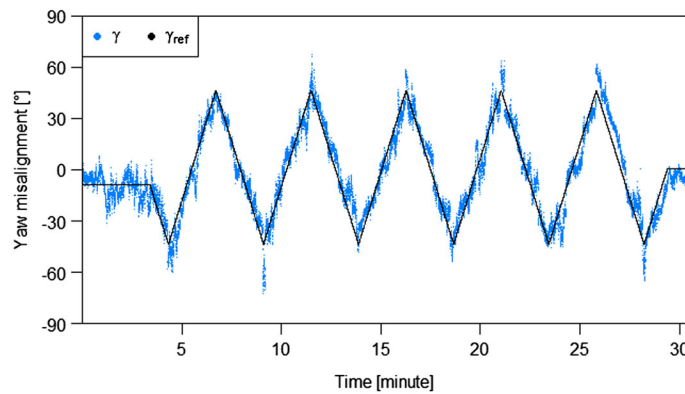


Figure 13. Calibrated time series of reference and spinner anemometer yaw misalignment data with method 1.

which normally increase the variability of the wind direction. Figure 10 shows the measured wind speed on the met mast during the calibration. The spinner anemometer data $U_{hor,d}$, γ_d and β_d , the rotor yaw direction θ_{yaw} and the met-mast data were sampled at 20 Hz during the measurements. The rotor yaw direction is now converted to a reference yaw misalignment with reference to the average wind direction: $\gamma_{ref} = \overline{\theta_{dir}} - \theta_{yaw}$. In Figure 11, the spinner anemometer yaw misalignment γ_d and the reference yaw misalignment γ_{ref} are plotted with time, and in Figure 12, the parameters are plotted against each other.

In order to use the tangent relations in equation (40), the reference yaw misalignment from Figure 9 must be offset to zero yaw misalignment with the averaged wind direction $\overline{\theta_{dir}}$. This was made with a linear regression between reference yaw misalignment data and default yaw misalignment measured by spinner anemometer. The offset was subtracted in Figures 11 and 12(a). Now, the tangent relation can be plotted, Figure 12(b), and a linear regression be made to find $F_\alpha = 0.7141$. The calibrated yawing is shown in Figure 13.

5.2. Calibration of F_α method 2: forced yawing of wind turbine in stopped condition and use of minimization procedure

Calibration method 2 used the same measurement procedure and database as method 1. For a calibrated instrument, where F_α has been found, the slope of the linear regressed line for the reference and calibrated yaw misalignments shall be equal to one (Figure 14(b)). This constraint is used to find the value of F_α with a minimization function $f(m) = |m - 1|$, where m is the slope of the linear regressed line of the reference and back and forth converted measured yaw misalignment data. The minimization routine utilizes a golden section search and successive parabolic interpolation on F_α . The back and forth conversion follows the procedure in Figure 6. The non-calibrated data are shown in Figure 14(a), while the calibrated data are shown in Figure 14(b), with $F_\alpha = 0.6881$.

5.3. Calibration of F_α method 3: forced yawing of wind turbine in stopped condition and use of direct expression

Calibration method 3 uses the same measurement procedure and database as methods 1 and 2. In method 3, F_α is found from a direct expression of F_α for each measured dataset with the tangent relation, (equation (40)). The default inflow angle to the rotor shaft axis α_d is found from the spinner anemometer output values through combination of the transformation equations derived in Section 3, considering also whether the default yaw misalignment γ_d is positive or negative:

$$\begin{aligned} \text{for } \gamma_d \geq 0 : \tan \alpha_d &= \frac{\sqrt{\sin^2 \gamma_d + (\cos \gamma_d \sin \delta + \tan \beta_d \cos \delta)^2}}{\cos \gamma_d \cos \delta - \tan \beta_d \sin \delta} \\ \text{for } \gamma_d < 0 : \tan \alpha_d &= -\frac{\sqrt{\sin^2 \gamma_d + (\cos \gamma_d \sin \delta + \tan \beta_d \cos \delta)^2}}{\cos \gamma_d \cos \delta - \tan \beta_d \sin \delta} \end{aligned} \quad (47)$$

The reference inflow angles are found from the rotor yaw direction measurements and calculated with equation (48). The reference yaw misalignment γ_{ref} is determined with the inverse transformation (Section 2.4). With a good approximation, one can set the reference flow inclination angle equal to the measured flow inclination angle with the default spinner anemometer constants: $\beta_{ref} = \beta_d$:

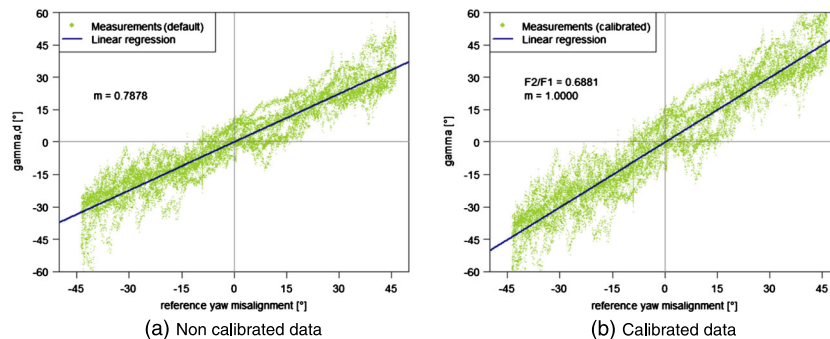


Figure 14. Reference and spinner anemometer yaw misalignment data before and after calibration with method 2. (a) Non-calibrated data and (b) calibrated data.

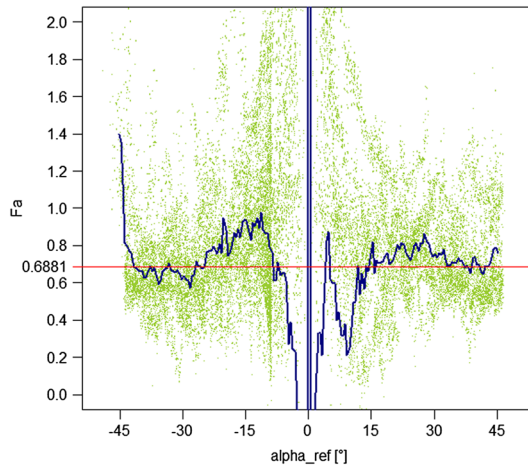


Figure 15. Method 3 yawing turbine in and out of wind in stopped condition and direct calculation of F_α . Red line is F_α from method 2 with the use of minimization function.

$$\begin{aligned} \text{for } \gamma_{ref} \geq 0 : \tan \alpha_{ref} &= \frac{\sqrt{\sin^2 \gamma_{ref} + \cos(\gamma_{ref} \sin \delta + \tan \beta_{ref} \cos \delta)^2}}{\cos \gamma_{ref} \cos \delta - \tan \beta_{ref} \sin \delta} \\ \text{for } \gamma_{ref} < 0 : \tan \alpha_{ref} &= -\frac{\sqrt{\sin^2 \gamma_{ref} + (\cos \gamma_{ref} \sin \delta + \tan \beta_{ref} \cos \delta)^2}}{\cos \gamma_{ref} \cos \delta - \tan \beta_{ref} \sin \delta} \end{aligned} \tag{48}$$

Although F_α is expected to be constant for different inflow angles and wind speeds, the ratio $\tan \alpha_d / \tan \alpha_{ref}$ of equation (40) diverges significantly, see blue line in Figure 15. This is not appropriate for a robust determination of F_α , and thus, we will not present a result for this method.

5.4. Calibration of F_α method 4: use of met mast during operation and use of minimization procedure

Calibration method 4 utilizes a hub height wind direction measurement on a met mast together with measurement of rotor yaw direction to determine the reference yaw misalignment,⁷ defined as the measured wind direction minus the rotor yaw direction:

$$\gamma_{ref} = \theta_{dir,10} - \theta_{yaw,10} \tag{49}$$

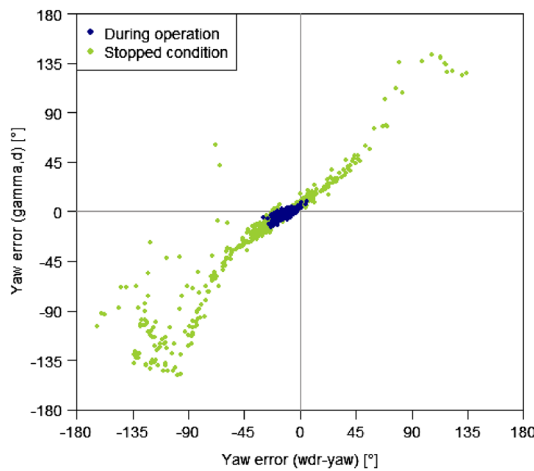


Figure 16. Method 4 calibration during operation with the use of met mast. Rotating (blue) and stopped (green).

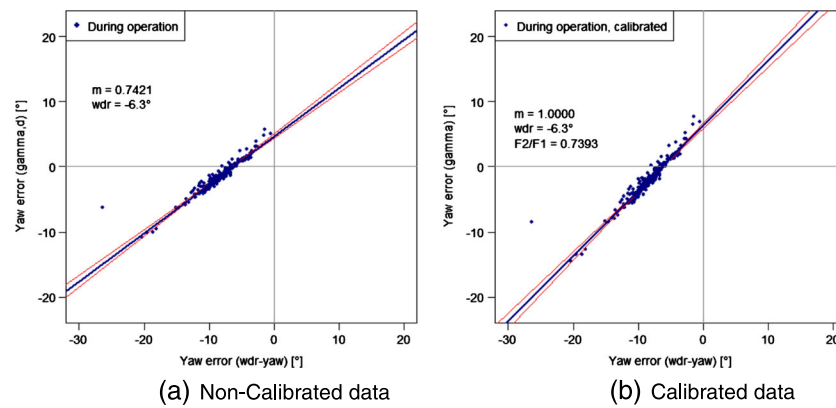


Figure 17. Yaw misalignment measurements during operation of the wind turbine with method 4, filtered for free wake sector and turbulence intensity less than 10% (red lines are linear fitting with x - and y -axis, while the blue line is the average). (a) Non-calibrated data and (b) calibrated data.

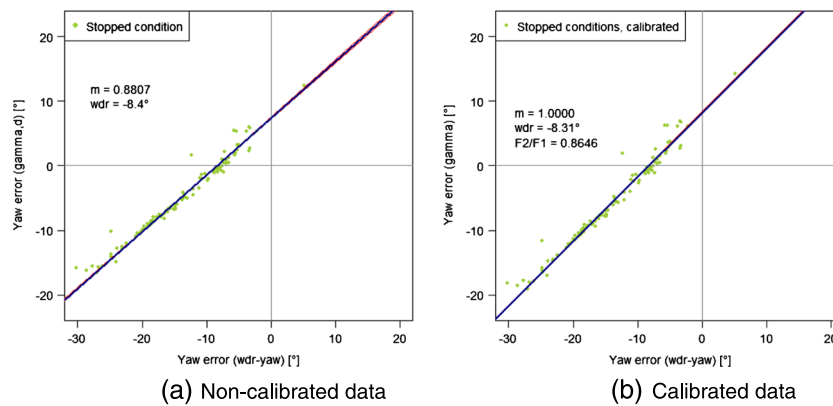


Figure 18. Yaw misalignment measurements during stopped conditions of the wind turbine with method 4, filtered for free wake sector and turbulence intensity less than 10% (red lines are linear fitting with x - and y -axis, while the blue line is the average). (a) Non-calibrated data and (b) calibrated data.

Because of the physical distance between the met mast and the wind turbine, it is necessary to use 10 min averaging to ensure good correlation. This means longer time is required to acquire an appropriate database. The yaw misalignment measured by the spinner anemometer with default constants $k_1 = k_2 = 1$ versus mast-measured reference yaw misalignment is shown in Figure 16 (before filtering). The influence of the non-linearity of the spinner anemometer algorithm at reference yaw misalignments larger than $\pm 45^\circ$ is clearly seen.

The measurements collected over 1 year were filtered for wind directions from 238° to 328° (free wake sector), for a turbulence intensity less than 10% and temperature above 2° to avoid icing conditions of the cup anemometer, resulting in 245 measurements during operation and 109 in stopped condition. Figure 17(a) shows a plot of uncalibrated spinner anemometer data during operation, while Figure 17(b) shows the corresponding calibrated data. Figure 18(a) shows a plot of uncalibrated spinner anemometer data in stopped conditions, while Figure 18(b) shows the corresponding calibrated data. Although filtering for a 90° sector, the measurements are seen to cover only a small range of yaw misalignment data. The minimization linear fitting procedure from method 2 is then used to find F_α . The results are $F_\alpha = 0.8646$ for stopped condition and $F_\alpha = 0.7393$ for operation.

5.5. Calibration of F_α method 5: use of CFD during operation and stopped

Calibration method 5 uses CFD for determination of F_α . The wind turbine rotor was modelled with the Ellipsys CFD software,^{9–11} including detailed modelling of spinner, nacelle, blade roots and profiled blades. The flow was simulated for a free wind speed of 8 m s^{-1} and for inflow angles of 0° , 10° , 20° and 30° . For each inflow case, two simulations were

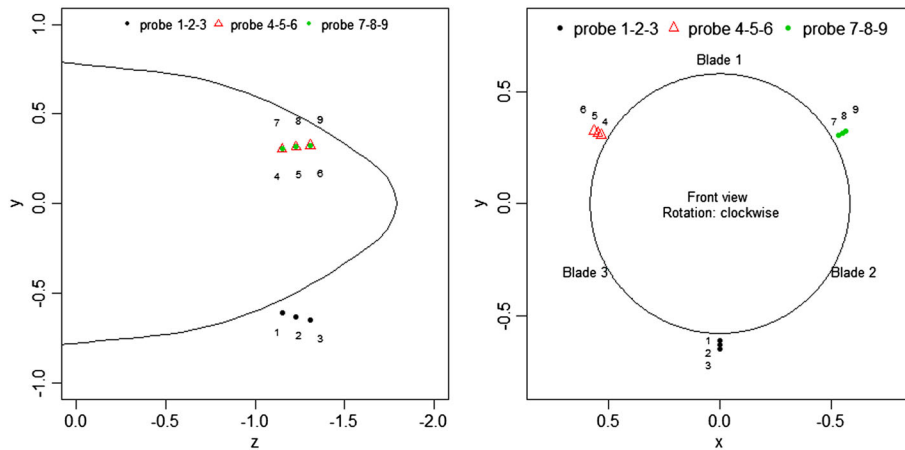


Figure 19. Side view and front view of spinner, indicating the coordinate system used for the CFD simulations (x-axis to the left, y-axis upwards, z-axis inwards along shaft axis).

performed, one with rotating rotor, the other with rotor stopped and blade number one pointing upwards ($\phi = 0^\circ$). This gives eight test cases (rotating/stopped and four inflow angles). Tilt angle and flow inclination angles were set equal to zero; hence, the reference yaw misalignment corresponds to the inflow angle $\gamma_{ref} = \alpha_{ref}$.

The CFD simulation gives three velocity components (u, v, w) at three points along each sonic sensor path (nine points overall; Figure 19). For the non-rotating case, only one single rotor position was considered. For the rotating case, a full rotor rotation was divided into 2000 steps (0.18° each).

All the calculations consider the full rotor, with its blade profiles, over a simulation volume 10 times bigger than the rotor diameter. The simulation of the rotating cases also takes account of the induction due to the rotor at the spinner position.

In post-processing of the data, the components u, v, w in the global coordinate system were combined to a vector velocity $U(u, v, w)$. The vector of the sensor path $V(x, y, z)$ was calculated as the difference between the coordinates of the end points of the path and normalized to one. The sensor path wind speed was calculated as the dot product $U \cdot V$. The sensor path wind speeds and k_α for the rotating cases are shown in Figure 20 for $10^\circ, 20^\circ$ and 30° , respectively. k_α was calculated with equation (5) rearranged as

$$k_\alpha = \frac{k_2}{k_1} = \frac{\sqrt{3(V_1 - V_{ave})^2 + (V_2 - V_3)^2}}{\tan(\alpha_{ref})\sqrt{3}V_{ave}} \quad (50)$$

k_α was expected to be independent of rotor position, but unstable dynamic effects, dependent on rotor position and inflow angle, are seen to be pronounced, especially for greater inflow angles, as shown in Figure 20 to the right.

Figure 21 shows a summary of the nine k_α values for the different flow calculation cases.

The highest three values in Figure 21 are rotor averaged k_α values during rotation (black), while the points just below (red) are k_α values for rotor azimuth position $\phi = 0^\circ$ of the same rotating case. The difference between the two cases (black and red points) does not represent a trend but is purely due to the variations of k_α over one revolution (Figure 20). The difference between the second case (red) and the third (blue) is small for the 10° inflow angle case, while the differences at 20° and 30° are in the order of about 15%.

6. DISCUSSION

A summary of the results of the five calibration methods to find F_α is shown in Table I.

The calibration measurements and simulations were made for both operating and stopped conditions.

Method 1 with forced yawing and high sampling rate in stopped condition is a robust procedure that is easy and fast to perform in the field. The yaw misalignments can be forced to reasonably high values, which is also necessary because the spreading of data due to variations in wind direction during measurements is high. The resulting calibration factor $F_\alpha = 0.7141$ is 7% higher than for the CFD calculation at 10° inflow angle. F_α for higher flow angles of the CFD calculations are somewhat smaller (up to 20%).

Method 2 using a minimization function to achieve correct slope gave a result close to method 1 (3% lower). The two methods are quite similar. Method 2 is a little more cumbersome as a minimization, and iterative procedure is needed while method 1 is more direct.

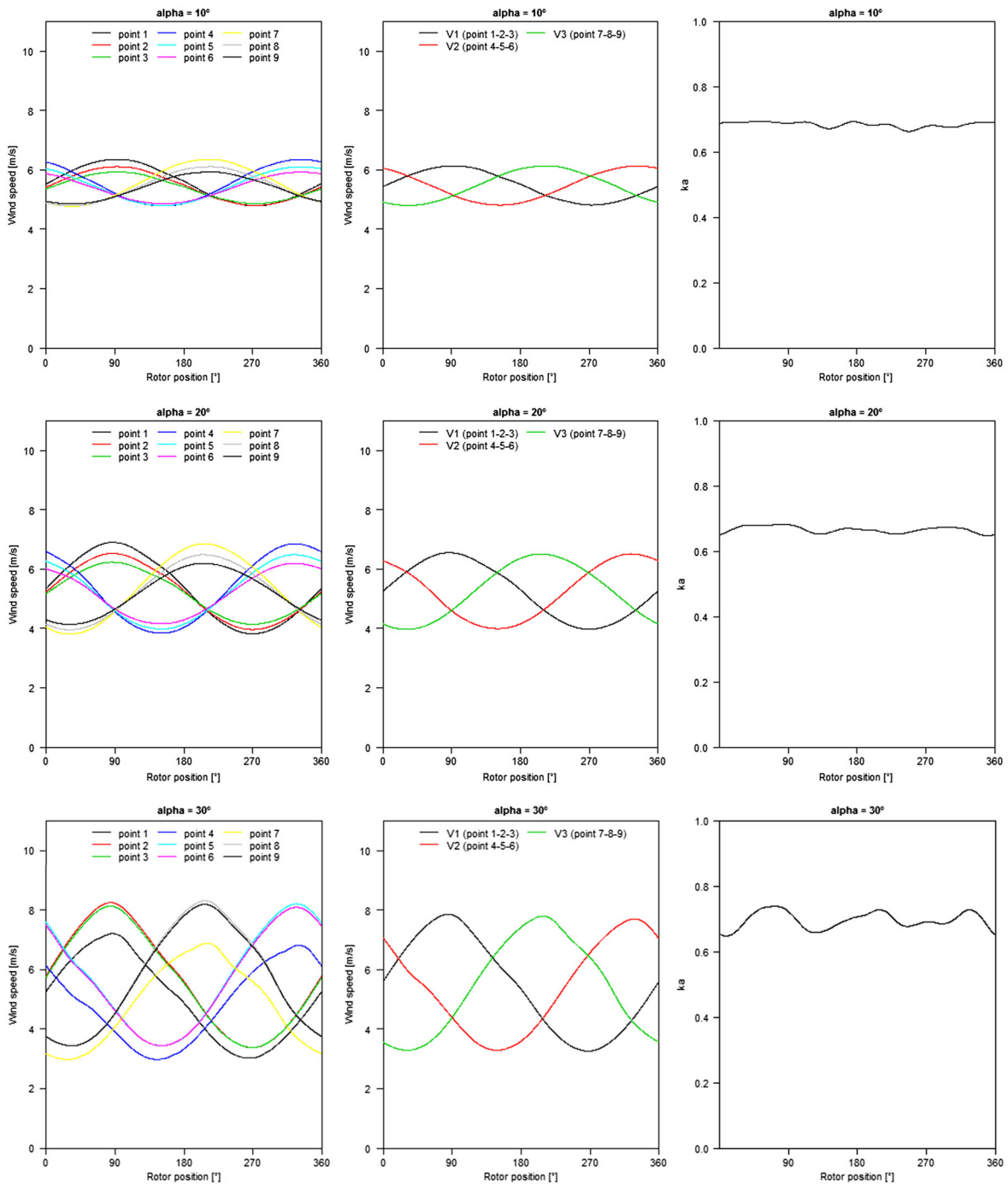


Figure 20. The CFD calibration simulations during rotation, method 5, for $\alpha = 10^\circ, 20^\circ$ and 30° from top to bottom. Wind speeds along sonic sensor paths to the left, averaged wind speeds in the middle and k_α to the right.

Method 3 using the direct expression of F_α seemed to fail to give useful results. Especially, the large variations of F_α in the range $\pm 15^\circ$ is disappointing. The singularity at 0° was expected, but the influence in the surroundings of the singularity is spoiling the method.

Method 4 used 10 min averages recorded during normal operation and in stopped condition. The 10 min averaging ensures reasonably robust measurement points, but the yaw misalignment range during operation is rather small. For stopped condition, F_α is significantly larger than for operating condition (about 17%), and it is also significantly larger than the value for methods 1 and 2 (about 20%).

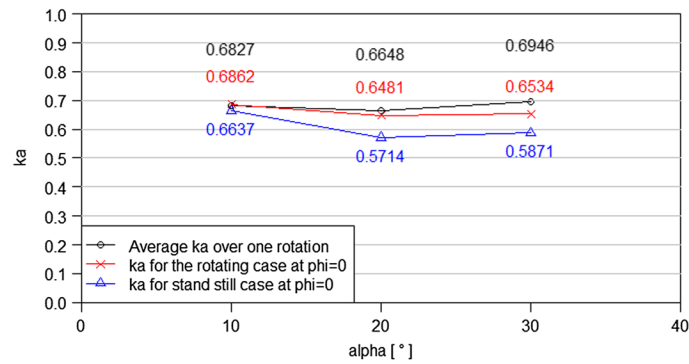


Figure 21. Calibration coefficient from different CFD simulation cases; rotating and averaged (black), rotating at $\phi = 0^\circ$ (red), stopped at $\phi = 0^\circ$ (blue).

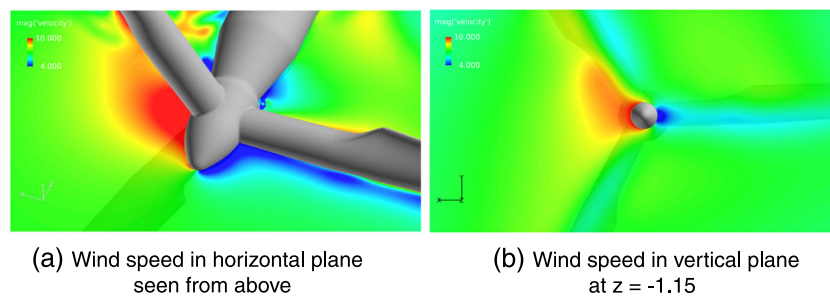


Figure 22. Graphic presentation of a CFD result for 8 m s^{-1} and inflow angle $\alpha_{ref} = 30^\circ$ from the right, rotor position $\phi = 90^\circ$ (blade 1 horizontal). (a) Wind speed in horizontal plane seen from above and (b) wind speed in vertical plane at $z = -1.15$.

Table I. Summary of results of calibration methods for angular measurements.

Method	Test method description	Analysis to determine F_α	F_α	Condition
Method 1	Forced yawing of wind turbine with stopped rotor, acquisition of data from spinner anemometer and yaw direction at 1 Hz or faster at wind speed $>6 \text{ m s}^{-1}$	Correction of data for average wind direction, plotting data with tangent relations and linear regression	0.7141	Stopped
Method 2	Same as method 1	Minimization of slope function with golden search and successive parabolic interpolation routine using back and forth conversions	0.6881	Stopped
Method 3	Same as method 1	Direct calculation of F_α	0.6–1.0	Stopped, high scatter
Method 4	Acquisition of 10 min averaged data from spinner anemometer, yaw direction and met mast over months long period	Operation and stopped data from condition of wind turbine analysed separately.	0.8646 0.7393	Stopped Operating
Method 5	Full rotor CFD simulation for different inflow angles, for rotating and non-rotating conditions	Post-processing of three-dimensional wind field to calculate sensor path wind speeds and F_α with forward transformation	0.6637 0.5714 0.5871 0.6862 0.6481 0.6534 0.6827 0.6648 0.6946	Stopped, $\alpha = 10^\circ, \phi = 0^\circ$ Stopped, $\alpha = 20^\circ, \phi = 0^\circ$ Stopped, $\alpha = 30^\circ, \phi = 0^\circ$ Operating, $\alpha = 10^\circ, \phi = 0^\circ$ Operating, $\alpha = 20^\circ, \phi = 0^\circ$ Operating, $\alpha = 30^\circ, \phi = 0^\circ$ Operating, $\alpha = 10^\circ, \phi = ave$ Operating, $\alpha = 20^\circ, \phi = ave$ Operating, $\alpha = 30^\circ, \phi = ave$

The difference in F_α from stopped to operating might be due to induced wind speed from the operating and thrust-generating rotor. The induced wind speed reduces the longitudinal component U_x , while the transversal component U_y is the same. The effect is that the local yaw misalignment at the spinner is larger than in the far field. With a known induction function $a(U) = (U_\infty - U)/U_\infty$, the correction of locally measured yaw misalignment to the far field is

$$\gamma_\infty = \arcsin((1 - a) \sin \gamma) \quad (51)$$

For a yaw misalignment measured at the spinner of 10° and an induction factor of 10%, the yaw misalignment measured at the far field is 9.0° (10% lower). When a yaw misalignment at the spinner is higher during operation than when stopped, then the F_α value for operating condition should be higher than for stopped condition. Method 4 in Table I shows the opposite. This is a controversy. However, the measurements in stopped condition are made during operating periods of the wind turbine. Stopped conditions do only occur for very low wind speeds where the wind turbine stops or is idling because of low wind conditions. The measurements for stopped conditions are thus far from the requirements in methods 1–3 of wind speeds above 6 m s^{-1} . The stopped condition measurements of method 4 should therefore be considered with reservation. The measurements during operation comply well with the measurements in stopped condition of methods 1 and 2 considering a calculated induction factor in the range 2.5% to 7.4%, using equation (51). This level of the induction factor is, however, lower than what should be expected. A reason for an increased uncertainty in use of method 4 is the quite small yaw misalignment range during operation.

Method 5 with CFD simulations results in quite some variety. Figure 20 shows increasing variability of k_α over a rotation with increasing inflow angle. The variability pattern is without a 3P similarity. This indicates fluctuations in the aerodynamic flow over the spinner or unsteadiness in the CFD calculations. The wind speed flow pattern in Figure 22(b) indicates flow separation at the spinner nose at 30° inflow angle. At lower inflow angles, Figure 20 right, the variability is reduced. The most trustworthy calibration values with CFD for angular measurements must therefore be found in the 10° inflow angle simulations, as this is the area where actual yaw misalignment measurements are expected. For stopped condition, k_α is significantly higher for 10° inflow angle than for 20° or 30° . For operating condition, k_α is 3.4% higher for 10° , while it is 11–13% for 20° to 30° .

Overall, methods 1 and 3, with quite comparable results, are in good agreement with method 4 for operating conditions, with a calculated increase in k_α of 3.5% for operating conditions due to induction. This is equivalent to CFD simulations for 10° inflow angle with an increase of 3.5% due to induction. The CFD simulations just give k_α values about 8% lower values than field calibrations, as seen in Table I. The reason for the lower k_α values from CFD simulations might be due to calculation uncertainties connected with flow separation on the spinner nose because of the pointed spinner. This might be a disadvantage specifically on this type of spinner and might not be found on more rounded spinners.

6.1. Uncertainty of yaw misalignment measurements

Angular measurements with the spinner anemometer has some uncertainties connected to calibration as well as some other relations. The influence of induced wind speeds raises the question whether the measured yaw misalignment is defined as a local inflow angle at the spinner or a far field inflow angle. We find it most appropriate to define the yaw misalignment as a local inflow angle, as well as we find it most appropriate to define the measured wind speed as a local wind speed. The induction function, as mentioned earlier, should be used to correct the measurements to the far field. The induction function should be found as part of the calibration of F_1 . This could be made according to the International Electrotechnical Commission standard,⁸ as a determination of the nacelle transfer function. Defining the yaw misalignment as a local measurement reduces the uncertainty because of a clear definition of the measurand. Calibration methods 1 and 2 are therefore also the preferred methods.

The sonic sensors must always be zero wind calibrated, as they are from factory. A traceable wind tunnel calibration could be made if required, but this should normally not be necessary for angular measurements because the uncertainty is relatively low. The internal calibration must be made prior to calibration for angular measurements to smooth out variations during each rotation, so that the rotor azimuth position during calibration yawing does not influence on the calibration. The uncertainty related to the calibration factor F_α with methods 1 and 2, where we have taken the non-linearity of the spinner anemometer algorithm into account, is estimated at $\pm 2\%$, for use of either of the two methods and a linearization uncertainty with a standard deviation of 10%. The uncertainty of the yaw direction sensor is estimated at $\pm 2^\circ$. However, the uncertainty on the linearity is estimated to be close to zero, so we do not need to take this into account. If we assume rectangular uncertainty distributions for use of methods 1 or 2 and linearization, and combine the uncertainty components, we get a standard uncertainty of 10% of F_α .

The uncertainty of F_α , and thus k_α , provides an uncertainty of α of the same order. The yaw misalignment and flow inclination angles are directly derived from α and have the same uncertainty connected to them. A spinner anemometer that measures for example 10° yaw misalignment, and where the standard uncertainty of F_α is 10%, will have a standard uncertainty on the yaw misalignment of 1° .

7. CONCLUSIONS

In the first part, the spinner anemometer conversion algorithm that converts the measured wind speeds by the sonic sensors to horizontal wind speed, yaw misalignment and flow inclination angle is described. The inverse conversion is derived in order to use earlier measured wind data (measured with default constants k_1 and k_2) to find the calibration factor F_α . F_α is used to correct the default spinner anemometer ratio $k_{\alpha,d} = k_{2,d}/k_{1,d}$ to the calibrated ratio $k_\alpha = k_2/k_1$ by $k_\alpha = F_\alpha k_{\alpha,d}$. It was found that F_α was the only single calibration factor that angular measurements depend on. It was further found that calibration for angular measurements should be made after internal calibration of the spinner anemometer and before wind speed calibration.

Five different methods for calibration of a spinner anemometer for yaw misalignment measurements were presented for a stall-regulated 500 kW wind turbine with a spinner anemometer mounted on a pointed spinner. The first three calibration methods 1–3 consist of stopping the turbine in a steady and low turbulent wind ($>6 \text{ m s}^{-1}$) and yawing the turbine several times in and out of the wind. These methods used fast-sampled measurements (20 Hz, $>1 \text{ Hz}$). Time required was about half an hour. Method 1 used a tangent relation with a linear regression to find $F_\alpha = 0.7141$ and was the highest recommended method with method 2 using a minimization function and an iterative process with back and forth conversion algorithms to find $F_\alpha = 0.6881$, following very close. Method 3 failed to give a satisfactory result.

Method 4 used 10 min average data during normal operation and standstill of the wind turbine, combined with wind direction measurements from a met-mast upwind of the wind turbine. Data for stopped condition were found to be made at too low wind speeds. For operation condition, we found $F_\alpha = 0.7393$. The higher value than for methods 1 and 2 was assumed to be due to rotor induction.

Method 5 used CFD to calculate the flow over the spinner for axial and skew airflow during operating and stopped conditions. F_α was found directly from the calculations. The calculations for 10° inflow angle were considered to be the most trustworthy, deriving F_α values approximately 8% lower than for field calibrations. The differences were considered to be due to separation on the pointed spinner.

The influence of rotor induction increases the yaw misalignment measurements locally at the spinner compared with the far field. We define the yaw misalignment measurements to be a local measurement; therefore recommending calibrations by yawing the wind turbine in and out of the wind in stopped conditions and eventually using an induction function for correction to the far field. The uncertainty connected with the calibration was found to be approximately 10%, resulting in an uncertainty of 1° for a 10° yaw misalignment measurement.

ACKNOWLEDGEMENTS

This work was performed as part of an EUDP project funded by the Danish Energy Agency and by Vattenfall, Metek and Vestas. (J.nr 64009-0273). The authors would like to thank the people from Metek, Vattenfall and ROMO Wind for the help with technical support and for their good collaboration in the project.

REFERENCES

1. Frandsen S, Sørensen N, Mikkelsen R, Pedersen TF, Antoniou I, Hansen K. The generics of wind turbine nacelle anemometry. *EWEC 2009*, Bruxelles, 2009.
2. Zahle F, Sørensen NN. Characterization of the unsteady flow in the nacelle region of a modern wind turbine. *Wind Energy* 2011; **14**: 271–283.
3. Højstrup J, Nielsen D, Hansen K, Lauritzen L. Maximise energy production by minimizing yaw misalignment. Large scale field deployment of spinner anemometer. *Poster 0162, EWEC 2013*, Vienna, 2013.
4. Pedersen TF. Spinner anemometer—an innovative wind measurement concept. *EWEC 2007*, Milan, 2007.
5. Pedersen TF, Sørensen N, Evevoldsen P. Aerodynamics and characteristics of a spinner anemometer. *Journal of Physics: Conference Series* 75 012018 2007.
6. Spinner anemometer user manual version 9.27-3. *Metek Meteorologische Messtechnik GmbH*, Germany, 2012.
7. Paulsen US, *Vindmølleafprøvning Nordtank NTK 500/41, Måling af Effektkurve*, Technical Report Risø-I-889 DA, Risø National Laboratory, Roskilde, Denmark, November 1995.
8. IEC 61400-12-2 Wind turbines - part 12-2: Power performance of electricity producing wind turbines based on nacelle anemometry, Edition 1.0, 2013-03.
9. Michelsen JA, Basis3D—a platform for development of multiblock PDE solvers. *Technical Report AFM 92-05*, Technical University of Denmark, 1992.

10. Michelsen JA, Block structured multigrid solution of 2D and 3D elliptic PDEs. *Technical Report AFM 94-06*, Technical University of Denmark, 1994.
11. Sørensen NN, General purpose flow solver applied to flow over hills. *Technical Report Risø-R-827(EN)*, Risø National Laboratory, 1995.

Chapter 3

Innovative method for calibration of flow angle measurements

Chapter 2 presented five methods for calibration of a spinner anemometer for flow angle measurements, consisting in yawing the wind turbine several times of $\pm 60^\circ$ in and out of the wind in stopped condition. The recommended method required the yaw position to be measured at high sampling frequency (1-10 Hz) along with the spinner anemometer output. The signal of the wind turbine yaw position sensor is often difficult to access, therefore a second position sensor was generally installed by Romo Wind A/S. The installation of the sensor is difficult and requires the technician to access a confined and dirty space by the yaw rack under the nacelle.

A new innovative method that does not require the yaw position to be measured was investigated in this chapter. The new method leverage on the non linearity of the spinner anemometer algorithm to find the calibration factor F_α by an optimization process that minimizes the dependency of the wind speed to the yaw misalignment. The new calibration method was found to be rather robust with F_α values within $\pm 2.7\%$ of the mean value for four successive tests at the same rotor position.

The following article describes the calibration method and the verification of the method with field experiments.

An innovative method to calibrate a spinner anemometer without use of yaw position sensor

Giorgio Demurtas¹ and Nick Gerardus Cornelis Janssen²

¹DTU Wind Energy, Frederiksborgej 399, 4000 Roskilde, Denmark.

²Romo Wind A/S, Olof Palmes Alle 47, 8200 Aarhus N, Denmark.

Correspondence to: Giorgio Demurtas (giord@dtu.dk)

Abstract. A spinner anemometer can be used to measure the yaw misalignment and flow inclination experienced by a wind turbine. Previous calibration methods used to calibrate a spinner anemometer for flow angle measurements were based on measurements of a spinner anemometer with default settings (arbitrary values, generally $k_{1,d} = 1$ and $k_{2,d} = 1$) and a reference yaw misalignment signal measured with a yaw position sensor. The yaw position sensor is normally present in wind turbines for control purposes, however, such a signal is not always available for a spinner anemometer calibration. Therefore, an additional yaw position sensor was installed prior to the spinner anemometer calibration. An innovative method to calibrate the spinner anemometer without a yaw positions sensor was then developed. It was noted that a non calibrated spinner anemometer that overestimate (underestimate) the inflow angle will also overestimate (underestimate) the wind speed when there is a yaw misalignment. The new method leverage on the non linearity of the spinner anemometer algorithm to find the calibration factor F_α by an optimization process that minimizes the dependency of the wind speed to the yaw misalignment. The new calibration method was found to be rather robust with F_α values within $\pm 2.7\%$ of the mean value for four successive tests at the same rotor position.

Nomenclature

V_1	Speed along the sensor path of probe 1.	α	Inflow angle respect to the shaft axis.
V_2	Speed along the sensor path of probe 2.	δ	Shaft tilt angle.
V_3	Speed along the sensor path of probe 3.	β	Flow inclination angle.
V_{ave}	Mean value between V_1, V_2, V_3 .	γ	Yaw misalignment.
U	Wind speed vector modulus.	γ_{ref}	Reference yaw misalignment.
U_{hor}	Horizontal wind speed component.	ϕ	Rotor position
$U_{hor,d}$	Horizontal wind speed (non calibrated).	$\overline{U_{hor}}$	Mean horizontal wind speed.
$U_{hor,d,c}$	Horizontal wind speed component (calibrated with correct k_α but not yet k_1).	θ	Azimuth position of flow stagnation point on spinner (relative to sonic sensor 1).

k_1	Calibration constant mainly related to wind speed calibration.	F_1	Calibration correction factor mainly related to wind speed calibration.
k_α	Calibration constant mainly related to angle calibration.	F_α	Calibration correction factor mainly related to angle calibration.
k_2	Calibration constant (equal to $k_\alpha \cdot k_1$).	F_2	Calibration correction factor ($F_\alpha \cdot F_1$).
RMSE	Root Mean Square Error	TI	Turbulence Intensity.
QSC	Quality Score	WSR	Wind Speed Response method
GGref	Gamma-Gamma reference method	TanTan	Tangent-Tangent method

1 Introduction

The spinner anemometer (Pedersen et al. (2007)) measures the horizontal wind speed U_{hor} , yaw misalignment γ and flow inclination β experienced by a wind turbine by measuring the flow on the spinner by using three 1D sonic sensors. The three 1D sonic sensors are mounted on the spinner and connected to a so called "conversion box". Each sonic sensor arm also contains a 1D accelerometer which measurements are used in the conversion box to calculate the rotor position. The main purpose of the conversion box is to execute the conversion algorithm that transform the 1D sonic sensors readings which are in a rotating coordinate reference system (Fig. 1) to the fixed nacelle coordinate reference system as U_{hor} , γ and β . The conversion algorithm takes into consideration the wind turbine tilt angle δ which is set in the conversion box as a constant. The shape of the spinner is accounted for by two calibration coefficients, k_1 and k_2 . The first coefficient mainly relates to wind speed measurements, while the ratio of the two coefficients $k_\alpha = k_2/k_1$ mainly relates to flow angle measurements. The relations between the wind speed U , flow angle α and azimuth position of the stagnation point θ producing V_1 , V_2 and V_3 measured by the three 1D sonic sensors are:

$$V_1 = U (k_1 \cos(\alpha) - k_2 \sin(\alpha) \cos(\theta)) = U \cdot k_1 (\cos(\alpha) - k_\alpha \sin(\alpha) \cos(\theta)) \quad (1)$$

$$V_2 = U \left(k_1 \cos(\alpha) - k_2 \sin(\alpha) \cos\left(\theta - \frac{2\pi}{3}\right) \right) = U \cdot k_1 \left(\cos(\alpha) - k_\alpha \sin(\alpha) \cos\left(\theta - \frac{2\pi}{3}\right) \right) \quad (2)$$

$$V_3 = U \left(k_1 \cos(\alpha) - k_2 \sin(\alpha) \cos\left(\theta - \frac{4\pi}{3}\right) \right) = U \cdot k_1 \left(\cos(\alpha) - k_\alpha \sin(\alpha) \cos\left(\theta - \frac{4\pi}{3}\right) \right) \quad (3)$$

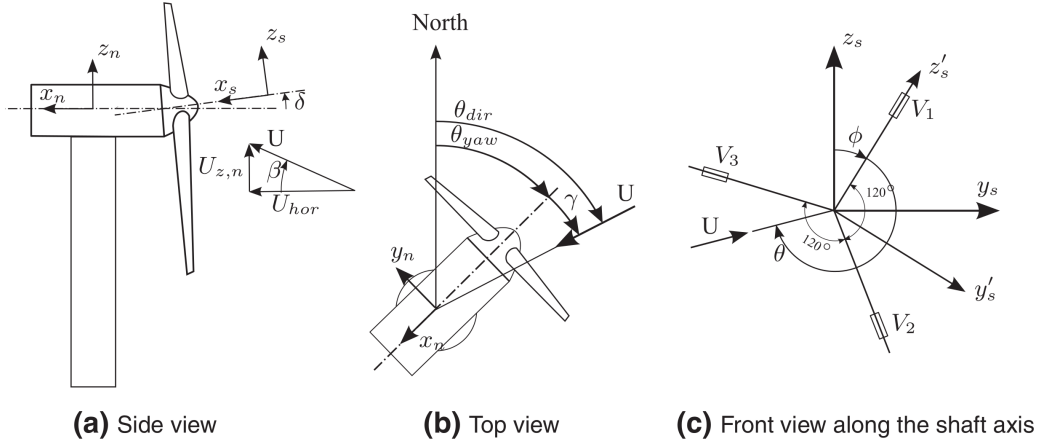


Figure 1. Coordinate systems and definition of angles: rotating spinner coordinate system x'_s , y'_s and z'_s , non-rotating shaft coordinate system x_s , y_s and z_s , fixed nacelle coordinate system x_n , y_n and z_n , yaw direction θ_{yaw} , yaw misalignment γ , flow inclination angle β , tilt angle δ , azimuth position of flow stagnation point on spinner θ (relative to sonic sensor 1) and rotor azimuth position ϕ (position of sonic sensor 1 relative to vertical). From Demurtas et al. (2016).

The conversion algorithm (Eq. 5 to Eq. 18) was derived from Eq. 1, 2 and 3. The values of k_1 and k_2 constants are generally not known when the spinner anemometer is installed on a wind turbine for the first time, they are therefore set to an arbitrary value, generally $k_{1,d} = 1$ and $k_{2,d} = 1$. The calibration procedure will then provide the correction factors F_1 and F_α to correct the default values to calibrated values (Eq. 4). The output values relative to a spinner anemometer which is measuring with default calibration settings has the subscript 'd' ($U_{hor,d}$, γ_d , β_d).

$$k_1 = F_1 \cdot k_{1,d} \quad k_2 = F_2 \cdot k_{2,d} = k_\alpha \cdot k_1 = k_{\alpha,d} \cdot F_\alpha \cdot k_1 \quad (4)$$

$$\alpha = \arctan \left(\frac{k_1 \sqrt{3(V_1 - V_{ave})^2 + (V_2 - V_3)^2}}{\sqrt{3}k_2 V_{ave}} \right) \quad (5)$$

$$V_{ave} = \frac{1}{3}(V_1 + V_2 + V_3) \quad (6)$$

$$U = \frac{V_{ave}}{k_1 \cos \alpha} \quad (7)$$

$$V_1 < V_{ave} : \theta = \arctan \frac{(V_2 - V_3)}{\sqrt{3}(V_1 - V_{ave})} \quad V_1 \geq V_{ave} : \theta = \arctan \frac{(V_2 - V_3)}{\sqrt{3}(V_1 - V_{ave})} + \pi \quad (8)$$

$$U_{x,s} = U \cos(\alpha) \quad (9)$$

$$U_\alpha = U \sin(\alpha) \quad (10)$$

$$U_{y,s} = -U_\alpha \sin(\phi + \theta) \quad (11)$$

$$U_{z,s} = -U_\alpha \cos(\phi + \theta) \quad (12)$$

$$5 \quad U_x = U_{x,s} \cos(\delta) + U_{z,s} \sin(\delta) \quad (13)$$

$$U_y = U_{y,s} \quad (14)$$

$$U_z = U_{z,s} \cos(\delta) - U_{x,s} \sin(\delta) \quad (15)$$

$$U_{hor} = \sqrt{U_x^2 + U_y^2} \quad (16)$$

$$\gamma = \arctan\left(\frac{U_y}{U_x}\right) \quad (17)$$

$$10 \quad \beta = \arctan\left(\frac{U_z}{U_{hor}}\right) \quad (18)$$

1.1 Existing calibration methods for flow angle measurements

Two methods based on measurements to calibrate a spinner anemometer for flow angle measurements proposed in Pedersen and Demurtas (2014) consist in yawing the wind turbine of $\pm 60^\circ$ several times under manual control (as indicated by the turbine yaw position sensor, with respect to the mean wind direction). During this test, the output parameters of the spinner anemometer (U_{hor} , γ , β) are recorded at high sampling frequency (10 Hz). The analysis of the measurements provide the correction factor F_α that multiplied by the default $k_{\alpha,d}$ gives the correct k_α calibration value.

The methods are based on the assumption that the wind direction is constant during the test. Due to this requirement, Pedersen and Demurtas (2014) recommended to do the test at wind speeds above 6 m/s. Both methods need the yaw position to be measured in order to calculate the reference yaw misalignment γ_{ref} , defined as the mean wind direction minus the instantaneous yaw position during test (see Pedersen and Demurtas (2014) for details). In the first method (abbreviated as GGref) F_α was calculated by calibrating the measurements iteratively, until the linear fit of γ as a function of γ_{ref} was giving a line of slope equal to 1.

In the second method (abbreviated as TanTan), only one linear fitting was made to $\tan(\gamma)$ as a function of $\tan(\gamma_{ref})$. In this case, the slope coefficient of the fit was exactly F_α . The two calibration methods were found to be sensitive to the width of the yawing span. In fact, different F_α values were obtained sub-setting the data-set to a variable span of γ_{ref} .

A new method to find the F_α value, that does not require a yaw position measurement, and use the non linearity of the spinner anemometer conversion algorithm is proposed.

2 The wind speed response method

The method (abbreviated WSR) is based on the assumption that the wind speed is constant during the test. The turbulence of the real wind will add some scatter in the measurements which will reduce the repeatability of the result. While in principle a single yawing movement is sufficient, in practice the wind speed fluctuations needs to be averaged by yawing the wind turbine several times. The spinner anemometer is able to measure inflow angles (yaw misalignment γ and flow inclination β) and wind speed U . A wrong k_α value will result in a wrong value of the angle γ , which will turn into a wrong value of the horizontal wind speed U_{hor} . In other words, a wrong k_α makes the wind speed measurement dependent on the yaw misalignment. This property of the spinner anemometer model (Eq. 1, 2 and 3) was verified with a data-set consisting of constant wind speed U_{hor} and 13 values of yaw misalignment going from -60° to 60° in steps of 10° . The tilt angle and the flow inclination were set to arbitrary values (equal to zero for Fig. 2). In the real world the tilt angle of the wind turbine is typically between 3° and 6° while the flow inclination varies within approximately $\pm 10^\circ$. The conversion algorithm takes into consideration both the tilt angle δ and the measured flow inclination β_d when calculating the yaw misalignment γ_d , therefore they have no influence on the result of this method. V_1 , V_2 and V_3 were calculated with Eq. 1, 2 and 3 with $k_\alpha = 1$ and $k_2 = 1$.

Eq. 5 to Eq. 18 (which are the direct conversion algorithm presented in Pedersen and Demurtas (2014)) were used with new values of k_α equal to 0.5, 1 and 2, with the calculated V_1 , V_2 and V_3 to calculate $U_{hor,d}$ and α_d . k_1 was kept equal to one.

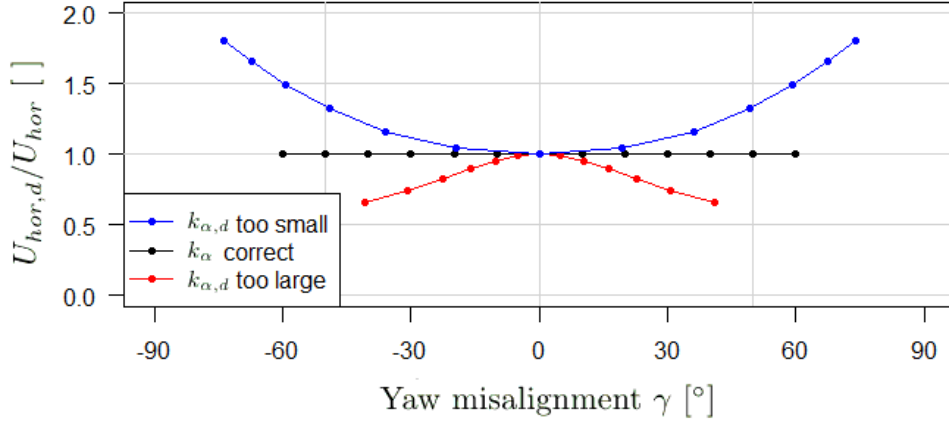


Figure 2. Effect of three k_{α} values on yaw misalignment and wind speed measurements. Black line shows data where the k_{α} is correct (equal to one for our theoretical spinner model). Blue curve shows k_{α} set to 0.5. To correct the blue curve to the black curve, the correction should be made with $F_{\alpha} > 1$ ($F_{\alpha} = 2$ in this case). Red line shows k_{α} set to twice the correct value, therefore we need $F_{\alpha} < 1$ to correct the measurements to the black line.

When the conversion was made with $k_{\alpha} = 1$, $U_{hor,d}$ and α_d matched the (correct) initial values of U_{hor} and α (black line in Fig. 2). On the other hand, when the conversion was made with $k_{\alpha,d} = 0.5$ the wind speed and angle were overestimated (blue curve in Fig. 2) because $k_{\alpha,d}$ is too small compared to the correct k_{α} value equal to one in this example. Similarly, with $k_{\alpha,d} = 2$ the angles and the wind speed were underestimated (red curve in Fig. 2).

- 5 From experience of calibration on several turbines the default settings of $k_{\alpha,d} = 1$ is too small. Therefore the wind speed response looks like a happy smile and an $F_{\alpha} > 1$ is required to correct the default calibration value. Note that the wind speed is still measured correctly for small inflow angle (where the three curves of Fig. 2 are close to each other).

The method to optimize F_{α} consists in minimizing the RMSE (Root Mean Square Error) of a horizontal linear fit made to the measurements of $U_{hor,d}$ for varying F_{α} . U_{hor} is obtained applying the F_{α} calibration to the measurements of $U_{hor,d}$, γ , d and β_d acquired with default values $k_{1,d}$, $k_{2,d}$. For this reason U_{hor} is a function of $U_{hor,d}$, γ_d , β_d , $k_{1,d}$, $k_{2,d}$ and F_{α} .

The function object of the optimization is

$$RMSE = f(U_{hor,d}, \gamma_d, \beta_d, k_{1,d}, k_{2,d}, F_{\alpha}) = \sqrt{\frac{1}{n} \sum_1^n (\overline{U_{hor}} - U_{hor})^2}, \quad (19)$$

where the first three variables comes from the measurements, fourth and fifth are the settings of the spinner anemometer at the time of acquisition of the measurements, and the last one (F_{α}) is the independent variable used in the optimization. The function of Eq. 19 was optimized to its minimum using a combination of golden section search and successive parabolic interpolation (Brent and N.J. (1973)).

3 Application of the method

The measurements were acquired in February 2016 on a Neg-Micon 2 MW wind turbine installed in Denmark. The wind turbine was yawed in and out of the wind several times with the rotor stopped with one blade pointing downwards. Figures 3 and 4 show the 10 Hz data recorded during the calibration procedure. Figure 3A, B and C show non calibrated measurements, while Fig. 4A, B and C show calibrated measurements. In both Fig. 3 and 4 the sub-figure A shows the time series of the yaw misalignment and yaw misalignment reference (measured with a yaw position sensor). Sub-figure B shows the time series of the wind speed. Sub-figure C shows the wind speed response as a function of yaw misalignment.

Figure 3D shows the value of F_α calculated with the three different methods (GGref and TanTan from Pedersen and Demurtas (2014) and the present method, WSR), for varying range of yawing the wind turbine out of the wind (data were filtered according to γ_{ref} in steps of 5° span per side). The F_α value was calculated with the WSR method only if there were at least 30 seconds of measurements in the outmost 5° of the considered range (which justifies the fact that the scatter plot of Fig. 4C appears wider than the maximum range shown in Fig. 3D by the green line).

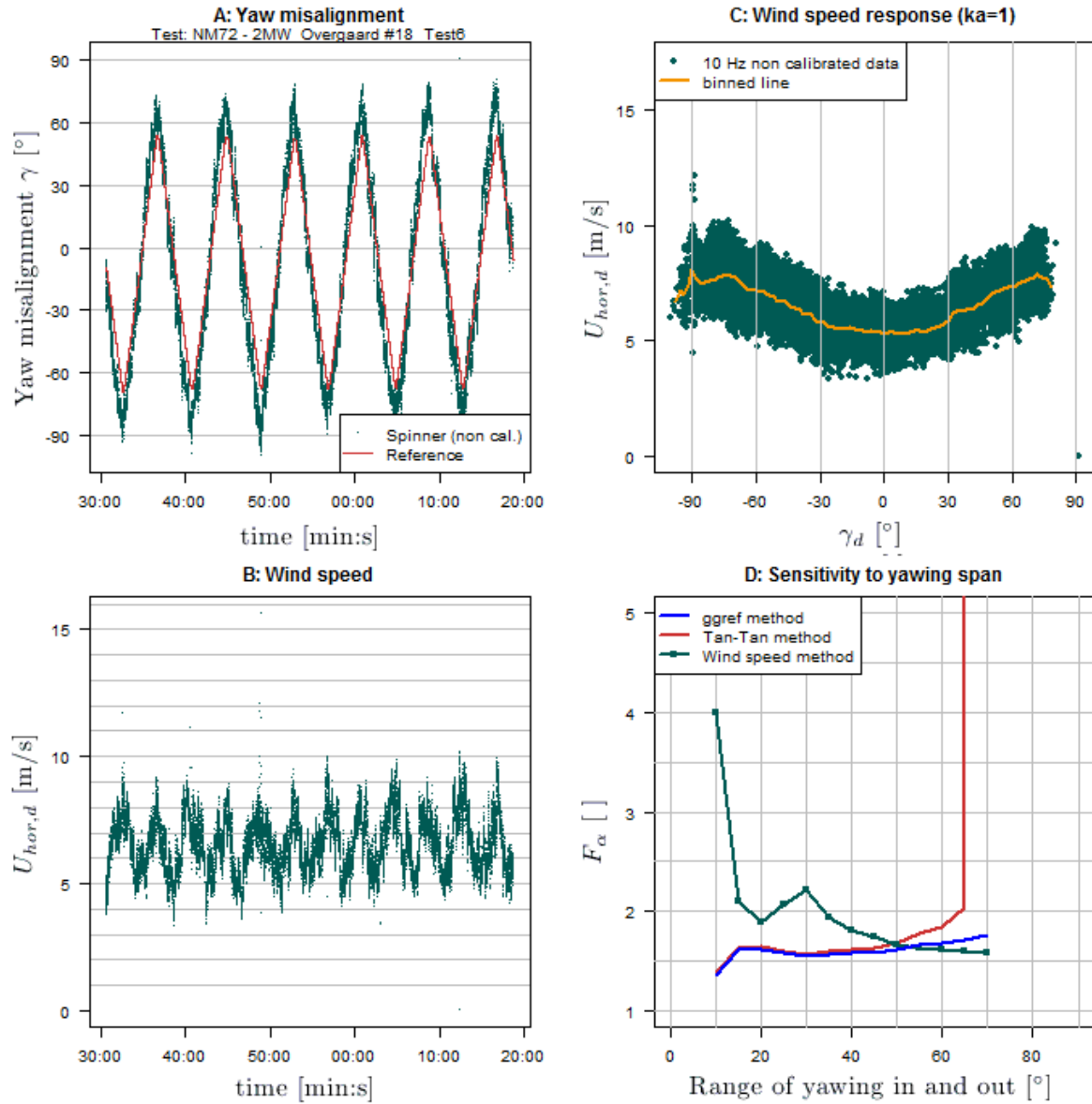


Figure 3. Before calibration, test 6. A: Time series of yaw misalignment as measured by the spinner anemometer and by the yaw position sensor. B: wind speed time series as measured by the spinner anemometer before F1 calibration. C: Wind speed as a function of yaw misalignment both measured by spinner anemometer. D: Calibration correction factor F_α calculated in three different methods, as a function of yawing span ranging from $\pm 10^\circ$ to $\pm 90^\circ$ in steps of $\pm 5^\circ$.

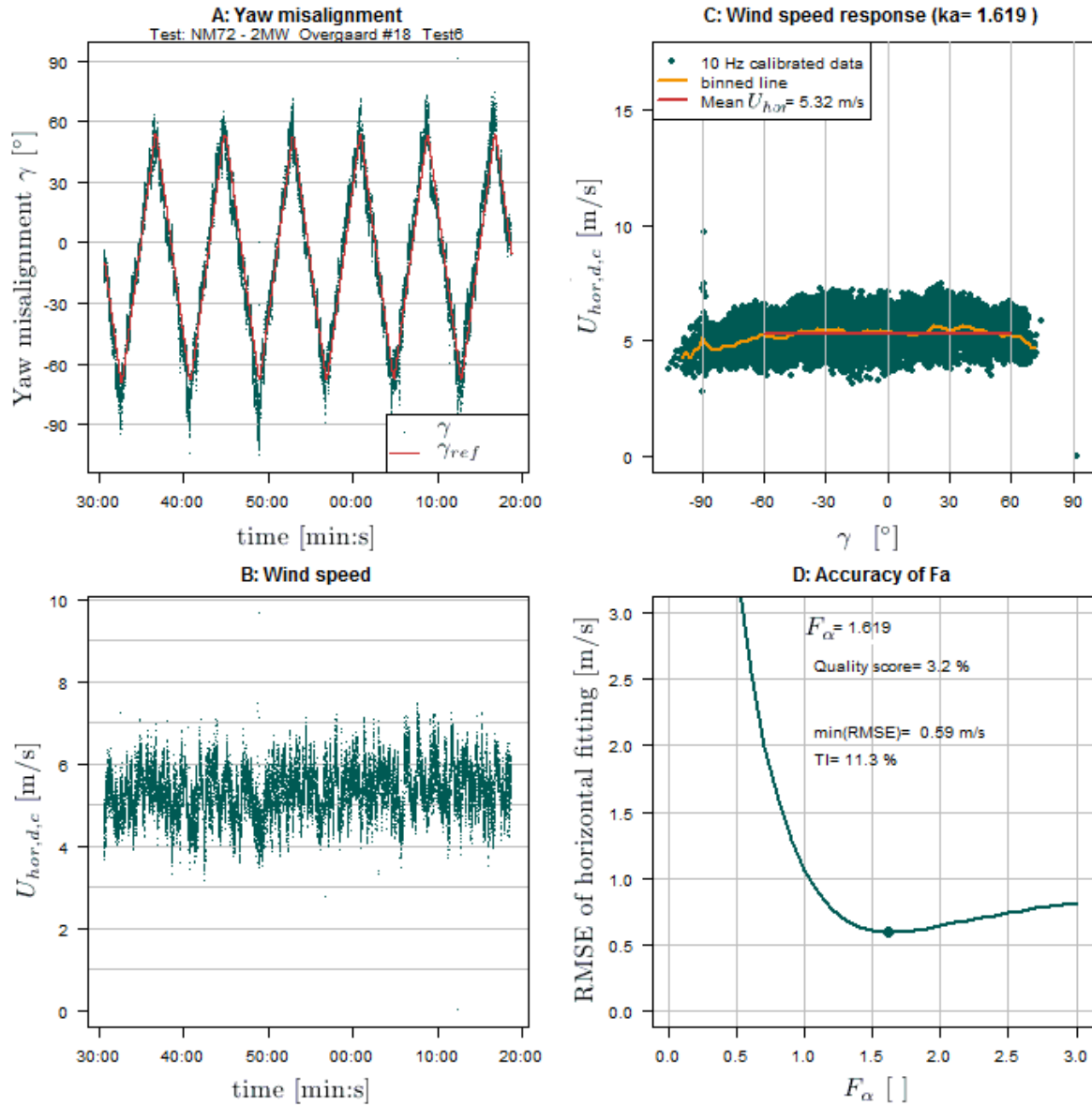


Figure 4. After calibration, test 6. A: Time series of yaw misalignment as measured by the spinner anemometer and by the yaw position sensor. B: wind speed time series as measured by the spinner anemometer before F1 calibration, after F_α calibration. C: Wind speed as a function of yaw misalignment both measured by spinner anemometer and calibrated with F_α . D: Root mean square error of the horizontal fit (red line in sub-figure C) as a function of F_α .

4 Discussion

As seen also in tests performed on other wind turbine models, the GGref and TanTan methods tend to give a higher F_α for increasing yawing span than the WSR method. This is especially true for the TanTan method, because of the tangent function properties, that tend to increase rapidly when approaching 90° angle.

5 As seen in Fig. 3D, the value of F_α is dependent on the chosen width of yawing the turbine in and out of the wind. For the TanTan and GGref methods, Pedersen and Demurtas (2014) suggested to limit the span to $\pm 45^\circ$. The value of F_α calculated with the WSR method tends to stabilize and be comparable with the previous two methods for a yawing span within 50° and 70° .

10 Above a certain large inflow angle (depending on the spinner shape) the air flow would separate from the spinner surface with the consequence of the downwind sensor measuring in a separated flow region. In this condition the spinner anemometer cannot measure correctly, since the relation between the sensor path velocities does not follow the spinner anemometer mathematical model (Eq. 1 to 3).

The F_α value calculated for yawing span of $\pm 60^\circ$ was 1.619. This value was used to calibrate the measurements, which are show in Fig. 4A, B and C. In Fig. 4C, the red line shows the mean wind speed for the measurements where the yawing span is 15 in the range $\pm 60^\circ$. Figure 4D shows how the RMSE varies as a function of F_α , and the optimum F_α with a dot at the minimum RMSE.

20 The method is based on the assumption of a constant wind speed. When applying the method to a spinner anemometer exposed to natural wind the wind speed will naturally vary in the time frame of about one hour needed to complete the six yawing cycles (Fig. 3A). The wind speed variations are clearly visible in the wide scatter of Fig. 3C, which are averaged when calculating the RMSE (Eq. 19). The turbulence reduces the repeatability of the result (F_α) since it introduces some randomness in the measurements. The result can be improved by a large number of tests or by using a stable wind source. A worst case is that the increase (and decrease) of wind speed is synchronized with the yaw position of the turbine, which is basically impossible to happen when the turbine is yawed several times.

5 Sensitivity analysis

25 The calibration test was performed several times on the exact same turbine. The rotor was stopped with one blade pointing downwards (so called bunny position) and the nacelle was yawed six times for each test, of $\pm 90^\circ$ (test 7 to 10) or $\pm 60^\circ$ (test 1 to 6) by operating manually from the turbine control panel. The yaw moves with a speed of about $0.5^\circ/\text{s}$, therefore one test of six sweeps takes approximately one hour. Tests 7 to 10 were made in the same day one after the other for the exact same rotor position. The WSR method was used to calculate F_α for each test and several yawing span (Fig. 6) also reported in Tab. 1 for 30 the case of $\pm 60^\circ$ yawing span. Test 3 and 5 faced some data acquisition problems and were discarded.

Regarding the ability of the method to give reproducible results, the variation of F_α for tests 7 to 10 are within $\pm 2.7\%$ of the mean value 1.52. Since the rotor position is the same for the four tests, the only ascribable responsible for the variations is the wind turbulence. The 8 results are within $\pm 8.5\%$ of the mean value 1.59. It seems that the F_α value relative to the first 4

tests (about 1.67) is higher than the last for tests (1.50), which could be due to a different rotor position which plays a role if the rotational symmetry of the spinner and sensor mounting positions are not accurate. The accuracy of the mounting position of the sonic sensors on this spinner was not investigated.

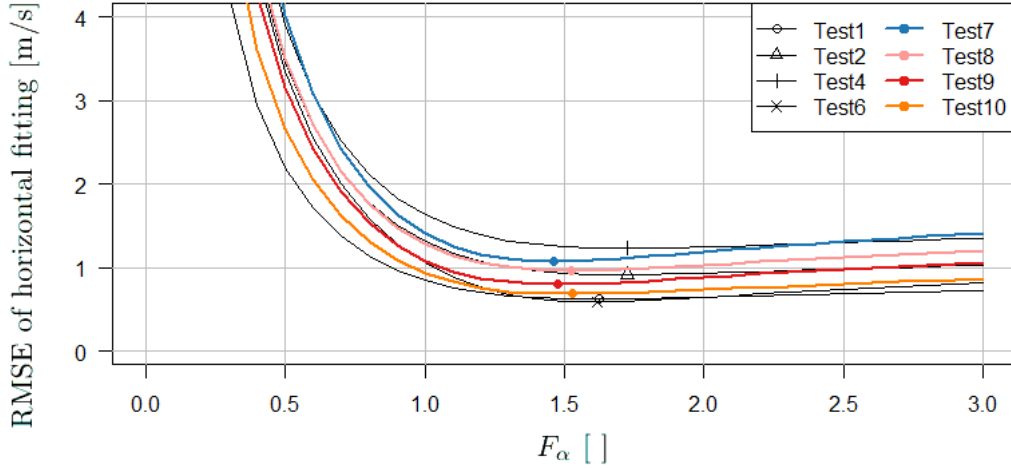


Figure 5. Root mean square error as a function of F_α . Markers locate the minimum value of RMSE and the corresponding F_α value. Colour bold lines are tests performed for the exact same rotor position.

Table 1. F_α values for eight calibration tests made on the same wind turbine. Tests 7 to 10 were made with exact same rotor position relative to a wind turbine yawing span of $\pm 60^\circ$.

Test	1	2	4	6	7	8	9	10
F_α value	1.63	1.72	1.73	1.62	1.46	1.53	1.48	1.53

6 Goodness of a calibration and benchmark on 17 wind turbine models

- 5 The variations encountered in the estimation of F_α call for the definition of a variable to judge the quality of the calibration. One indicator could be related to the shape of the curves of Fig. 5. The more flat and shallow minimum, the larger uncertainty on F_α . The indicator was named quality score (QSC, see Eq. 20), calculated as the slope to the left of the minimum point.

$$QSC = \frac{RMSE(F_\alpha - 0.1) - RMSE(F_\alpha)}{0.1} \quad (20)$$

Figure 7 shows QSC as a function of the span of yawing.

- 10 What minimum quality score should a test have to give meaningful F_α ? To answer this question, the wind speed response method was applied to a database of yawing tests consisting of 29 calibration tests made on 17 turbine models. Results are shown in Fig. 8 and Fig. 9.

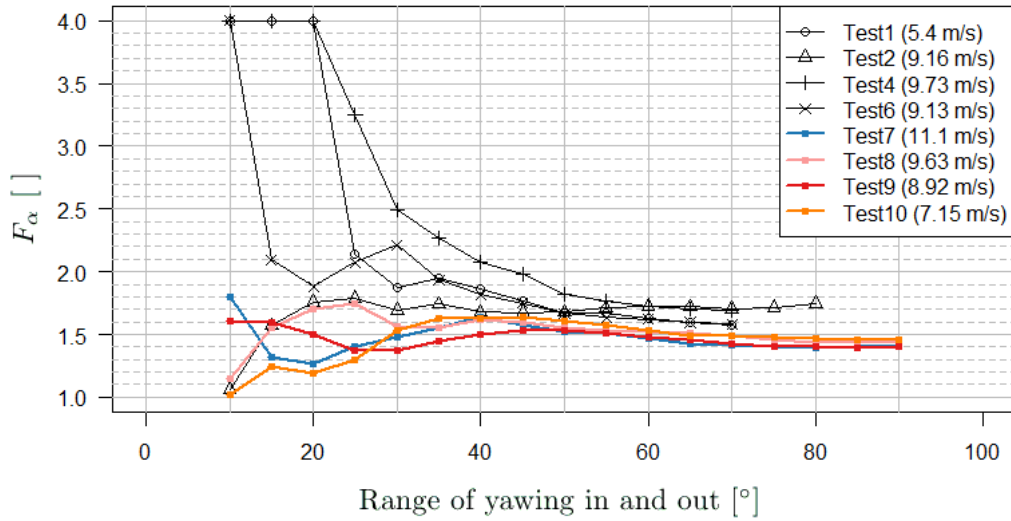


Figure 6. Sensitivity of the F_α to the yawing span. Colour bold lines are tests performed for the exact same rotor position. For test 2 the wind turbine was yawed of $\pm 60^\circ$ but an initial offset of the turbine with respect to the wind direction and a wind direction change during the test determined measurements up to 80° . The values in the legend shows the mean wind speed during the test.

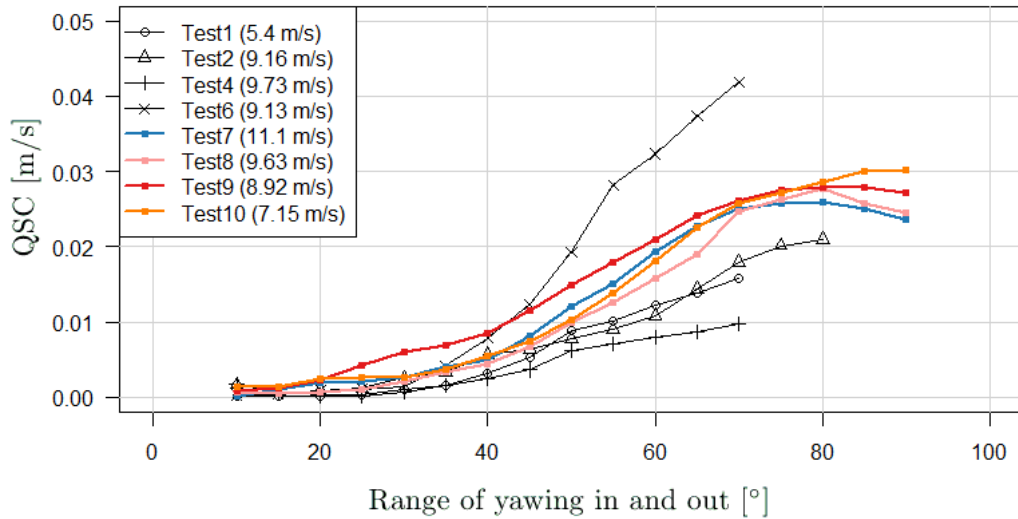


Figure 7. The quality score (QSC) is a measure of how much the RMSE as a function of F_α peaks at the minimum. A wide yawing span gives a more clear peak. The values in the legend shows the mean wind speed during the test.

Figure 8 can help to identify which conditions of wind speed and turbulence leads to a more precise estimate of F_α , which means a more steep $RMSE(F_\alpha)$ curve, or in other words a high QSC. Average wind speed and turbulence intensity were calculated from the measurements calibrated with F_α , for a range of yaw misalignments included in the interval -30° to 30° .

This is to ensure that there is not flow separation from the spinner surface and therefore ensure the spinner anemometer model validity (the spinner anemometer model is expressed by Eq. 1, Eq. 2 and Eq. 3). Figure 8 shows an inverse relation between the quality score and the turbulence intensity of the wind speed as measured by the spinner anemometer during the yawing test.

5 Figure 8 shows that the QSC increases with the wind speed U_{hor} .

The most pronounced correlation in Fig. 8 is between QSC and TI, where the QSC is increasing for decreasing turbulence intensity. This suggests that the ideal condition to perform the test is at low turbulence. The initial statement (in Sec. 2) that the wind speed turbulence would reduce the accuracy of the method is also confirmed by a QSC that reduces as the TI increases.

A condition of low turbulent wind can practically be found by night, when the atmosphere is stable, in a side that is flat with low roughness. It seems also that the QSC increases for increasing U_{hor} , however the scatter of QSC also increases and there are several points with a low QSC despite the high wind speed. This means that to achieve a high QSC it is more important a low TI than a high wind speed.

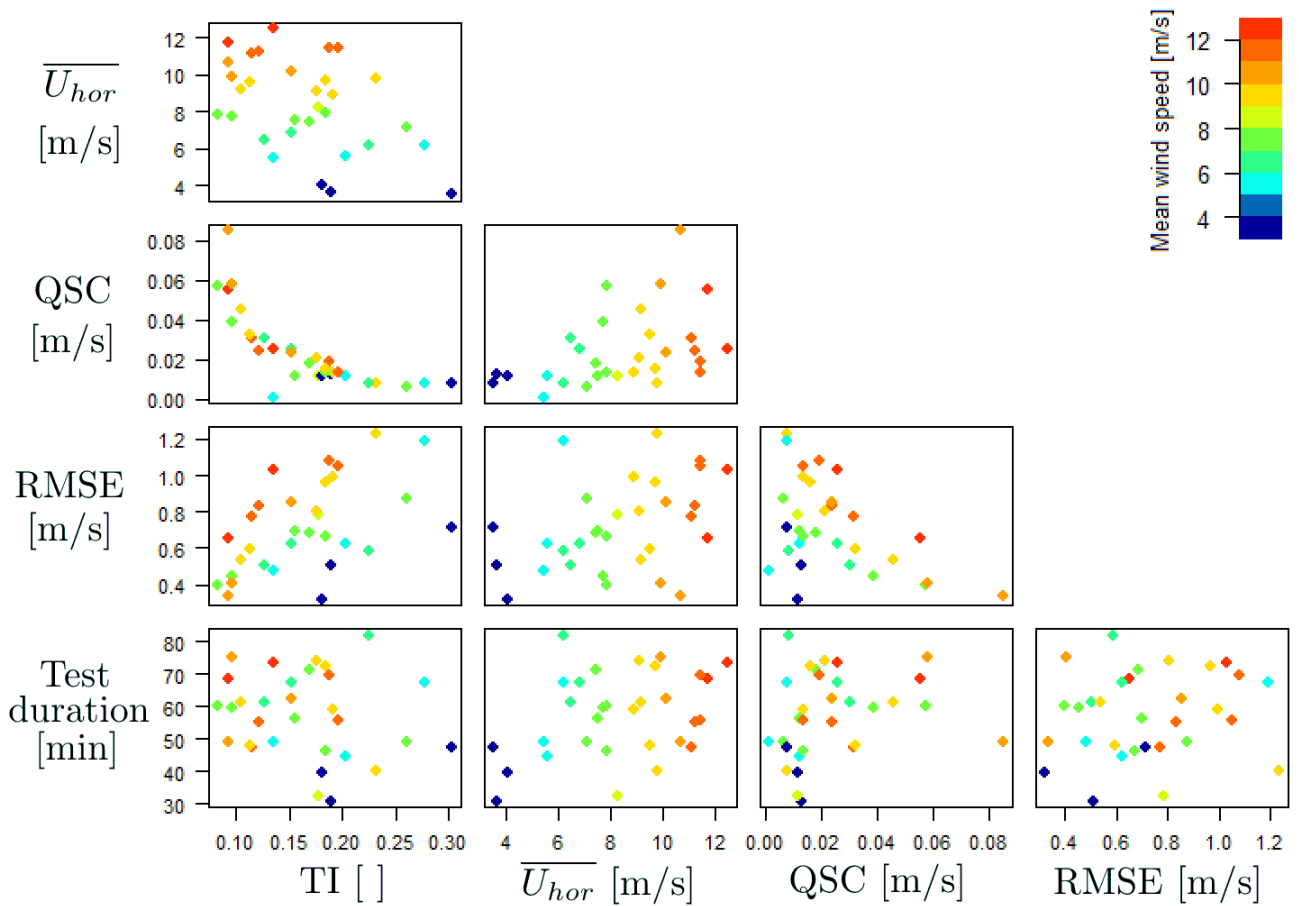


Figure 8. Application of the method to a large database of wind turbines. Colour coded with the mean wind speed.

7 Comparison with previous methods

The F_α was calculated with the three methods GGref, TanTan, and WSR for a range of yawing (γ_{ref}) of $\pm 45^\circ$, $\pm 45^\circ$ and $\pm 60^\circ$, respectively. Figure 9 shows a comparison of F_α values for 29 tests made on 17 wind turbine models. All the spinner anemometer were initially set with the same default calibration values ($k_{1,d} = 1$, $k_{2,d} = 1$) therefore it is possible to compare directly the F_α values. Most of the turbines present a F_α between 1 and 2, values which are attributable to a pointed spinner shape (like a Vestas V52) or a rounded spinner (like a Neg-Micon NM80). The four tests with F_α between 2.5 and 3.5 belong to a flat spinner like the one of a Siemens SWT-6.0-154.

The two methods which agrees the most are the GGref and the TanTan methods. This good agreement however does not implies that the F_α estimate is accurate, but rather that the two methods are similar (in fact they are both based on a linear fitting of the measurements, as described in Sec. 1.1).

The value of F_α calculated with the WSR method shows a lower level of agreement with the other two methods, being it based on a completely different principle.

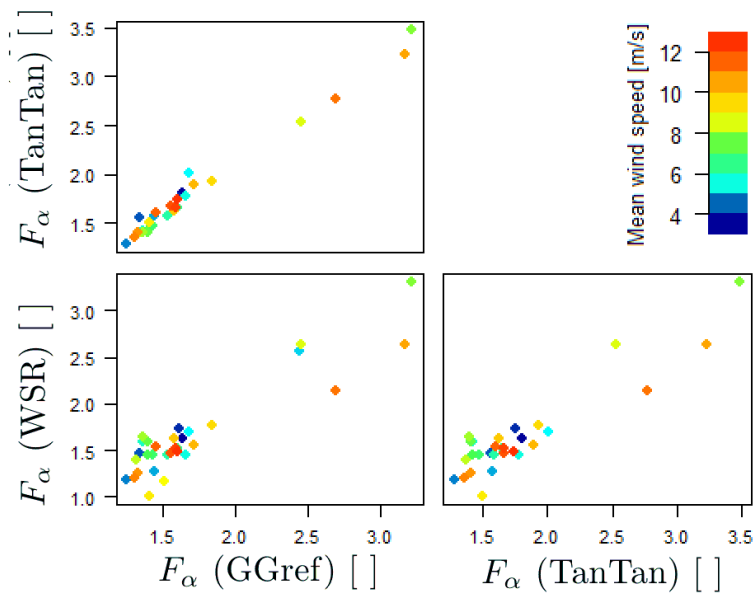


Figure 9. F_α calculated with three methods over a large database of wind turbines. Colour coded with the mean wind speed.

8 Conclusions

The article presented a new method to calibrate spinner anemometer flow angle measurements (yaw misalignment). The advantage of the method is that it does not need the yaw position of the nacelle to be measured.

5 The robustness of the method was investigated by repeating the calibration test on the same turbine several times, with the rotor locked in the exact same rotor position to avoid sensor mounting deviations to play a role. The F_α values found for 4 tests for the exact same rotor position were within $\pm 2.7\%$ of the mean value.

The quality score parameter (QSC) was introduced to quantify goodness of the F_α estimate. The QSC was found inversely dependent on the turbulence intensity. To have a sharp estimate of F_α it is therefore better to perform the test in low turbulence
10 wind conditions. The relation found between the QSC and the width of yawing suggests to yaw the turbine further than $\pm 60^\circ$, up to $\pm 80^\circ$ (this values might be different for other spinner shapes). Another issue to consider is that the test could start with an offset, and end up being -90° to 70° instead of -80° to 80° . This is easily avoidable yawing the wind turbine a bit further than the desired yawing span.

The sensitivity of the method to the width of yawing the turbine in and out of the wind was investigated by applying the
15 calibration method to a subset of the original database. The subset was obtained filtering for $\gamma_{ref} \in [-s, s]$, where s was the span ranging from 10° to 90° in steps of 5° . Significant variations of the F_α value were found for yawing span s below approximately 60° .

The F_α calculated with the wind speed response method was compared with the F_α calculated with previous methods
(GGref, TanTan) using 29 calibration tests performed by Romo Wind A/S on 17 wind turbine models. The sensitivity to span
20 of yawing showed that the WSR method tends to stabilize to same values as GGref for yawing span larger than approximately 50° . Both the GGref and TanTan methods gave similar values up to $\pm 40^\circ$, then the TanTan method gave higher F_α and diverged for a yawing span larger than 70° .

A recommended yawing span to use to calculate F_α seems to be $\pm 60^\circ$ for the WSR method and $\pm 40^\circ$ for the TanTan and
GGref methods, however the turbine shall be yawed further than this angle ($\pm 90^\circ$ recommended) to compensate for initial
25 offset error in the yaw position and wind speed direction change during the test.

It is best to perform the test at the lowest possible turbulence intensity, which might be found in stable atmospheric condition (typically by night) in a flat site with low roughness.

It is recommended to verify the variation of F_α as a function of span of yawing (using the calibrated yaw misalignment if the yaw sensor is not available), since substantially different spinner shapes might give a stable F_α at different yawing span.

Acknowledgements. Romo wind A/S for financing one third of the PhD project this article is part of.

References

Brent, R. and N.J., E. C.: Algorithms for Minimization without Derivatives., Prentice-Hall, 1973.

Demurtas, G., Pedersen, T. F., and Zahle, F.: Calibration of a spinner anemometer for wind speed measurements, Wind Energy, 2016.

- 5 Pedersen, T., Madsen, H., M, R., Courtney, M., S, N., Enevoldsen, P., and Egedal, P.: Spinner Anemometry - An Innovative Wind Measurement Concept, 2007.

Pedersen, T. F. and Demurtas, G.: Calibration of a spinner anemometer for flow angle measurements, Wind Energy, 2014.

Chapter 4

Calibration for wind speed measurements

What has been presented in chapter 2 and 3 closes the topic of the calibration for flow inclination and yaw misalignment measurements. This chapter will address the topic of calibration for wind speed measurements.

The calibration of a wind sensor to be used for power performance measurements is always needed to ensure traceability to reference wind speed sensors such as the Pitot tube of a wind tunnel. The large size of a spinner anemometer does not allow to place it directly into a wind tunnel, therefore each sonic sensor is first calibrated in the wind tunnel in order to measure the wind speed correctly at the sonic sensor positions, and then (once mounted on the spinner) internally calibrated and k_α calibrated [14, 15]. It is then calibrated with k_1 as described in this chapter. k_1 is calibrated as the ratio between spinner anemometer horizontal wind speed and met-mast wind speed in a zero induction condition.

When the turbine is in operation the calibrated spinner anemometer wind speed will be corrected again to the free wind speed by the NTF (Nacelle Transfer Function) to compensate for the rotor induction.

One could in principle neglect the calibration of the k_1 constant and correct everything (spinner shape, sensor mounting position and rotor induction) with the NTF alone, but there were found good reasons to keep the two corrections independent. The following article explains why.

RESEARCH ARTICLE

Calibration of a spinner anemometer for wind speed measurements

Giorgio Demurtas, Troels Friis Pedersen and Frederik Zahle

Technical University of Denmark, Frederiksborgvej 399, PO Box 49, 4000 Roskilde, Denmark

ABSTRACT

The power curve of a wind turbine can be measured, according to IEC 61400-12-2 with a nacelle-mounted anemometer. Typically, a sonic anemometer or a cup anemometer and a wind vane are mounted on the back of the nacelle roof. Another option is to use a spinner anemometer.

The measurement principle of the spinner anemometer is based on the flow distortion caused by the wind turbine spinner. The flow on the spinner surface is measured by means of three 1D sonic sensors mounted on the spinner and a conversion algorithm to convert the wind velocity components measured by the three sonic sensors to horizontal wind speed, yaw misalignment and flow inclination angle. The algorithm utilizes two calibration constants that are specific to the spinner shape, blade root design and to the mounting positions of the sonic sensors on the spinner.

The present analysis describes methods to determine the calibration constant related to wind speed measurements. The first and preferred method is based on the definition of the calibration constant and uses wind speed measurements during the stopped condition of the wind turbine. Two alternative methods that did not require the turbine to be stopped were investigated: one used relatively high wind speed measurements during normal operation of the wind turbine, while the other one used a CFD simulation of the flow over the spinner. The method that entails stopping the turbine in good wind conditions showed the best results and is recommended. The evaluation of uncertainty was not included in the present analysis. Copyright © 2016 The Authors Wind Energy Published by John Wiley & Sons Ltd.

KEYWORDS

anemometer; spinner anemometer; spinner anemometer calibration; iSpin; nacelle anemometry; calibration; wind speed

Correspondence

Giorgio Demurtas, Technical University of Denmark, Frederiksborgvej 399, 4000 Roskilde, Denmark.

E-mail: giod@dtu.dk

This is an open access article under the terms of the Creative Commons Attribution License, which permits use, distribution and reproduction in any medium, provided the original work is properly cited.

Received 15 April 2015; Revised 10 December 2015; Accepted 22 December 2015

LIST OF SYMBOLS

- V_1 velocity component of the wind speed along sensor path 1
- V_2 velocity component of the wind speed along sensor path 2
- V_3 velocity component of the wind speed along sensor path 3
- V_{ave} average of V_1 , V_2 , V_3
- U_d wind speed vector modulus measured by the spinner anemometer prior to calibration
- U wind speed vector modulus at the spinner anemometer (reference value to calibrate U_d , equal to the free wind speed vector modulus in stopped conditions or conditions of null rotor induction)
- U_{hor} horizontal wind speed component measured with the spinner anemometer (calibrated value)
- $U_{hor,d}$ horizontal wind speed component measured with the spinner anemometer (non-calibrated value)
- $U_{hor,d,c}$ horizontal wind speed component measured with the spinner anemometer (corrected with F_α but not F_1)
- U_α wind velocity component in the plane perpendicular to the shaft axis x_s
- U_x wind velocity component along x
- U_y wind velocity component along y
- U_z wind velocity component along z

- $U_{x,n}$ wind velocity component along x_n
 $U_{y,n}$ wind velocity component along y_n
 $U_{z,n}$ vertical wind velocity component, along z_n
 $U_{x,s}$ wind velocity component along x_s
 $U_{y,s}$ wind velocity component along y_s
 $U_{z,s}$ wind velocity component along z_s
 δ shaft tilt angle
 β flow inclination angle (positive when upwards)
 γ yaw misalignment
 α inflow angle with respect to the shaft axis
 α_d inflow angle with respect to the shaft axis measured by the spinner anemometer prior to calibration
 ϕ rotor position (equal to zero when sonic sensor one is at top position, positive clockwise)
 θ azimuth position of flow stagnation point on spinner (relative to sonic sensor 1)
 θ_{yaw} yaw direction referred to geographical coordinate system
 θ_{dir} wind direction referred to geographical coordinate system
 k_1 calibration constant mainly related to wind speed calibration
 k_α calibration constant related to angle calibration
 k_2 calibration constant mainly related to angle calibration (equal to $k_\alpha \cdot k_1$)
 F_1 calibration correction factor mainly related to wind speed calibration
 F_α calibration correction factor related to angle calibration
 F_2 calibration correction factor mainly related to angle calibration (equal to $F_\alpha \cdot F_1$)
 σ standard deviation
 N number of measurements
 I rotor induction, calculated as $I = (U_{mm} - U_{hor})/U_{mm}$
 U_{mm} horizontal wind speed component (free wind speed measured with the met-mast)
 U_{free} horizontal wind speed component measured with the spinner anemometer and corrected with the nacelle transfer function to free wind speed
 $U_{N,i}$ nacelle wind speed average value in bin i of the nacelle transfer function
 $U_{F,i}$ free wind speed average value in bin i of the nacelle transfer function

LIST OF ABBREVIATIONS

- s.a. spinner anemometer
 NTF nacelle transfer function
 IEC International Electrotechnical Commission
 CFD Computational Fluid Dynamics

1. INTRODUCTION

The spinner anemometer¹ can be used to measure the inflow wind speed to a wind turbine and to measure its power performance. For this last purpose, spinner anemometers need to be calibrated similarly to nacelle cup anemometers. Previous research^{2,3} described problems related to cup anemometers and wind vanes, or 2D sonic anemometers, mounted on top of the nacelle. The flow distortion caused by the blade roots and nacelle affects even state-of-the-art nacelle anemometry instruments. This flow distortion is normally corrected for in the wind turbine control system. However, corrections in the controller might not take all situations into account, for example, when the wake swirl from upstream wind turbines introduces upwards and downwards flow on the nacelle.⁴ Such corrections are not required for a spinner anemometer, which is not affected by blade wakes since it measures the wind upstream of the rotor (Figure 1). The measurement principle used by the spinner anemometer is actually based on the flow distortion created by the spinner. Because of the size of a modern wind turbine spinner and imperfections of the spinner shape, such as poor rotational symmetry, it is challenging to mount the sensors equally distant from the spinner center and spaced 120°. These challenges in the spinner anemometer mounting could be easily solved in the future by integrating the sensor mounting holes in the spinner mold and by improving the spinner quality control during manufacture of the spinner.

The calibration of a spinner anemometer accounts for the shape of the spinner, mounting position of the sonic sensors and characteristics of the sensors, while the rotor induction is accounted for with the nacelle transfer function (NTF) as defined in IEC 61400-12-2.⁶ It is important to keep the wind speed calibration separate from the NTF, so that changes due to the spinner anemometer (mounting position of the sonic sensors, spinner geometry) can be accounted for with a new calibration only, whereas changes in the wind turbine control system or blades can be accounted with a new NTF only.

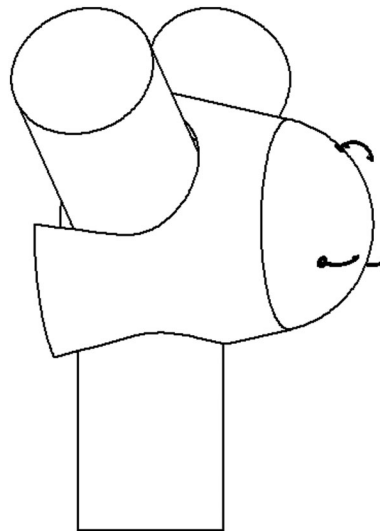


Figure 1. A drawing showing a spinner anemometer with three sonic sensors.⁵

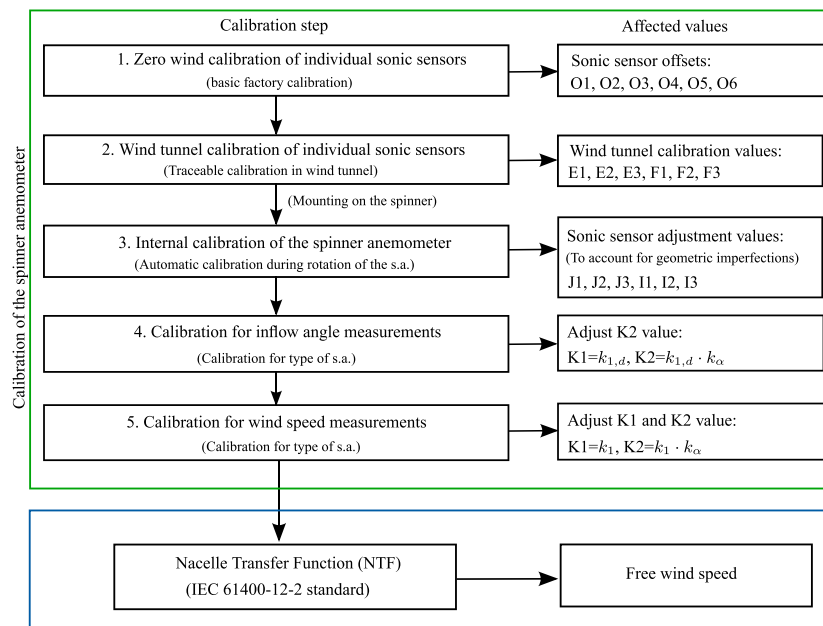


Figure 2. Overview of the sequence of steps necessary to calibrate a spinner anemometer (from the work of Demurtas and Pedersen⁷). Elements enclosed in the green contour are related to the calibration, while those in the blue box refer to the nacelle transfer function needed to calculate the free wind speed as described in the IEC standard.⁶ The boxes on the right side within the green box specify which parameters of the spinner anemometer needed to be updated.

This separation between calibration of the spinner anemometer and the NTF of the wind turbine allows for direct use of the calibration values k_1 and k_2 determined on one turbine for several other turbines with the same spinner shape, verifying the sensors mounting positions with photos and estimating an additional uncertainty associated with the mounting position. The NTF determined on the first turbine can then be used on all other turbines to measure the power curve according to IEC 61400-12-2,⁶ as long as the induction at the center of the rotor can be assumed unchanged.

The calibration of the spinner anemometer requires five steps (Figure 2). Depending on the intended use of the spinner anemometer, it is not required to execute all the steps. See Table I for clarification of which steps are required depending on the intended use of the spinner anemometer.

Table I. Indication of which calibration steps should be performed depending on the intended use of the spinner anemometer.

Calibration steps 1 to 5	Wind speed for power performance measurement according to IEC 61400-12-2	Wind speed for operation of the wind turbine	Yaw misalignment for operation of the wind turbine.
1) Zero wind calibration	Required	Required	Required
2) Wind tunnel calibration	Required		
3) Internal calibration	Required ^a	Required ^a	Required ^a
4) Calibration for inflow angle measurement	Required	Required	Required
5) Calibration for wind speed measurements	Required	Required	
Nacelle Transfer Function (NTF)	Required		

^aOnly required to average out spinner and sonic sensor installation imperfections over a full rotation. For 10 min. average measurements, this calibration has no effect, while it has an effect on turbulence measurements and non-averaged measurements.

The zero wind calibration is executed by the manufacturer (Figure 2). If power performance measurements are performed according to IEC 61400-12-2,⁶ the sonic sensors must be individually calibrated in a wind tunnel. The internal calibration (Figure 2) is an automatic calibration made during normal operation of the wind turbine soon after the installation of the spinner anemometer. The calibration for inflow angle measurements is then made at a stand still.⁵ A practical guide⁷ describes in more detail the execution of each calibration step.

The present article describes the calibration for wind speed measurements (fifth step in Figure 2) and gives a demonstration of the use of the NTF to calculate the free wind starting from spinner anemometer measurements. The ability to calculate the free wind based on spinner anemometer measurements is useful for power performance measurements. The correlation between wind turbine power and wind speed was found to be higher for the spinner anemometer than for a nacelle roof anemometer or a met-mast. This allows to reduce the averaging time (which is typically 10 min). The Fast-wind Project report⁸ found that a power curve made with 2 min averaging time was very close to the one made with 10 min averages and was ranging up to a much higher wind speed.

For calibration purposes, the horizontal wind speed $U_{hor,d}$ measured by the (non-calibrated) spinner anemometer is related to a met-mast hub-height wind speed measurement U_{mm} by means of the default $k_{1,d}$ constant.

The relationship between $U_{hor,d}$ and U_{mm} is linear as long as the angular measurements are calibrated with the correct k_{α} (fourth step in Figure 2).⁵ For this reason, it is best to set the calibration value for inflow angle measurements in the spinner anemometer conversion box before the wind speed calibration is performed.

The experimental setup used for the present article is a Nordtank 500 kW wind turbine located at DTU Risø campus, Denmark, and a met-mast with hub height measurements of wind speed and wind direction.

The next two sections describe the coordinate system and the conversion algorithm (see the literature⁵ for a detailed explanation of the conversion algorithm).

2. COORDINATE SYSTEM

The coordinate systems for transforming the spinner anemometer parameters are shown in Figure 3. The inflow angle α , which is not shown, is the angle between the shaft axis and the vector of the inflow wind speed U . The yaw misalignment γ is defined as $\gamma = \theta_{dir} - \theta_{yaw}$.

3. OVERVIEW OF THE SPINNER ANEMOMETER CONVERSION ALGORITHM

A detailed description of the conversion algorithm is given in the literature.⁵ Here, we show the equations in the order they are used in the conversion. The measurement principle of the spinner anemometer is based on the flow over the spinner, which is measured close to the spinner surface with three wind velocity sensors. One dimensional sonic sensors are used typically with a sensor path placed approximately 10 cm above the spinner surface. Accelerometers integrated in the sonic sensors are used to calculate the rotor position.

The fundamental mathematical model (equations 1, 2 and 3) assumes that the flow is uniform in a section upstream of the spinner in a circle of 0.5 m in diameter and that the wind velocity component measured by the sensors (V_1 , V_2 and V_3) are sinusoidal as a function of the position θ of the flow stagnation point for a constant inflow wind speed U .

$$V_1 = U (k_1 \cos \alpha - k_2 \sin \alpha \cos \theta), \quad (1)$$

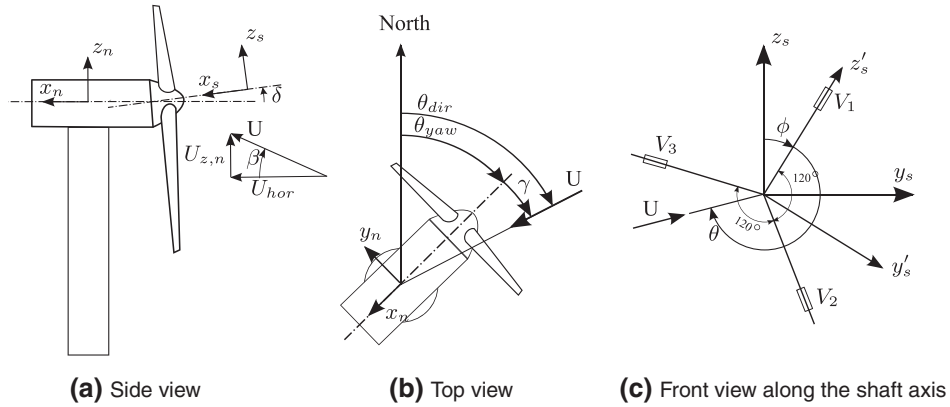


Figure 3. Coordinate systems and definition of angles: rotating spinner coordinate system (x'_s, y'_s and z'_s), non-rotating shaft coordinate system (x_s, y_s and z_s), fixed nacelle coordinate system (x_n, y_n and z_n), yaw direction yaw , yaw error γ , flow inclination angle β , tilt angle δ , azimuth position of flow stagnation point on spinner θ (relative to sonic sensor 1) and rotor azimuth position ϕ (position of sonic sensor 1 relative to vertical).

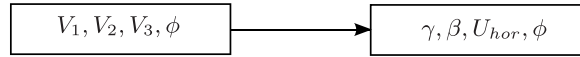


Figure 4. Direct transformation from sonic sensor wind speeds to spinner anemometer parameters.

$$V_2 = U \left(k_1 \cos \alpha - k_2 \sin \alpha \cos \left(\theta - \frac{2\pi}{3} \right) \right), \quad (2)$$

$$V_3 = U \left(k_1 \cos \alpha - k_2 \sin \alpha \cos \left(\theta - \frac{4\pi}{3} \right) \right). \quad (3)$$

The spinner anemometer conversion algorithm transforms the sonic sensor wind velocity components V_1 , V_2 and V_3 and the rotor azimuth position ϕ measurements into the spinner anemometer output parameters: horizontal wind speed U_{hor} , yaw misalignment γ and flow inclination angle β . This transformation (Section 3.1 and Figure 4) is called direct transformation and runs inside the spinner anemometer conversion box.

The inverse transformation (Section 3.2) transforms the output of the spinner anemometer into the input values V_1 , V_2 and V_3 . This is needed to post-calibrate measurements that were acquired with certain (default) calibration constant to new calibration constants, as described in Section 3.3.

3.1. Direct transformation

The mathematical expressions of the conversion algorithm implemented in the spinner anemometer are as follows:

$$\alpha = \arctan \left(\frac{k_1 \sqrt{3(V_1 - V_{ave})^2 + (V_2 - V_3)^2}}{\sqrt{3}k_2 V_{ave}} \right) \quad (4)$$

$$V_{ave} = \frac{1}{3}(V_1 + V_2 + V_3) \quad (5)$$

$$U = \frac{V_{ave}}{k_1 \cos \alpha} \quad (6)$$

$$V_1 < V_{ave} : \theta = \arctan \frac{(V_2 - V_3)}{\sqrt{3}(V_1 - V_{ave})} \quad (7)$$

$$V_1 \geq V_{ave} : \theta = \arctan \frac{(V_2 - V_3)}{\sqrt{3}(V_1 - V_{ave})} + \pi \quad (8)$$

$$U_{x,s} = U \cos(\alpha) \quad (9)$$

$$U_{\alpha} = U \sin(\alpha) \quad (10)$$

$$U_{y,s} = -U_{\alpha} \sin(\phi + \theta) \quad (11)$$

$$U_{z,s} = -U_{\alpha} \cos(\phi + \theta) \quad (12)$$

$$U_x = U_{x,s} \cos(\delta) + U_{z,s} \sin(\delta) \quad (13)$$

$$U_y = U_{y,s} \quad (14)$$

$$U_z = U_{z,s} \cos(\delta) - U_{x,s} \sin(\delta) \quad (15)$$

$$U_{hor} = \sqrt{U_x^2 + U_y^2} \quad (16)$$

$$\gamma = \arctan\left(\frac{U_y}{U_x}\right) \quad (17)$$

$$\beta = \arctan\left(\frac{U_z}{U_{hor}}\right) \quad (18)$$

3.2. Inverse transformation

The mathematical expressions of the inverse transformation are as follows:

$$U_x = U_{hor} \cos(\gamma) \quad (19)$$

$$U_y = U_{hor} \sin(\gamma) \quad (20)$$

$$U_z = U_{hor} \tan(\beta) \quad (21)$$

$$U_{x,s} = U_x \cos(\delta) - U_z \sin(\delta) \quad (22)$$

$$U_{y,s} = U_y \quad (23)$$

$$U_{z,s} = U_x \sin(\delta) + U_z \cos(\delta) \quad (24)$$

$$U = \sqrt{U_{x,s}^2 + U_{y,s}^2 + U_{z,s}^2} \quad (25)$$

$$U_{\alpha} = \sqrt{U_{y,s}^2 + U_{z,s}^2} \quad (26)$$

$$\alpha = \arctan\left(\frac{U_{\alpha}}{U_{x,s}}\right) \quad (27)$$

$$U_{z,s} > 0 : \theta = \arctan\left(\frac{U_{y,s}}{U_{z,s}}\right) - \phi \quad (28)$$

$$U_{z,s} \leq 0 : \theta = \arctan\left(\frac{U_{y,s}}{U_{z,s}}\right) - \phi + \pi \quad (29)$$

$$V_1 = U(k_1 \cos(\alpha) - k_2 \sin(\alpha) \cos(\theta)) \quad (30)$$

$$V_2 = U\left(k_1 \cos(\alpha) - k_2 \sin(\alpha) \cos\left(\theta - \frac{2\pi}{3}\right)\right) \quad (31)$$

$$V_3 = U\left(k_1 \cos(\alpha) - k_2 \sin(\alpha) \cos\left(\theta - \frac{4\pi}{3}\right)\right) \quad (32)$$

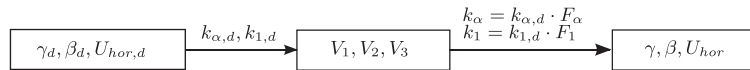


Figure 5. Application of correction factors to measurements taken with default calibration constants.

3.3. Post-calibration of measurements

Knowledge about the conversion algorithm is generally not necessary for the calibration and normal use of a spinner anemometer. It becomes necessary when the user needs to correct measurements taken with a calibration set into the conversion box ($k_{1,d}$, $k_{2,d}$) to different calibration constants (Figure 5). The default calibration values are corrected to the new values by the use of the correction factors

$$F_1 = \frac{k_1}{k_{1,d}}, \quad (33)$$

$$F_2 = \frac{k_2}{k_{2,d}}, \quad (34)$$

which relates default values to the new values.

The calibration for angular measurements (step 4) provides the ratio

$$F_\alpha = \frac{k_\alpha}{k_{\alpha,d}} = \frac{k_2/k_1}{k_{2,d}/k_{1,d}} = \frac{F_2}{F_1}, \quad (35)$$

used to calibrate inflow angle measurements. When F_1 is calculated (step 5) with the method described in this article, the value of F_2 will be adjusted to keep the correct ratio.

4. CALIBRATION METHOD FOR WIND SPEED MEASUREMENTS

The objective of the wind speed calibration is to find a single value of k_1 that makes the spinner anemometer wind speed (U_{hor}) equal to the free wind speed (U_{mm}) in stopped conditions of the wind turbine. U_{hor} represents the wind speed at the rotor center as if the turbine was not present, since it is a value calibrated to the free wind speed. If the calibration for angular measurements has been made and inserted into the conversion box, then the relation U_{mm} to U_{hor} is linear.

Three methods have been developed to calculate the value of the calibration constants—one based on CFD calculations and two based on measurements. When using measurements, the calibration constants are initially set in the spinner anemometer conversion box to default values (for example, $k_{1,d} = 1$ and $k_{2,d} = 1$). Based on measurements taken with default constants, the method gives the correction factor F_1 , which is then used to correct the default calibration constant $k_{1,d}$ to $k_1 = F_1 k_{1,d}$.⁵

It is important to note that U_{hor} is not the wind speed at the spinner. The actual wind speed at the spinner will be lower than U_{hor} at the front part of the spinner, and it will be higher than U_{hor} on the sides of the spinner and between the blades.

U_{hor} is lower than the free wind speed when the turbine is operating because of the rotor induction. To calculate the free wind speed during operation of the wind turbine, the spinner anemometer wind speed U_{hor} must be corrected by the use of the NTF (as defined in the standard IEC 61400-12-2).⁶

The induction is taken into account with the NTF only, and not with k_1 . In other words, k_1 only accounts for the spinner and blade root shapes and mounting positions of the sonic sensors.

Table II explains in the first two rows the calculation steps to go from default to calibrated values, and in the third and last row, how to go from calibrated value to free wind speed. The present article, however, focuses on the calibration of the spinner anemometer k_1 constant.

4.1. Application of k_α calibration

The application of the calibration k_α has little effect on the wind velocity component along the shaft axis, while it has a large influence on the angular measurements, as found in the literature.⁵ Correcting the measurements to the correct value of k_α gives the important simplification that the relationship between the free reference wind speed and the spinner anemometer wind speed becomes linear. It is therefore recommended to set the correct k_α value in the spinner anemometer conversion box as soon as it is known. If not set, measurements have to be post-calibrated with the method explained in Section 3.3 and in the work of Pedersen *et al.*⁵ As explained in the literature,⁵ the post-calibration of averaged measurements will introduce an error.

Table II. Calculation steps to convert default values to calibrated values and finally to free wind speed.

From	Action	To
$U_{hor,d}$	Application of F_{α} (determined in ⁵)	$U_{hor,d,c}$
$U_{hor,d,c}$	Determination and application of F_1 (chapters 5.4, 5.5 and 5.6)	U_{hor}
U_{hor}	Determination and application of the NTF (IEC 61400-12-2) ⁶	$U_{hor,free}$

4.2. Calculation of the calibration correction factor F_1

As derived in the work of Pedersen *et al.*⁵ and summarized in Section 3, the calibration factor F_1 is defined as

$$F_1 = \frac{k_1}{k_{1,d}} = \frac{U_d \cos(\alpha_d)}{U \cos(\alpha)}, \quad (36)$$

where U_d is the magnitude of the wind velocity measured by the non-calibrated spinner anemometer and U is the magnitude of the wind velocity used as a reference for the calibration.

When the measurements of the spinner anemometer have been corrected with F_{α} , we can neglect the cosine ratio, since $\alpha = \alpha_d$ (the value of the measured inflow angle is correct). This is also the case when the correct $k_{\alpha} = k_2/k_1$ was set in the conversion box at the time when the measurements were acquired, or the measurements have been corrected with the procedure schematized in Figure 5.

The calibration test is performed using the natural wind. The reference wind speed U shall be measured at hub height at a distance upstream of the wind turbine according to IEC 61400-12-1.⁹ U can be measured with a 3D sonic anemometer or with a specifically designed cup anemometer that measures the vector wind speed rather than the horizontal velocity component. Most of the cup anemometers available on the market are however designed to measure the horizontal component of U . Therefore, under the assumption that the flow inclination at the spinner is equal to the flow inclination at the met-mast, we can turn equation 36 into

$$F_1 = \frac{U_{hor,d,c}}{U_{mm}}, \quad (37)$$

so that we compare the horizontal components, instead of the modulus of the wind vectors.

5. APPLICATION OF THE CALIBRATION METHOD ON A SPECIFIC WIND TURBINE SPINNER ANEMOMETER

A spinner anemometer was mounted on a Nordtank 500 kW wind turbine located at DTU Risø Campus test site, approximately 6 km north of Roskilde, Denmark. The wind turbine has been used for many years for research and educational purposes and is very well instrumented (see description of the site and of the instrumentation in the work of Paulsen and Wagner¹⁰).

Three methods to calibrate the k_1 constants are presented here: for Method 1 the wind turbine is stopped, for Method 2 the wind turbine is in operation, while Method 3 is based on CFD simulation of the stopped rotor.

According to the definition of k_1 (equal to the ratio between the spinner anemometer horizontal wind speed and the free horizontal wind speed in a condition of zero induction), the correct method to determine k_1 is Method 1, which uses a stopped turbine. The drawback of this method is that it requires the wind turbine to be stopped for several hours in good wind conditions, which is generally not acceptable by the wind turbine owner. Therefore, we investigated the possibility of determining the calibration constant using measurements during operation of the wind turbine (Method 2) and CFD simulation of the stopped turbine (Method 3). The following subsections describe the instrument setup, data selection, as well as present an analysis of the three methods.

5.1. Spinner anemometer mounting evaluation

Figure 6 shows the spinner of the Nordtank turbine and two of its sonic sensors. Figure 6 is an overlay of three photos taken from ground level during rotation of the rotor in a way that each photo shows one of the three sensors when it is clearly visible on the side of the spinner. The sides of the spinner were used as reference to align the photos. Due to the height of the wind turbine, in order to obtain a good resolution of the photo, it was necessary to use a digital camera with a 300 mm zoom optic (12 Megapixel, 18×24 mm CCD sensor). The camera was standing on a tripod at ground level under the spinner, 1.8 m from the tower.

The purpose of the photos was to both determine the absolute position of the sensor paths to define the geometry for the CFD calculations and verify the relative accuracy of the mounting of the sonic sensors. We scaled the photos to a known dimension of the spinner to be able to measure the position of the sensor path.

In Figure 6, the red line drawn in the sonic sensor path (which is 160 mm long) indicates the mean path in which the wind velocity components V_1 , V_2 and V_3 are measured. The CFD results (Section 5.6) were extracted in five points along this line.

The deviations between the three sonic sensors show a variation of about 1.8° in the sonic sensor path angle and about 5 mm in longitudinal direction (Figure 7). For simplicity in the CFD simulation, we considered that all the sensors were mounted in the exact same position. However, this photographic method could be used to determine the uncertainty in the wind speed measurements because of mounting tolerances and spinner geometry imperfections. The impact of such geometric deviations has not been investigated in detail here because the spinner anemometer was internally calibrated (step 3 of the calibration procedure in Figure 2) to compensate for the geometric imperfections. As described in the literature,¹¹ the internal calibration ensures that the three sensors measure the same average wind speed over one rotation.

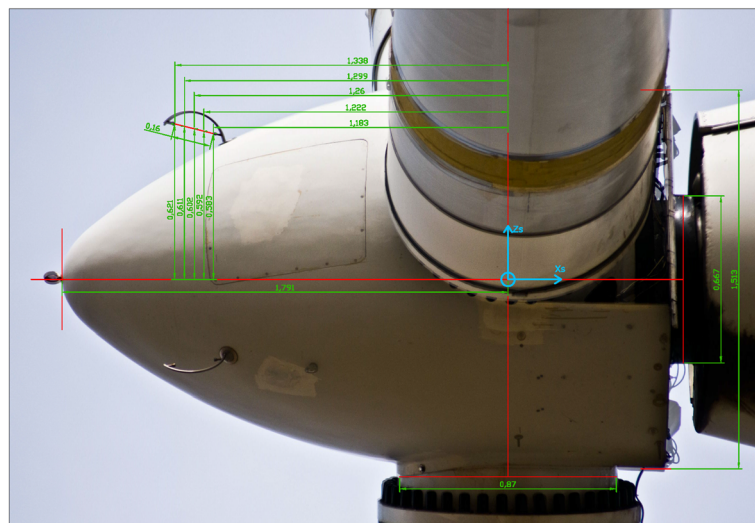


Figure 6. Overlay of three photos of the spinner anemometer mounted on the Nordtank 500 kW wind turbine, which allows a comparison of the position of the three sonic sensors. The short red line in the sensor path indicates the mean sensor path. The green dimensions show the coordinates of the five points along the sensor path used in the CFD simulation. The points of sensor 1 are numbered 1 to 5 going from left to right. Table IV gives the coordinate values of each point.



Figure 7. Zoomed in view of the overlay of Figure 6 to highlight the relative position of the three sonic sensors.

Table III. Calculation steps to convert default values to calibrated values and finally to free wind speed.

Period	Turbine condition	Date span	10 min averages	Calibration set in the conversion box
A	Operation	7/12/2012–01/02/2013	525	$k_1 = 1, k_2 = 1$
B	Operation	24/05/2014–30/06/2014	883	$k_1 = 0.703, k_2 = 0.500$
C	Stopped	01/01/2013–23/05/2014	353	$k_1 = 1, k_2 = 1$

5.2. Free wind measurement

The met-mast was positioned at 2.5 rotor diameters in a westerly direction with respect to the wind turbine (283°). The measurement of wind speeds at hub height was used to calibrate the spinner anemometer wind speed measurements. The reference instrument was a cup anemometer mounted on a boom perpendicular to the main wind direction, calibrated in a MEASNET compliant wind tunnel.

The wind direction was measured with a 3D sonic anemometer placed on a second boom 2 m below the cup anemometer, which was not calibrated for wind speed measurements. The valid wind direction sector was $283^\circ \pm 45^\circ$ (238° to 328°). Temperature was measured at the met-mast at hub-height.

5.3. Data selection

The measurement system was active on the wind turbine and met-mast since January 2012. Useful measurements for the present analysis were found in three different measurement periods, A, B and C (Table III). Periods A and B were filtered for measurements during operation of the wind turbine, while period C for measurements during stopped condition due to various reasons.

The selection of the measurement periods were made to present broad range of wind speed values. The reason for having three periods instead of two is that the calibration settings of the spinner anemometer were changed during the measurement campaign (in date 23/05/2014) from $k_{1,d} = 1, k_{2,d} = 1$ to $k_1 = 0.703$ and $k_2 = 0.500$ (which makes $k_\alpha = k_2/k_1 = 0.711$, as found in the literature).⁵ Having the correct k_α set in the spinner anemometer conversion box allows for a much easier use of the measurements present in the database. It would not make sense to merge data acquired with different calibration settings. Therefore, the measurements of periods A were corrected to the same k_1 and k_2 of period B (using the inverse and direct transformation in chapter 3.3) and only then merged with period B. This merge resulted in 1408 10 minute averages where the met-mast wind speed U_{mm} ranged from 3.6 to 19 m s⁻¹.

Measurements of all periods were filtered for temperature larger than 1°C to avoid rime and icing on the cup anemometer. Faulty mast wind speed measurements were removed by deleting the 10 min data sets, where U_{mm} was larger than 50 m s⁻¹.

The control system on the turbine reports a status signal of the generator (on-line/of-line) and status of the blade tip brakes (released/retracted). In order to avoid the period of time where the turbine was available but not producing due to low wind speeds, the measurements during operation were obtained by filtering for electrical power output larger than 1 kW.

Measurements during stopped and idling conditions (period C) were obtained by filtering for generator rotations per minute smaller than 20. The data set included measurements from when the wind turbine was stopped for faults, maintenance or cut-outs. The met-mast wind speed U_{mm} span was from 1 to 27 m s⁻¹. The yaw misalignment in stopped conditions never exceeded 40°.

5.4. Calibration of F_1 , method 1: comparison with met-mast during stopped conditions

As introduced previously, the scope of the calibration is to find the value of k_1 that makes the spinner anemometer wind speed measurements (U_d) equal to the free wind speed at the rotor center (U) in stopped conditions. Based on measurements taken with default $k_{1,d}$ and $k_{2,d}$ constants, the calibration method gives the correction factor F_1 , which is then used to correct the default calibration constant $k_{1,d}$ to $k_1 = F_1 k_{1,d}$.⁵

Measurements of horizontal wind speed by the spinner anemometer ($U_{hor,d,c}$), as a function of met-mast horizontal wind speed (U_{mm}), are shown in Figure 8. Since the turbine was stopped (data set C), there is no rotor induction effect, and the correction factor F_1 is expected to be independent of the wind speed. This assumption is verified in Figure 9, where F_1 is calculated with equation 37.

There is some increased scatter at low wind speeds (below 5 m s⁻¹), due to the lower correlation between the met-mast and spinner anemometer. The reason for the high scatter at wind speed lower than 5 m s⁻¹ as seen in Figure 9 is that at low wind speeds the correlation between the wind speeds measured at distant locations in space is reduced. This might also be

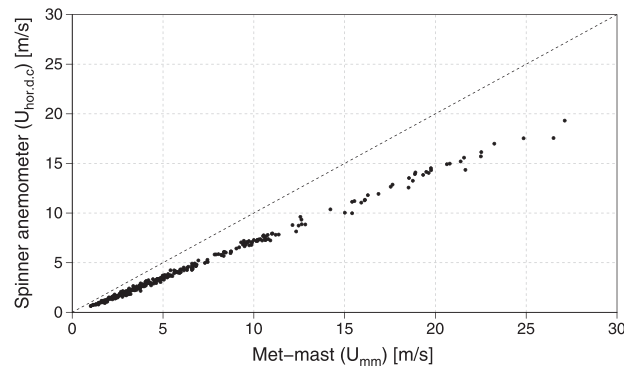


Figure 8. Non-calibrated horizontal wind speed by the spinner anemometer as a function of met-mast horizontal wind speed (period C, stopped condition). Black points are 10-min averages. Dashed black diagonal line is 1:1.

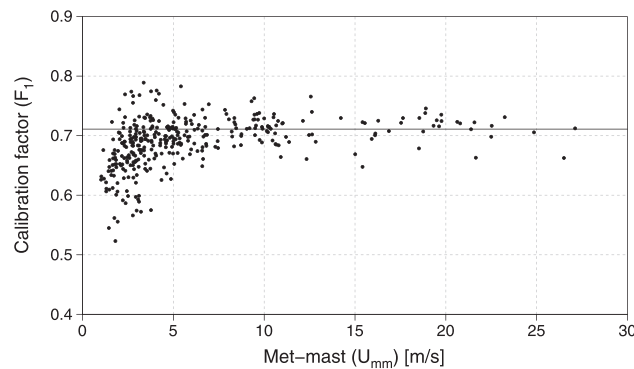


Figure 9. F_1 correction factor as a function of met-mast wind speed (period C, stopped condition). Black points are 10 min averages. Horizontal black line is at $F_1 = 0.711$.

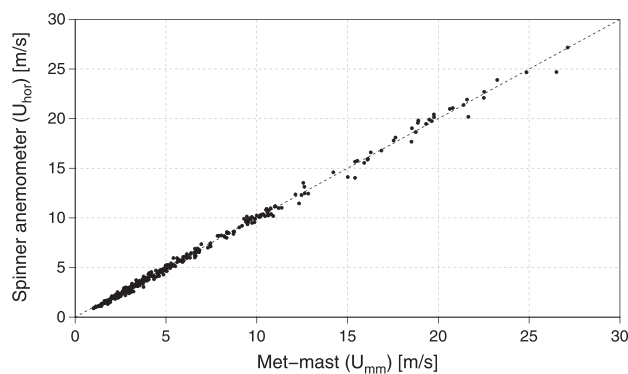


Figure 10. Calibrated horizontal wind speed by the spinner anemometer as function of met-mast horizontal wind speed (period C, stopped condition). Dashed black diagonal line is 1:1.

seen by plotting the ratio between two cup anemometers mounted on two met-masts with a horizontal displacement similar to the one between spinner anemometer and met-mast of the present experiment.

The average value of $F_1 = 0.711$ was calculated for wind speeds above 5 m s^{-1} , which resulted in the standard deviation of F_1 lower than 2.5% while still keeping 42% of the measurements (149 out of 353). The statistical uncertainty (σ/\sqrt{N} , where N is the number of samples and σ is the standard deviation) of the mean value is less than 0.002. Since $k_{1,d} = 1$, then $k_1 = 0.711$.

The measurements during stopped conditions calibrated with $F_\alpha = 0.714$ and $F_1 = 0.711$ ($F_2 = F_\alpha F_1 = 0.508$) are shown in Figure 10. In the same figure, the 1:1 relationship between spinner anemometer measurements and met-mast measurements confirms a correct calibration of F_1 and absence of rotor induction.

5.5. Calibration of F_1 , method 2: comparison with met-mast at high wind speeds

This second method to determine F_1 uses measurements during operation of the wind turbine (Figure 11).

During operation, however, the rotor induction reduces the wind speed at the rotor plane with respect to the free wind speed, introducing a significant error in the calculation of F_1 . This slow down is small when the turbine is operating at high wind speeds, with a low power coefficient, as seen in the works of Pedersen *et al.*,^{4,11} where the induction was found to be smaller than 1% above 17 m s^{-1} , for a pitch-regulated Vestas V80* wind turbine.

A set of F_1 values was determined from the measurements with equation 37 and plotted as a function of wind speed (Figure 12).

The red line is a bin average with 1 m s^{-1} bin size, centered at integer wind speeds. The horizontal black line shows the value of F_1 found for stopped conditions (Section 5.4). As expected, the red line tends asymptotically to the value of F_1 calculated for the stopped rotor (method 1) shown with a horizontal black line. There were unfortunately no measurements between 18 and 25 m s^{-1} . It is not possible to determine a value of F_1 for an induction free condition during operation for the measured data (the red line does not seem to reach an asymptotic value and increases with the wind speed as a result of the induction decreasing).

The measurements of the period during operation calibrated with $F_\alpha = 0.714$ (found in the literature⁵) and $F_1 = 0.711$ (found in Section 5.4 for a stopped rotor) are shown in Figure 13 as a function of the met-mast wind speed.

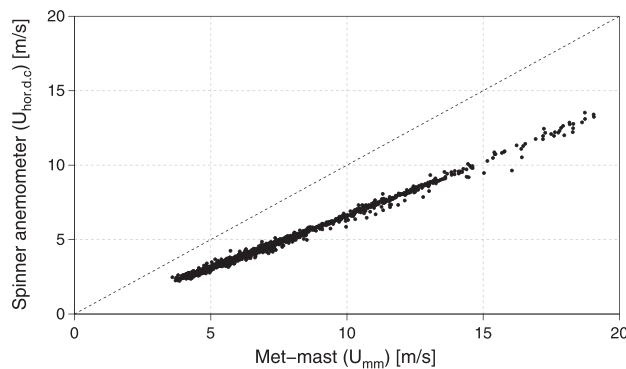


Figure 11. Non-calibrated horizontal wind speed by the spinner anemometer as a function of met-mast horizontal wind speed (merge of periods A and B, during operation). Dashed black diagonal line is 1:1.

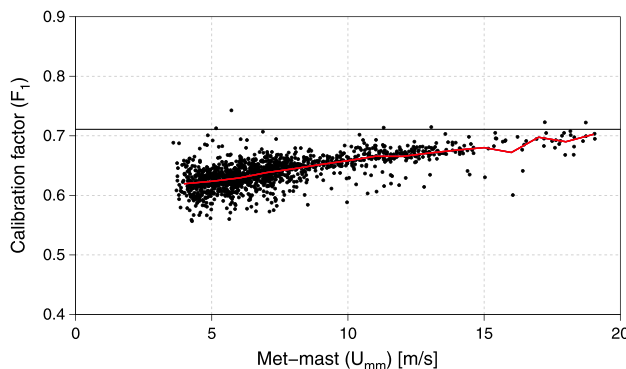


Figure 12. F_1 correction factor as a function of met-mast wind speed, disturbed by the rotor induction during operation of the wind turbine (data sets A and B). The black horizontal line at $F_1 = 0.711$ shows the calibration result obtained with method 1 (stopped condition). Black points are 10 min averages. Red line is 1 m s^{-1} bin average.

*Vestas Wind Systems A/S, Hedeager 42, 8200 Aarhus N, Denmark.

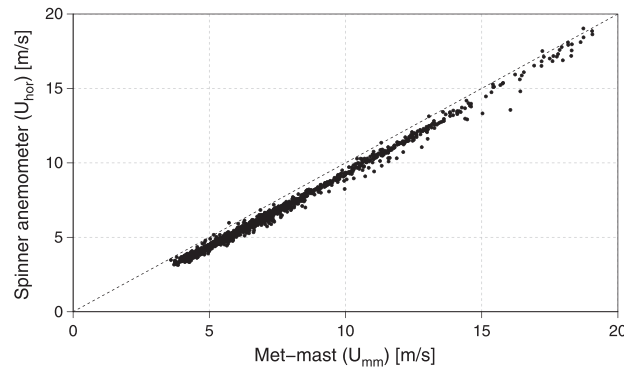


Figure 13. Calibrated horizontal wind speed by the spinner anemometer as a function of met-mast horizontal wind speed (merge of periods A and B, during operation). The deviation from the 1:1 dashed line is due to the rotor induction, which makes the wind speed at the turbine lower than the wind speed at the met-mast. This deviation will be accounted for with the NTF, see chapter 6.

5.6. Calibration of F_1 , method 3: CFD simulation

Calibration method 3 used CFD for the determination of k_1 for a stopped condition of the wind turbine. The flow field around the turbine was modeled using the EllipSys3D[†] flow solver,^{12–15} which solved the incompressible Reynolds-averaged Navier–Stokes equations using the finite volume method in general curvilinear coordinates in a collocated grid arrangement to facilitate complex mesh geometries.

In all simulations, the EllipSys3D code was used in steady state mode, running local time stepping towards a steady state solution. Furthermore, the coupled momentum and pressure-correction equations were solved using the SIMPLE¹⁶ algorithm, while the convective terms were discretized using the QUICK¹⁷ scheme.

In the simulations, all three blades, spinner and nacelle were modeled according to the actual geometry of the turbine, while the tower was omitted. The total number of cells in the domain was 14 million cells. A grid independence study was conducted, and a so-called mixed order extrapolation was used to compute the numerical error associated with the sonic sensors on the spinner. This study showed that the velocities extracted in the sensor paths had an error associated with them of approximately 2%. To decrease this error, a finer mesh would have to be used.

5.6.1. CFD reference system and geometry description.

Looking at the spinner from the front, the CFD reference system has the x axis pointing left, the y axis upwards and the z axis aligned with the shaft axis (positive in the main stream flow direction). Blade 1 is pointing upwards; hence, sensor 1 is at the bottom of the spinner, sensor 2 at the top left and sensor 3 at the top right.

The CFD simulation gives three velocity components (u , v and w , aligned with x_s , y_s and z_s) at each of the five points in each sonic sensor path (red line in Figure 6). The coordinates of the points presented in Table IV are obtained by measuring from the photo of Figure 1, with fifteen points in total. Points P_1 to P_5 belong to sonic sensor 1 (P_5 being the closest to the spinner surface), P_6 to P_{10} to sensor 2 and P_{11} to P_{15} to sensor 3.

5.6.2. Projection along sensor path.

The result of the CFD simulation is given as three wind speed components in the global coordinate system. The velocity along the sensor path was calculated as the dot product between the vector velocity $\mathbf{U}(u, v \text{ and } w)$ and the unit vector of the sensor path $\mathbf{V}(x_s, y_s \text{ and } z_s)$. The unit vector of the sensor path 1 was calculated as $(\mathbf{r}_{P_5} - \mathbf{r}_{P_1})/|\mathbf{r}_{P_5} - \mathbf{r}_{P_1}|$.

Figure 15 shows the velocity projected along each sensor path for a free wind speed of 10 m s^{-1} . As seen in both Figures 14 and 15, the velocity at the point closer to the surface (P_5 for sensor 1) is higher than for the point further from the surface (P_1 for sensor 1). There is full agreement between the three sensors.

5.6.3. Calculation of the k_1 calibration constant from CFD simulations.

The flow is simulated for eight wind speeds in the range $4\text{--}20 \text{ m s}^{-1}$, at a flow angle $\alpha = 0$. For this inflow angle, the generic spinner anemometer wind speed relations (equations 1, 2 and 3) simplify to equation 38 where the dependency of θ and k_2 vanish. It becomes therefore easy to calculate k_1 using equation 39.

[†]In-house flow solver EllipSys3D is developed in co-operation between the Department of Mechanical Engineering at DTU and The Department of Wind Energy at Risø National Laboratory, Denmark.

Table IV. Coordinates of the points of the sensor paths.

Sensor	Point	x_s [m]	y_s [m]	z_s [m]
Sensor 1	1	0.000	-0.621	-1.338
	2	0.000	-0.611	-1.299
	3	0.000	-0.602	-1.260
	4	0.000	-0.592	-1.222
	5	0.000	-0.583	-1.183
	6	0.538	0.310	-1.338
Sensor 2	7	0.529	0.305	-1.299
	8	0.521	0.301	-1.260
	9	0.513	0.296	-1.222
	10	0.505	0.291	-1.183
	11	-0.538	0.310	-1.338
	12	-0.529	0.305	-1.299
Sensor 3	13	-0.521	0.301	-1.260
	14	-0.513	0.296	-1.222
	15	-0.505	0.291	-1.183

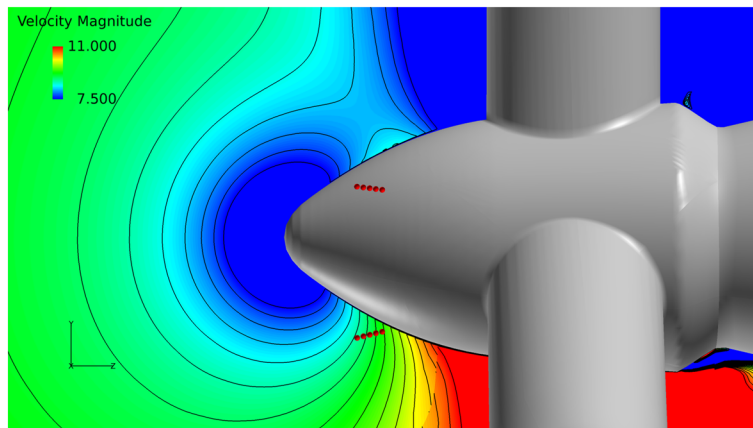


Figure 14. Side view of the wind turbine spinner with one blade vertically upwards. Color represents velocity modulus on a vertical plane in m s^{-1} for a free wind speed of 10 m s^{-1} . The red dots indicate the position on the sensor path of the CFD results (Figure 6). Low wind speed is found at the stagnation point in front of the spinner and in front of the vertical blade pointing upwards.

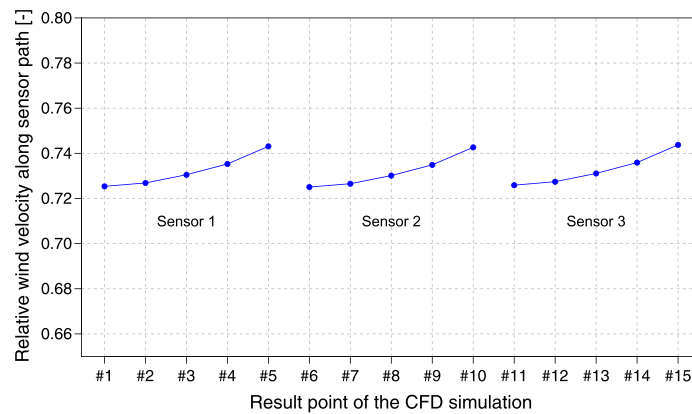


Figure 15. Wind velocity component along the sensor paths in each of the 15 result points in which the CFD results were computed, for a free wind speed of 10 m s^{-1} .

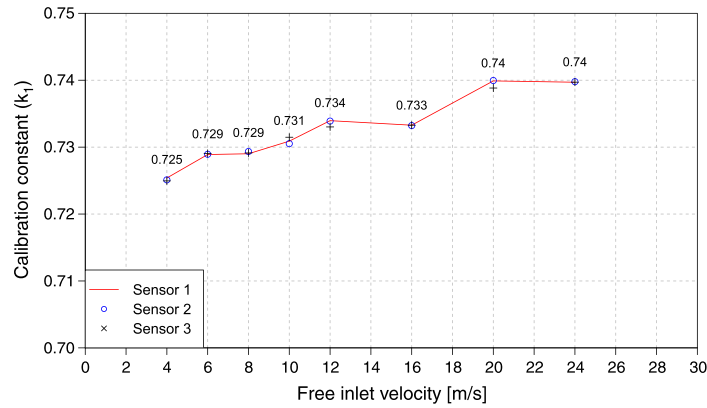


Figure 16. Calibration constant k_1 calculated from CFD simulations at various free wind speeds. The red line, blue circles and black crosses show the k_1 value determined for each of the three sensors. Numeric values are the mean of the three sensors.

$$V_1 = V_2 = V_3 = Uk_1, \quad (38)$$

$$k_1 = \frac{V_1}{U} = \frac{V_2}{U} = \frac{V_3}{U}. \quad (39)$$

The geometry of the sonic sensors was not included in the CFD simulation. Therefore, the velocity calculated at the points located at the extremes of the sensor path differs from the real velocity, which is influenced by the presence of the sensor heads. Due to this influence, the CFD results at the points closer to the sensor heads were neglected (P_1 and P_5 for sensor 1). The velocity along each sensor path was calculated as the average of the three velocities projected along the sensor path (result points P_2 , P_3 and P_4 for sensor 1).

The calculation of k_1 was repeated for each test wind speed in the range 4–24 m s^{-1} . The result is shown in Figure 16. There is a good agreement between the three sonic sensors. k_1 was expected to be independent of wind speed. However, Figure 16 shows a positive trend, with a mean value of 0.7326 and a variation of about $\pm 1\%$. The maximum difference between the values of k_1 calculated for different wind speeds is 0.0226, and the minimum is 0.0095. The increase of k_1 value in the range of wind speeds relevant for power performance measurements (4–16 m s^{-1}) is about 1.2%, as seen in Figure 16.

6. NACELLE TRANSFER FUNCTION TO ACCOUNT FOR THE ROTOR INDUCTION

The focus of the analysis is the calibration of the spinner anemometer for wind speed measurements. However, this chapter will consider the effect of the induction and the effect of the application of the NTF to the measurements during operation (periods A and B). A complete description of the method and uncertainty evaluation is available in the report.¹⁸ The induction is defined as the slow down of the wind relative to the free wind as

$$I = \frac{U_{mm} - U_{hor}}{U_{mm}}. \quad (40)$$

As seen in the previous equation, the induction is a function of the calibrated spinner anemometer horizontal wind speed U_{hor} . It is not possible to measure the induction if the spinner anemometer is not calibrated for wind speed measurements.

Figure 17 shows the induction at the center of the rotor measured by the calibrated spinner anemometer. At 4 m s^{-1} , it is 10–15% and gradually decreases for increasing wind speed. At 19 m s^{-1} , it has not yet reached zero induction.

The calibrated horizontal wind speed measured with the spinner anemometer was used to determine the NTF according to the method described in the literature.⁶ The NTF was derived from the measurements of periods A and B with the method of bins as shown with a red line in Figure 18.

The measurements of the calibrated spinner anemometer were then converted to free wind speed using the bin values of the NTF ($U_{F,i}$ and $U_{N,i}$) and linear interpolation between bins.

$$U_{free} = \frac{U_{F,i+1} - U_{F,i}}{U_{N,i+1} - U_{N,i}} \cdot (U_{hor} - U_{N,i}) + U_{F,i}. \quad (41)$$

A nice linear pattern is shown between calculated free wind speed and measured met-mast wind speed in Figure 19.

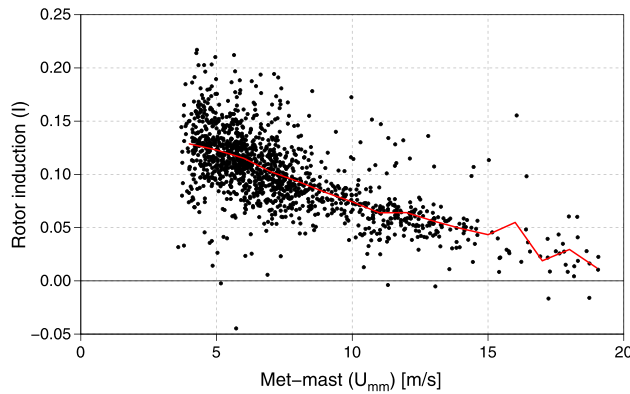


Figure 17. Rotor induction for the stall regulated turbine (during operation). The horizontal black line is showing the ordinate equal to zero. The red line shows the mean induction for wind speed bins of 1 m s^{-1} .

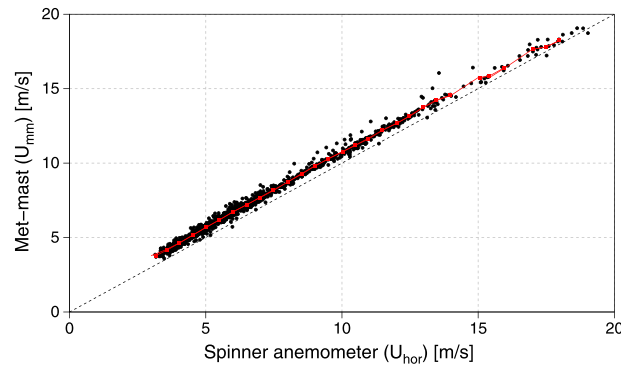


Figure 18. Red dots showing the NTF determined as described in IEC61400-12-2.⁶ The NTF is interpolated to adjacent bins at the bins 14.5 and 16.5 m s^{-1} because of the amount of 10 min averages lower than three. The dashed black diagonal line is 1:1.

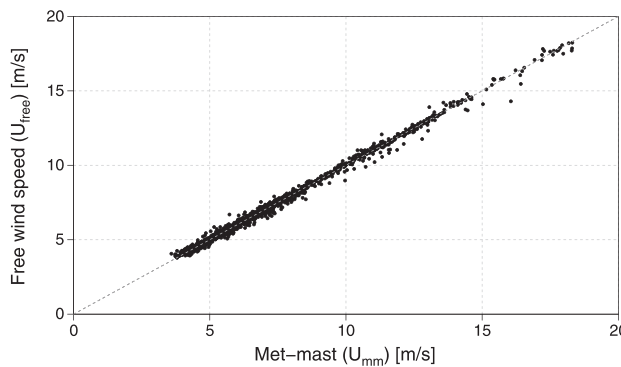


Figure 19. Free wind speed calculated from spinner anemometer measurements corrected with the NTF as a function of met-mast wind speed. The gray dashed line is a 1:1 line.

7. DISCUSSION

Methods 1 and 2 were based on field measurements, comparing the spinner anemometer wind speed with a met-mast wind speed. Ten minute averages were used to compare the measurements.

Method 1 used measurements of the wind turbine in a stopped condition or while idling. The 353 observations (equivalent to 2.5 days) were acquired over a period of almost 5 months when the wind turbine was stopped for maintenance or other reasons. However, measurements could have been acquired by intentionally stopping the turbine for a number of

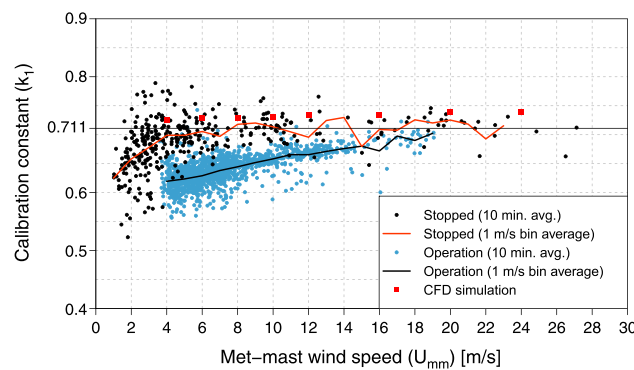


Figure 20. Comparison between the three methods used to calculate k_1 . The horizontal black line marks the value of k_1 calculated as average of the values during stopped condition for wind speed above 5 m s^{-1} .

hours when the wind was at the desired speed and direction, but this was not the case. Still, the results seemed satisfactory.

Method 2 used measurements at moderate wind speeds during operation. As a consequence of the low probability of occurrence of high wind speeds (also combined with the requirements of the valid direction sector), the collection of an appropriate amount of measurements for determination of an induction free k_1 constant was not possible. In the present analysis, an observation period of about 3 months was used to collect an amount of measurements of about 10 days, 90% of which the wind speed was below 15 m s^{-1} .

Method 3 used a CFD simulation of the velocity in the three sensor paths, in combination with basic equations of the spinner anemometer algorithm to calculate k_1 . Different inlet velocities (free wind speed) were used. A summary of the k_1 values found by use of the different methods is shown in Figure 20, merging results of Figures 9, 12 and 16.

Measurements during operation showed a k_1 that is heavily influenced by induction at the rotor center. For this reason, the calibration must be made in stopped conditions or during operation ensuring that the induction at very high wind speeds is negligible. This condition of negligible induction was not reached by our stall-regulated wind turbine, for the available measurements (up to $U_{mm} = 19 \text{ m s}^{-1}$). A modern pitch-regulated turbine however might have a negligible induction at lower wind speeds than a stall-regulated turbine, as experienced in the literature.⁴

The difference between the CFD results (2.2% to 4.2% overestimation with respect to $k_1=0.711$) might be due to the uncertainty of the CFD simulation, uncertainty of the cup anemometer on the met-mast or an underestimation of the wind speed measured by the spinner anemometer in the order of 3%. The spinner anemometer sensors were not in this case calibrated in an accredited wind tunnel as required according to the calibration overview of Figure 2. The CFD simulations show a trend of slightly increasing k_1 values for increasing wind speed, about $\pm 1\%$ of mean value. The cause of this trend has not been investigated. The effect is not present in the measurements in stopped condition.

8. CONCLUSIONS

This paper investigated and described three methods to calibrate a spinner anemometer for wind speed measurements and gave introduction to the consequent use of the NTF needed to measure the power performance of a wind turbine with the spinner anemometer.

Three methods to determine the k_1 calibration constant for wind speed measurements of a spinner anemometer were presented and compared. Additionally, the use of the NTF according to IEC 61400-12-2 was introduced to correct measurements to free wind speed.

- Method 1 used a stopped turbine and a comparison between the spinner anemometer wind speed and the free wind speed measured by the met-mast at hub height.
- Method 2, which was based on the same comparison but during operation of the wind turbine.
- Method 3 used CFD simulation to calculate the wind speeds at the sonic sensor paths and basic equations of the conversion algorithm to calculate the calibration constant k_1 .

According to the definition of k_1 (k_1 is the ratio between spinner anemometer horizontal wind speed and free horizontal wind speed in a condition of zero induction), the correct method to determine k_1 is Method 1, which used a stopped turbine. For Method 1, it was found that the relation between $U_{hor,d}$ and U_{mm} was linear, and hence, the F_1 correction factor was constant with respect to the free wind speed. The big drawback of this method is that it requires the wind turbine to be stopped for several hours in good wind conditions, which is generally not desirable for the wind turbine owner. Therefore,

we investigated the possibility of calculating the calibration constant using measurements during operation of the wind turbine (Method 2) and CFD simulation of the stopped turbine (Method 3).

Method 2 was notably influenced by the rotor induction. We tried to identify a range of high wind speeds in which F_1 was stabilizing to an asymptotic value. However, this condition was not met for our stall-regulated turbine at wind speeds up to 19 m s^{-1} . Method 2 seems to be more applicable on a pitch regulated turbine, where induction decreases more than for a stall-regulated turbine because of the pitching of the blades. This will make the F_1 values approach an asymptote.

Method 3, CFD simulation of the stopped turbine, has the obvious advantage of not requiring wind measurements to determine k_1 . The method showed a low dependency of k_1 on the wind speed (about 1.2% linear increase from 4 to 16 m s^{-1}) and 2.2% to 4.2% difference from the value obtained with method 1. In the absence of a free wind speed measurement, this method is appropriate to determine an initial value of the calibration coefficients.

The analysis shows the important simplification of the equations used to calculate k_1 arising from having set the correct k_α value in the spinner anemometer conversion box. Failing to do so means that the full conversion algorithm of sampled data has to be used to calculate back to sonic sensor wind speeds and forth to spinner anemometer wind speed for different k_1 and k_2 values. This was needed in this analysis because data was gathered with k_1 and k_2 values not representing a calibrated k_α value. It is recommended to follow the order of the five steps calibration procedure described in the work of Demurtas and Pedersen.⁷

The calibration of k_1 in addition to determination of the NTF is needed to measure the nacelle power curve of a wind turbine, ensuring separation between the instrument characteristics and the slow down of the wind due to the rotor induction. It is important to keep the calibration of the spinner anemometer separated from the NTF because the calibration of the spinner anemometer is invariant to control system settings and blade design.

Since the physics of extracting power from the wind is similar between different wind turbines, future research will investigate the possibility of defining a general NTF as a standard correction of the rotor induction. The specificity of the spinner shape and sonic sensors mounting will be accounted by the calibration of the spinner anemometer alone, on each turbine.

ACKNOWLEDGEMENTS

This work was performed as part of an EUDP project iSpin funded by the Danish Energy Agency (J.nr 64012-0107). The authors would like to thank all the people from Vattenfall, Metek and ROMO Wind for their good collaboration. This work was performed under the EUDP-2012-I project: iSpin (J.nr 64012-0107).

REFERENCES

1. Cuerva A, Pedersen TF, Sánchez Luengo S, Alamillo Pastor JD, SanzAndrs A, Franchini SA. Theoretical model on spinner anemometry based on ultrasonic paths. *Proceedings of EWECE 2008*, Brussels, 2008.
2. Frandsen S. Nacelle anemometry. *Proceedings of EWEA 2006*, Bruxelles, 2006.
3. Zahle F, Srensen NN. Characterization of the unsteady flow in the nacelle region of a modern wind turbine. *Wind Energy* 2011; **14**: 271–283.
4. Pedersen TF, Demurtas G, Sommer A, Hjrstrup J. Measurement of rotor centre flow direction and turbulence in wind farm environment. *Torque 2014, Journal of Physics*, Denmark, June 2014.
5. Pedersen TF, Demurtas G, Zahle F. Calibration of a spinner anemometer for yaw misalignment measurements. *Wind Energy* 2014.
6. IEC 61400-12-2: *Power Performance of Electricity Producing Wind Turbines Based on Nacelle Anemometry*. Edition 1. International Electrotechnical Commission: Geneva, Switzerland, 2012.
7. Demurtas G, Pedersen TF. Summary of the steps involved in the calibration of a spinner anemometer. *DTU Wind Energy Report I-0364*, Roskilde, 2014.
8. Pedersen TF, Wagner R, Demurtas G. Wind turbine performance measurements by means of dynamic data analysis. *DTU Wind Energy Report*, Roskilde, 2015.
9. 61400-12-1 IEC. *Power Performance Measurements of Electricity Producing Wind Turbines*. Edition 3. International Electrotechnical Commission: Geneva, Switzerland, 2005.
10. Paulsen US, Wagner R. IMPER Characterization of the wind field over a large wind turbine rotor—final report. (Chapter 4: Description of the experimental facility). *DTU Wind Energy report E-0002*, Roskilde, 2012.
11. Pedersen TF, Demurtas G, Gottschall J, Hjrstrup J, Nielsen JD, Christiansen W, Weich G, Sommer A, Kristoffersen JR. Improvement of wind farm performance by means of spinner anemometry. Section 2.3: Development of internal calibration method. *DTU Wind Energy report E-0040*, 2013.

12. Michelsen JA, *Basis3D—a platform for development of multiblock PDE solvers*, Technical Report AFM 92-05, Technical University of Denmark, 1992.
13. Michelsen JA, *Block structured multigrid solution of 2D and 3D elliptic PDEs*, Technical Report AFM 94-06, Technical University of Denmark, 1994.
14. Sørensen NN, *General purpose flow solver applied to flow over hills*, Technical Report Ris-R-827(EN), Risø National Laboratory, 1995.
15. Ivanell S, Mikkelsen R, Sørensen JN, Henningson D, *Validation of methods using EllipSys3D*, Technical Report, KTH TRITA-MEK, 2008.
16. Patankar SV, Spalding DB. A calculation procedure for heat, mass and momentum transfer in three-dimensional parabolic flows. *International Journal of Heat and Mass Transfer* 1972; **15**: 1787–1972.
17. Leonard PB. A stable and accurate convective modelling procedure based on quadratic upstream interpolation. *Computer Methods in Applied Mechanics and Engineering* 1979; **19**: 59–98.
18. Demurtas G. Power curve measurement with spinner anemometer according to IEC 61400-12-2. *DTU Wind Energy Report I-0440* 2015; **9**: 22–31.

Chapter 5

Power performance measurements and uncertainty analysis

Chapter 4 explained how to accurately measure the wind speed with a spinner anemometer and how to correct it to free wind speed by use of the NTF.

Measuring the performance of a wind turbine means establish the relation between electric power output and wind speed input. While the measurement of the electric power is straight forward, the challenge is to measure the wind speed. The IEC61400-12-1 standard describes the instrumentation requirements and the calculation procedures to determine the power curve with the method of bins, measuring the wind at hub height upstream of the wind turbine with a cup anemometer installed on a meteorological mast. Such structure is costly, therefore the IEC61400-12-2 standard was developed to define requirements and procedures to measure the wind on the wind turbine nacelle and on the spinner.

An experiment was set-up in the Nørrekær Enge wind farm, in the north of Denmark, near Løgstør. The wind farm consists of 13 Siemens 2.3 MW wind turbines (90 m diameter and 80 m hub height) aligned in a single row, almost east to west, in an open flat area. A met-mast was erected in a position suitable to measure the power curve of two adjacent wind turbines, the 4th and the 5th counting from west were both equipped with a spinner anemometer.

The met-mast was IEC61400-12-1 compliant and instrumented with a cup anemometer at hub height and a wind vane on a boom at 78 m height.

The reason for placing the met-mast in a position suitable to measure the power curve of both turbine 4 and 5 was to investigate if the calibration values and NTF determined on the reference turbine 4 could be applied on turbine 5.

The power curve comparison of turbines 4 and 5 presented in the report [16] was not satisfactory, and the cause was attributed to the excessive mounting tolerance of the sonic sensors on the spinner. The mounting was then improved and the analysis repeated. The position of the sonic sensors on each spinner was verified with photos taken from ground level. The power curves compared much better after the mounting improvement. The experiment and the analysis are presented in the following article, including a detailed evaluation of uncertainties.

Nacelle power curve measurement with spinner anemometer and uncertainty evaluation

Giorgio Demurtas¹, Troels Friis Pedersen¹, and Rozenn Wagner¹

¹DTU Wind Energy, Frederiksborgvej 399, 4000 Roskilde

Correspondence to: Giorgio Demurtas (giod@dtu.dk)

Abstract. The objective of this investigation was to verify the feasibility of using the spinner anemometer calibration and nacelle transfer function determined on one reference turbine, to assess the power performance of a second identical turbine. An experiment was set up with a met-mast in a position suitable to measure the power curve of the two wind turbines, both equipped with a spinner anemometer. An IEC 61400-12-1 compliant power curve was then measured for both turbines using the met-mast. The NTF (Nacelle Transfer Function) was measured on the reference turbine and then applied to both turbines to calculate the free wind speed. For each of the two wind turbines, the power curve (PC) was measured with the met-mast and the nacelle power curve (NPC) with the spinner anemometer. Four power curves (two PC and two NPC) were compared in terms of AEP (Annual Energy Production) for a Rayleigh wind speed probability distribution. For each turbine, the NPC agreed with the corresponding PC within 0.10% of AEP for the reference turbine and within 0,38% for the second turbine, for a mean wind speed of 8 m/s.

Keywords: Nacelle power curve, NPC, spinner anemometer, Nacelle transfer function, NTF

1 Introduction

Measuring the performance of a wind turbine means establishing the relation between wind speed (input) and electric power (output). While the measurement of the electric power is straight forward (because it is already in electrical form), the challenge is to measure the wind speed. The IEC61400-12-1 standard describes the instrumentation requirements and the calculation procedures to determine the power curve with the method of bins, measuring the wind at hub height upstream of the wind turbine with a cup anemometer installed on a meteorological mast. A met-mast is costly, therefore the IEC61400-12-2 standard was developed to define requirements and procedures to measure the wind speed on the wind turbine. While the use of the nacelle anemometer (mounted on the nacelle roof) for performance measurements is a well established procedure, the spinner anemometer is a less experienced option to measure the wind turbine performance. A spinner anemometer (Pedersen (2007)) consist of three one dimensional sonic wind speed sensors mounted on the spinner of the wind turbine. The advantage of a spinner anemometer over a nacelle anemometer is that it is measuring in front of the rotor rather than behind, where the flow is influenced by the wake of the blades and other elements present on the nacelle as described by Frandsen et al. (2009).

The spinner anemometer must be traceable calibrated using a met-mast in order to measure the wind speed accurately and to obtain an absolute power curve, according to the standard IEC61400-12-2 (2013) and as reported by Demurtas (2014).

Installation of a met-mast for each wind turbine is obviously not viable. Therefore the possibility of using the calibration found on a first -reference- turbine with a spinner anemometer to another one of same type was investigated in this work.

5 The objectives of the investigation were to:

- Install a met-mast to measure the power curve (PC) on two wind turbines next to each other.
- Install spinner anemometer on both wind turbines.
- Calibrate the spinner anemometer on the reference wind turbine.
- Measure the nacelle transfer function (NTF) on the reference wind turbine.

10 – Compute the NPC and PC for the reference turbine

- Apply the calibration values and NTF measured on the reference turbine to the second turbine.
- Compute the NPC and PC for the second turbine
- Compare the NPC with PC for both turbines.
- Evaluate the uncertainty related to spinner anemometer measurements

2 Site description

The measurements were taken at the Nørrekær Enge wind farm, located in the north of Denmark. This wind farm consist of a row of 13 Siemens 2.3 MW wind turbines (Fig. 1) in a very flat site, 80 m hub height and 93 m in rotor diameter. Every wind turbine was equipped with a spinner anemometer, but only the data from turbine T4 and T5 were used in this work. For this
5 experiment, an IEC61400-12-1 (2005) compliant met-mast was erected near turbine T4 and T5 (Fig. 2).

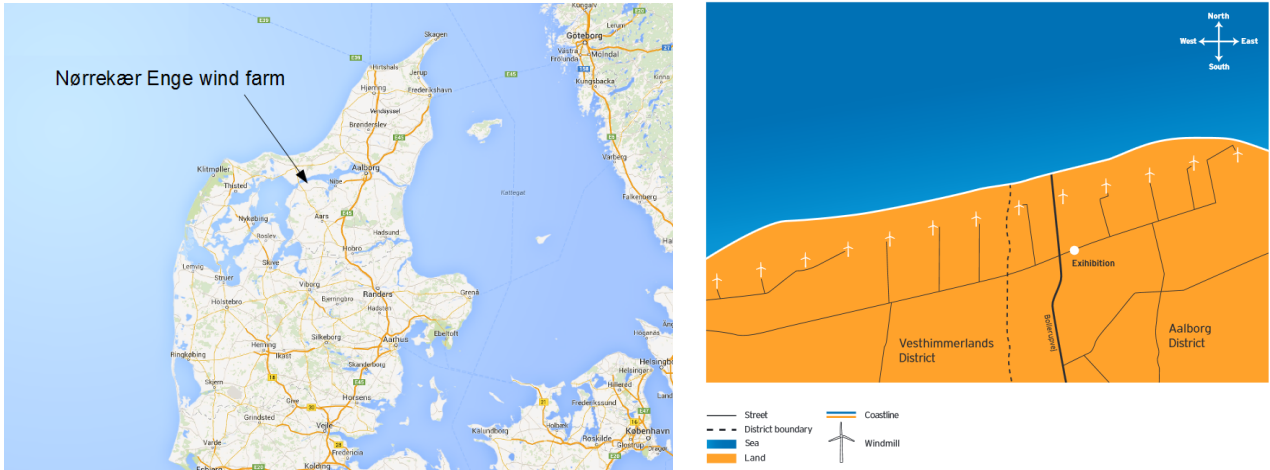


Figure 1. Left: Location of the wind farm in Denmark. Right: location of the 13 wind turbines in the wind-farm. The turbines are numbered 1 to 13 from the left to the right.

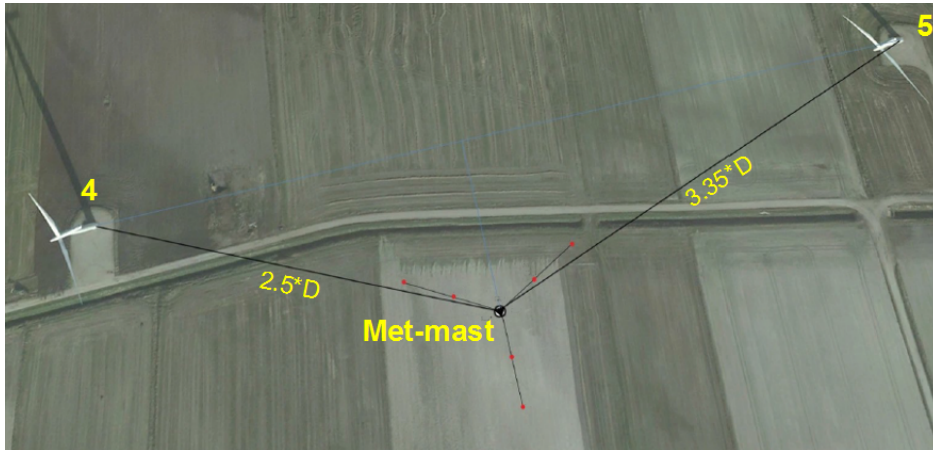


Figure 2. Relative position between reference turbine T4, met-mast and turbine T5.

The met-mast was positioned 2.5 rotor diameters from turbine T4 and 3.35 rotor diameters from turbine T5 (Fig. 2). The met-mast was equipped with a top mounted cup anemometer at 80 m a.g.l. (above ground level) at hub height, a wind vane at 78 m, barometer, thermometer and hygrometer at 78 m a.g.l.

5 The met-mast used a data-logger for meteorological measurements connected with a 3G modem to a server of DTU Wind Energy. In each turbine the spinner anemometer was connected to a local data-logger and with a 3G modem to a server of Romo Wind A/S. The electric power produced by the wind turbine was measured with additional voltage and current transducers and the same data logger used for the spinner anemometer (for more details see Demurtas (2015)).

3 Spinner anemometer calibration

Calibration of spinner anemometer has been analyzed and investigated in Pedersen et al. (2015) and Demurtas et al. (2016).
10 Due to the large size of the spinner of a modern wind turbine it is not feasible to place it directly into a wind tunnel. Therefore each sonic sensor was first calibrated in the wind tunnel, and then, once mounted on the spinner, internally calibrated (for details see the manual of the spinner anemometer by Metek (05-01-2009)). The internal calibration procedure ensures that the three sensors read the same average wind speed. The spinner anemometer on T4 was k_α calibrated to ensure that the inflow angle is measured correctly, and k_1 calibrated to ensure that the output value U_{hor} equals the free wind speed when the turbine
15 is stopped and pointed to the wind (see Demurtas (2014) for details). The k_α and k_1 calibration values found for T4 were used on both T4 and T5 (which is reasonable as long as the mounting of the sonic sensors and the spinner shapes are equal).

3.1 Sonic sensors wind tunnel calibration

The objective of the calibration of individual sonic sensors is to calibrate the wind speed measurements by the sonic sensors V_1 , V_2 and V_3 . Each sensor was calibrated individually in a MEASNET compliant wind tunnel. The sensor was mounted on a
20 support plate to hold it in the wind tunnel test section, Fig. 3. The mounting plate geometry was defined in Demurtas (2014) and the procedure described in IECRE (2015)). A calibration certificate was released for each sonic sensor. The values resulting from the wind tunnel calibration (slope m , offset q and sensor path angle ϕ_s , Tab. 1) should be set in the spinner anemometer conversion box (which converts V_1 , V_2 , V_3 and the rotor position into U_{hor} , γ and β) with the method described in Demurtas (2014). However this was not done, and a correction was applied to the measurements afterwards (see section 4). The sensor
25 path angle ϕ was not used.

Table 1. Sensor path angle (ϕ_s), slope (m) and offset (q) coefficients of the sonic sensor wind tunnel calibrations.

	Turbine 4 (SN: 107114721)			Turbine 5 (SN: 107114722)		
	m	q	ϕ_s	m	q	ϕ_s
Sensor 1	1.20746	0.18431	34.7°	1.22198	0.07906	34.7°
Sensor 2	1.22794	0.00168	34.8°	1.23066	-0.08116	34.6°
Sensor 3	1.23249	0.16930	35°	1.21517	-0.56490	34.1°
Average	1.22263	0.11843	34.7°	1.22198	0.07906	34.7°

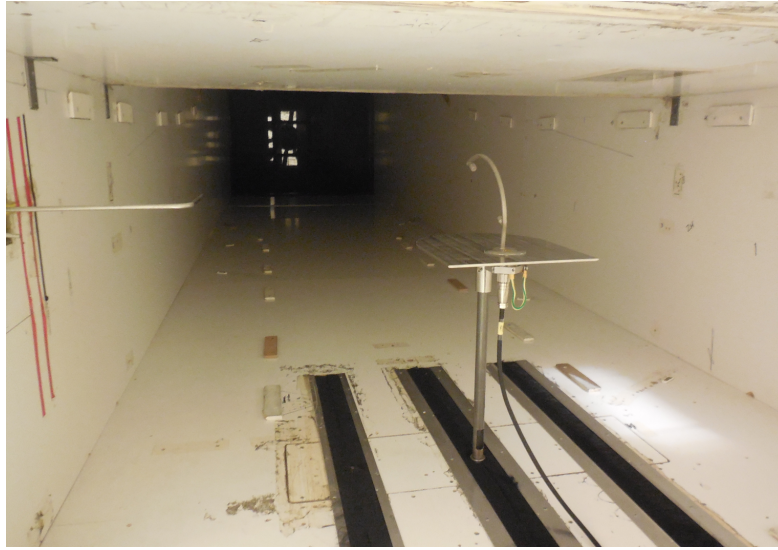


Figure 3. One sonic sensor mounted on the mounting plate in the test section of the SOHansen wind tunnel. The reference pitot tube is visible at the left hand side of the photo.

3.2 k_α calibration

The calibration for inflow angle measurements was made with the wind speed response method (WSR) described in Demurtas and Janssen (2016). The turbine was yawed several times of plus minus 60° in good wind conditions. The resulting calibration value $k_\alpha = 1.442$ was used to correct the measurements with the procedure described in Pedersen et al. (2015). The uncertainty on the k_α value could be calculated by repeating the test several times (as was done in Demurtas and Janssen (2016), which found a repeatability of the result within 8.5% of the mean value, for a different wind turbine model). In this case the calibration test was performed only once, and the uncertainty was estimated to $u_{k_\alpha} = 10\% \cdot k_\alpha$.

3.3 k_1 calibration

The objective of this calibration is to find the value of the k_1 calibration constant that makes U_{hor} to match the free wind speed U_{mm} when the turbine is stopped and is facing the wind. During operation of the wind turbine the rotor induction is accounted for with the nacelle transfer function (NTF) as described in the IEC61400-12-2 standard. To acquire the measurements needed for the calibration the wind turbine should be stopped, so that the wind seen by the spinner anemometer is not influenced by the induction. However, stopping the wind turbine would cause an energy loss, therefore the calibration was performed with the wind turbine in operation at high wind speed as proposed by Demurtas et al. (2016).

The k_1 calibration procedure was based on measurements acquired during operation of the wind turbine where k_1 was set to the default value $k_{1,d} = 1$ in the spinner anemometer conversion box. The correction factor F_1 was calculated as the ratio

$$F_1 = \frac{U_{hor,d,c}}{U_{mm}} \quad (1)$$

where $U_{hor,d,c}$ is the horizontal wind speed measured with default $k_{1,d}$ and calibrated k_α .

Since T4 is pitch regulated, F_1 should tend to an asymptote as the wind speed increase (Fig. 4) because the induction decreases for high wind speed. The value of $F_1 = 0.6019$ was calculated as the average of the values for free wind speed greater than 15 m/s. Since the default value was $k_{1,d} = 1$, the calibration value is:

$$k_1 = F_1 \cdot k_{1,d} = 0.6019 \quad (2)$$

k_1 is not subject to uncertainty because it is compensated with the uncertainty estimation of the NTF. This is further explained in section 9.

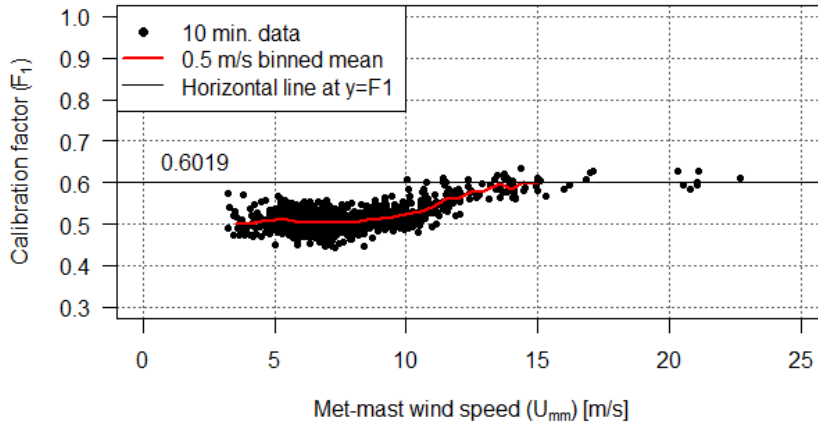


Figure 4. Calibration factor F_1 as a function of free wind speed during operation of the wind turbine.

4 Measurement database, data filtering and corrections

The measurement data-base consists of 237 hours of measurements acquired in a free wind direction sector between 101° and 229° as measured by the wind vane on the met-mast. The spinner anemometer measurements from both turbine 4 and 5 were calibrated with the k_α and k_1 values found for T4. Ten minute data sets where the minimum wind turbine rotor rotational speed was lower than 40 rpm were filtered out in order to keep data where the turbine is continuously in operation. Data sets where the ten minute mean power coefficient (measured with the met-mast) were higher than 16/27 (the Betz limit) were filtered out to remove four outliers (this is a deviation to the requirements of the IEC61400-12-1 (2005) standard). There was no need to filter for freezing temperature, since the temperature was between 6 and 14°C.

The sonic sensors wind tunnel calibration values were not set in the spinner anemometer conversion box as required in Demurtas (2014). However a correction was made on the measurements to take into account the results of the wind tunnel calibration. From the calibration certificates the sensors on turbine 5 has smaller slope coefficient (m_5) and smaller offset (q_5) than those on T4 (m_4 and q_4), which means that the sensors on T5 are reading a bit higher wind speed than sensors on T4. Measurements of T5 were reduced with the ratio of the mean slope and the difference in mean offset.

$$U_5 = U_{5,original} \cdot (m_5/m_4) + q_5 - q_4 \quad (3)$$

Figure 5 shows the ten minute mean values of power and calibrated wind speed. The wind speed was normalized with a value between 10 and 14 m/s for confidentiality reasons.

The traceability of the measurements of the spinner anemometer on T4 was ensured by the calibrated met-mast instruments and the NTF, while the traceability of the spinner anemometer on T5 was ensured by the NTF and wind tunnel calibration of the sonic sensors.

The air density was calculated from the met-mast measurements with Eq. 4 (from IEC61400-12-2 (2013)), where $P_w = 0.0000205 \cdot e^{(0.06138467 \cdot T)}$, $R_0 = 287.05$ J/kg K, and $R_w = 461.5$ J/kg K. T expressed in Kelvin, P in absolute Pascal.

$$\rho = \frac{1}{T} \left(\frac{P}{R_0} - RH \cdot P_w \left(\frac{1}{R_0} - \frac{1}{R_w} \right) \right) \quad (4)$$

Measured air density was between 1.2 and 1.27 kg/m³.

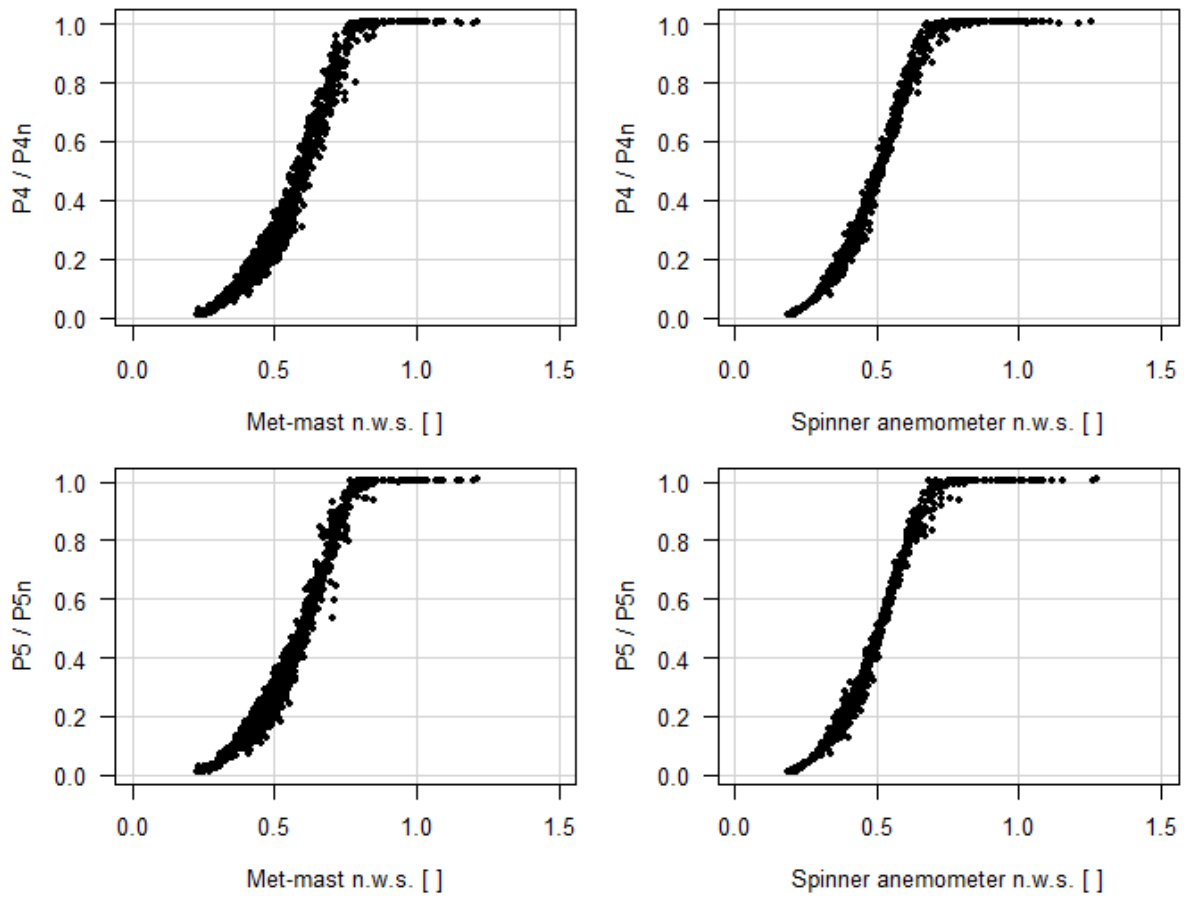


Figure 5. Scatter plot of power as a function of spinner anemometer normalized wind speed (n.w.s.) and met-mast normalized wind speed measurements, for turbines T4 and T5, before application of the NTF and before air density correction. Met-mast measurements to the left, and spinner anemometer measurements to the right. Turbine T4 measurements upper and turbine T5 measurements lower. Data refers to the same measurement period.

5 Nacelle transfer function measurement

The purpose of the NTF is to correct the spinner anemometer measurements to be representative of the free wind speed. U_{mm} is the free wind speed measured by the met-mast, and U_{free} is the free wind speed calculated by correcting the spinner anemometer measurements (U_{hor}) with the NTF.

- 5 The IEC61400-12-2 (2013) standard defines the NTF as the met-mast wind speed binned as a function of the nacelle wind speed. Krishna et al. (2014) investigated the root cause for high deviations in the self consistency check with the IEC61400-12-2 (2013) method and proposed an improved method, which consist of binning the spinner anemometer wind speed as a function of the met-mast wind speed. This procedure is used here. If a wind speed bin has less than 3 measurements, the value

of the NTF is calculated by linear interpolation from the adjacent bins if they both have at least 3 measurements each. No air density correction was made for the measurement of the NTF. The measured NTF for the spinner anemometer installed on turbine T4 is shown in Fig. 6 .

As expected the NTF is approximately 1:1 at high wind speed (around 11-15 m/s, thanks to the k_1 calibration), and is lower than 1:1 for the range of wind speeds where the turbine is operating with high C_p (high induction, which makes the wind speed by the spinner anemometer lower than the free wind speed).

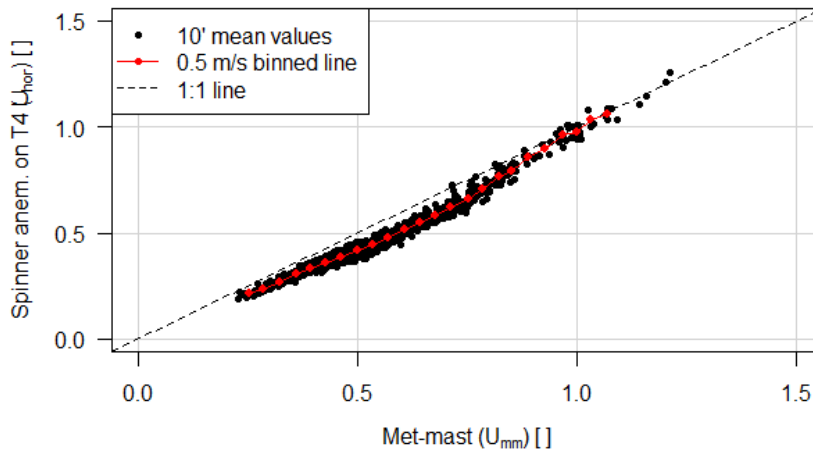


Figure 6. Nacelle transfer function measured with the spinner anemometer of turbine 4. Red line is the NTF obtained by linear interpolation between the red dots, which are the NTF binned values.

6 NTF self consistency check

The black line in Fig. 7 shows the power difference between the PC and the NPC of turbine 4. The blue and red curves shows the pass/fail boundaries defined in IEC61400-12-2 (2013) for the NTF. Both power curves were interpolated to the center of the bin with a cubic spline¹, so that the power values for the two power curves correspond to the same wind speed. Krishna et al. (2014) claimed that a NPC calculated from the same data-set used to measure the NTF (as it is the case for turbine 4) is identical to the PC (and therefore the self consistency check should return zero power difference for any wind speed bin). However in the present calculations the power difference was not zero. The PC was binned according to the met-mast wind speed (U_{mm}), and the NPC was binned according to the corrected nacelle wind speed (U_{free}). Krishna et al. (2014) suggested to bin both PC and NPC according to U_{mm} to keep uniformity in the binning process, but doing so would mean binning the exact same measurements for NPC and PC, resulting obviously in the same binned values of power.

¹as suggested in the draft of IEC61400-12-1, 88/460/CD, regarding presenting a power curve with values interpolated to the center of the bin.

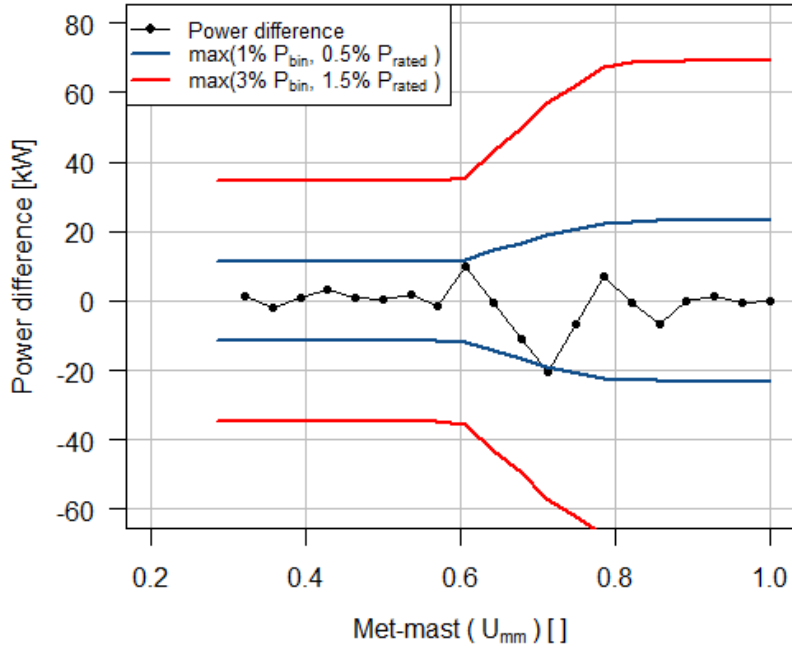


Figure 7. Nacelle transfer function self consistency check. The black curve shows the power difference between NPC and PC of the wind turbine used to measure the NTF. The NTF passes the test if the black curve is within the boundary marked by the blue curve. If the black curve crosses the red curve a new NTF shall be measured.

As mentioned, Krishna et al. (2014) suggest to bin the NTF corrected nacelle wind speed according to the met-mast wind speed U_{mm} to check the validity of the NTF. In the normal use of the NTF the met-mast is not available, and the power curve would be binned according to U_{free} . The procedure to calculate a NPC shall be the same on the reference turbine (where the NTF was measured and verified with the self consistency check) and on other turbines. Therefore it makes more sense
 5 always to calculate the bin averaged power curve binning according to U_{free} . In the procedure used in the present analysis, the bin average of the NTF corrected nacelle wind speed U_{free} are different from the bin average of the measured free wind speed U_{mm} (binning both according to U_{mm}). The cause is explained as follows.

The bin averages are computed by binning according to the same U_{mm} , therefore the binning itself should not make a difference. The spinner anemometer measurements that fall outside the range of definition of the NTF are lost during the
 10 application of the NTF. Therefore the bin average of those utmost bins will most likely be different from the original bin average value. One more reason for the bin average values to be different is that the correction applied with the NTF is applied to the time series through a linear interpolation, not to the bin average value. The binned values of U_{free} and U_{mm} would be equal only if the NTF correction was constant for all the measurements of the bin with a value corresponding to the NTF. When

the NTF is applied to the time series, the slopes of the linear interpolation segments are different on the two sides of the NTF definition point in a certain bin i . In fact in Fig. 9 top-right the red line is not a horizontal straight line.

7 Application of the nacelle transfer function

The NTF measured on turbine 4 was applied on spinner anemometer measurements of turbine 4 and then on turbine 5. Linear interpolation was used between the points that defines the NTF as described in the IEC61400-12-2 (2013) standard. The measurements that fall outside the range of the definition of the NTF are lost, since the NTF is undefined for these measurements. With the application of the NTF, part of the measurements were lost because the NTF was not defined above a certain wind speed (in Fig. 6 the red line does not extend as much as the black points, therefore about 2.5 hours of measurements are lost out of 237 hours).

The relation between free wind speed measured from the met-mast U_{mm} and free wind speed calculated from spinner anemometer measurements U_{free} is shown in the scatter plot of Fig. 8 for turbines 4 and 5.

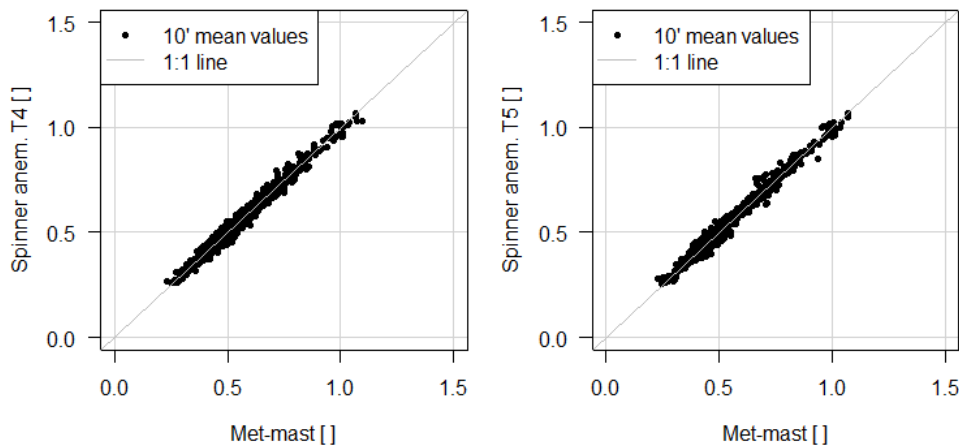


Figure 8. Calculated free wind speed as a function of measured free wind speed. Turbine 4 to the left and turbine 5 to the right.

$$R_{T4}^2 = 0.9839579, R_{T5}^2 = 0.9845664.$$

Since the spinner anemometer was calibrated following the method described in section 3, the spinner anemometer wind speed measurements are already matching the met-mast wind speed at high wind speeds ($U > 1.2$ times rated wind speed), that is when the rotor induction is low. From Fig. 9 we can see that the correction applied by the NTF is mostly localized below rated wind speed.

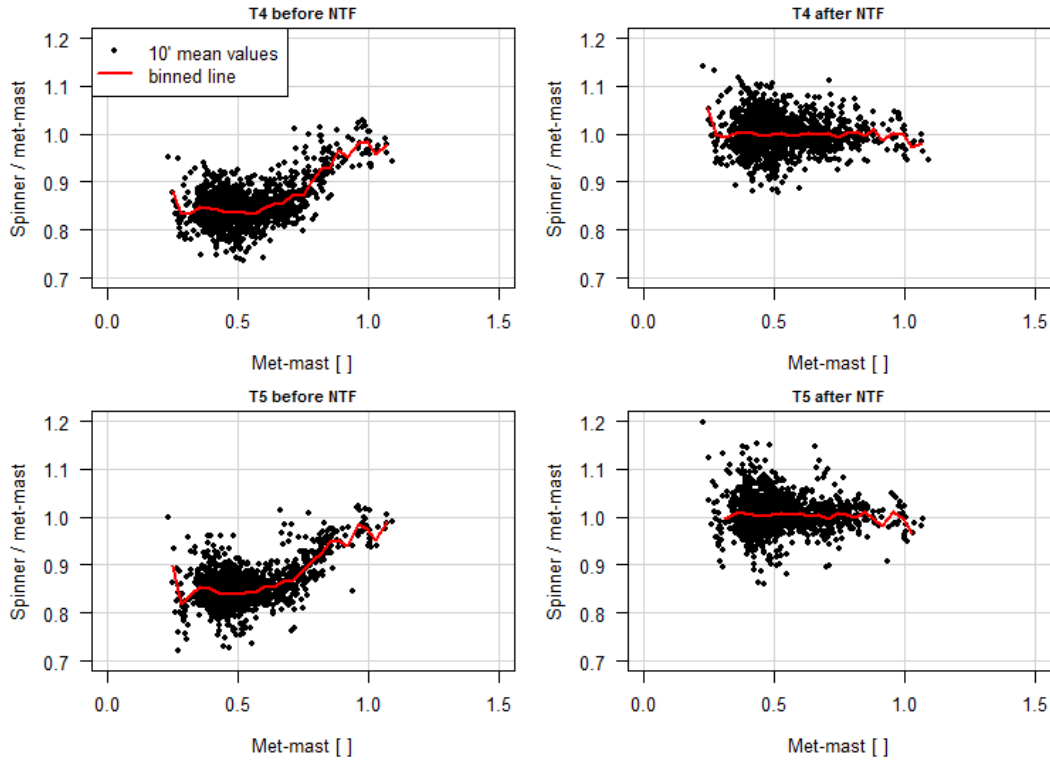


Figure 9. Ratio between calculated free wind speed and measured free wind speed (U_{free}/U_{mm}) as a function of measured free wind speed (U_{mm}).

8 Power curves and AEP

The calculated free wind speed and measured free wind speed were corrected to standard air density of 1.225 kg/m^3 with Eq. 5 after the application of the NTF. This is in accordance with IEC61400-12-2 (2013) for a pitch regulated turbine.

$$U_{free,n} = U_{free} \left(\frac{\rho}{1.225} \right)^{1/3} \quad (5)$$

- 5 The met-mast power curve was also corrected to standard air density of 1.225 kg/m^3 with Eq. 6 in accordance with IEC61400-12-1 (2005) for a pitch regulated turbine.

$$U_{mm,n} = U_{mm} \left(\frac{\rho}{1.225} \right)^{1/3} \quad (6)$$

The power curves of turbines 4 and 5 were obtained by averaging the power in each wind speed bin of 0.5 m/s , see Fig. 10. The value of power was interpolated with a cubic spline to the center of the wind speed bin so that the power values of the four
10 power curves are comparable (they all refer to the center of the wind speed bins).

Figure 10 shows the four power curves, NPC for T4, PC for T4, NPC for T5, PC for T5.

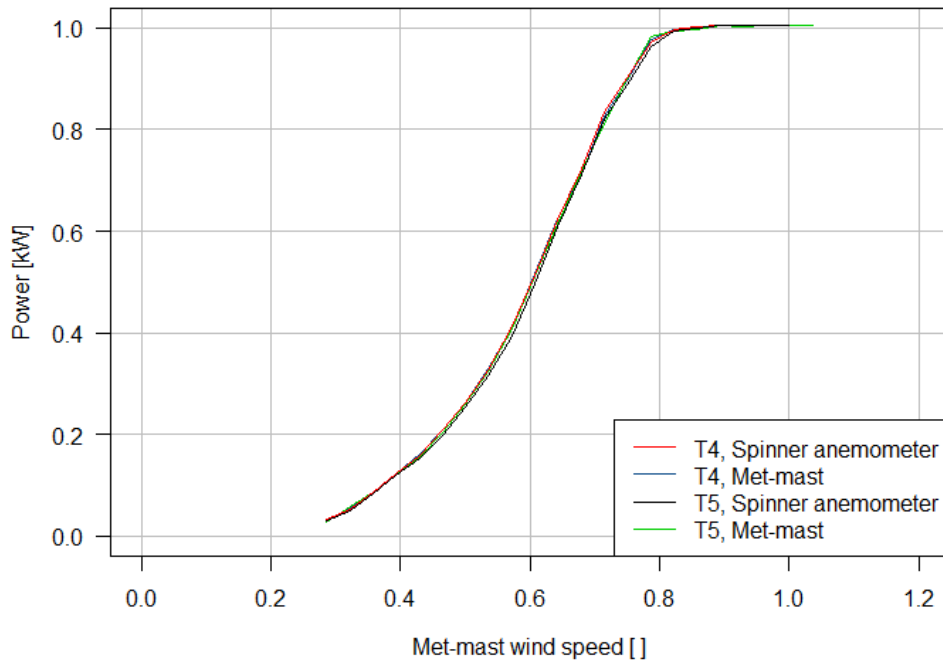


Figure 10. Power curves of turbines 4 and 5, measured with met-mast and with spinner anemometer.

A measure of the difference between the curves was evaluated by calculating the annual energy production (AEP) for a Rayleigh wind speed distribution with annual average wind speed between 4 m/s and 11 m/s. Table 2 shows the difference in AEP estimated for the four power curves. The AEP was calculated for the extrapolated power curve up to 25 m/s.

The nacelle power curve compared with the met-mast power curve within 0.10 % of AEP (at 8 m/s average wind speed) on the reference turbine, and within 0.38 % on the other turbine (see Tab. 2). The NPC is not identical to the PC, as well as the binned values of U_{free} are not equal to the binned values of U_{mm} even when binning both according to U_{mm} .

As expected, PC4 with NPC4 compares better than PC5 with NPC5, since the NTF was measured on T4. The uncertainty on AEP calculated for PC4 in the DTU report I-0440 Demurtas (2015) (with the same turbine and same measurement set-up, but not public for confidentiality of the data presented) was found to be 14.2% for $V_{avg} = 4$ m/s, 5.7% for $V_{avg} = 8$ m/s and 4.2% for $V_{avg} = 11$ m/s. The AEP difference is more than ten times smaller than the AEP uncertainty.

Table 2. Comparison between met-mast power curve (PC) and nacelle (spinner) power curve (NPC) in terms of annual energy production. The values in the table are calculated as $(from/to - 1) \cdot 100$. The AEP was calculated with the extrapolated power curve from valid data to 25 m/s.

V_{avg}	From:	NPC4	NPC5	PC5	NPC5
	to:	PC4	PC5	PC4	NPC4
m/s		%	%	%	%
4		0.10	-1.35	-1.04	-2.47
5		0.14	-0.95	-0.74	-1.82
6		0.13	-0.69	-0.55	-1.37
7		0.12	-0.51	-0.44	-1.06
8		0.10	-0.38	-0.36	-0.84
9		0.09	-0.30	-0.31	-0.69
10		0.07	-0.24	-0.28	-0.59
11		0.07	-0.19	-0.25	-0.51

9 Uncertainty analysis

This section will describe the evaluation of uncertainty of the free wind speed measured with the met-mast, and free wind speed calculated with an NTF applied to spinner anemometer measurements. The spinner anemometer measures the wind speed by means of three sonic sensors and a conversion algorithm. Each sensor was calibrated independently in a MEASNET compliant wind tunnel. The uncertainty of the three velocities were combined through the spinner anemometer conversion algorithm to give the uncertainty of the horizontal wind speed.

The uncertainty of spinner anemometer on T4 due to differences in mounting of the three sonic sensors is zero, since this spinner anemometer was used to measure the NTF. The mounting of the second spinner anemometer (on T5) was compared with the mounting of the reference spinner anemometer (on T4) and an additional uncertainty due to mounting differences with respect to T4 was added to the measurements of the spinner anemometer on T5.

9.1 Uncertainty related to wind tunnel calibration of sonic sensors

The relation between the wind tunnel speed and the velocity component in the sensor path is:

$$V_1 = V_t \cdot \cos(\phi_s) \quad (7)$$

If the angle ϕ_s of the sonic sensor path with respect to the horizontal mounting plate was not measured, one should assume that ϕ_s is within the manufacturing tolerance, $\phi_s = 35^\circ \pm 1.5^\circ$. The standard uncertainty on ϕ_s can therefore be expressed by the tolerance divided by the square root of three as:

$$u_{\phi_s} = (a_+ - a_-)/(2\sqrt{3}) = (36.5 - 33.5)/(2\sqrt{3}) = 0.866^\circ \quad (8)$$

In this case the angle ϕ_s was measured as part of the wind tunnel calibration (see Tab. 1). The uncertainty on ϕ_s depends on the accuracy of the protractor (the instrument to measure angles). In this case, a digital protractor with an accuracy of 0.2° was used, and therefore $u_{\phi_s} = 0.2^\circ$ was used instead of 0.866° .

The uncertainty on the wind tunnel calibration was expressed in the calibration certificates for a coverage factor $k_c = 2$ as a binned value as a function of wind tunnel speed. While the uncertainty is typically almost constant for a cup anemometer, the sonic sensor uncertainty showed increase with wind speed. The standard uncertainty ($k_c = 1$) was calculated by dividing the value reported in the certificates by two. The calibration standard uncertainty (function of wind speed) was fitted to a line as shown in Eq. 9.

$$u_t = (2.24 \cdot V_i + 0.855) \cdot 10^{-3} m/s \quad (9)$$

The uncertainty on the sonic sensor velocity V_1 is obtained combining the uncertainty u_t with the uncertainty u_{ϕ_s} , using the equation for combination of uncertainty of independent variables as expressed in Eq. 10 (according to section 5.1.2 of the GUM, JCGM/WG1 (2008)) and also shown in IECRE (2015) clarification sheet.

$$u_c^2(y) = \sum_{i=1}^N \left(\frac{\partial f}{\partial x_i} \right)^2 u^2(x_i) \quad (10)$$

Equation 10 applied to Eq. 7 results in Eq. 11:

$$u_1^2 = \left(\frac{\partial(V_t \cos \phi_s)}{\partial V_t} \right)^2 u_t^2 + \left(\frac{\partial(V_t \cos \phi_s)}{\partial \phi_s} \right)^2 u_{\phi_s}^2 = \cos^2 \phi_s \cdot u_t^2 + V_t^2 \sin^2 \phi_s \cdot u_{\phi_s}^2 \quad (11)$$

With u_t (Eq. 9) as the uncertainty of the wind tunnel wind speed and u_{ϕ_s} as the uncertainty on the sensor path angle (Eq. 8 or uncertainty of the protractor). The combined uncertainty on V_1 due to wind tunnel calibration is:

$$u_1 = \sqrt{(\cos \phi_s)^2 \cdot u_t^2 + (V_t \cdot \sin \phi_s)^2 \cdot u_{\phi_s}^2} \quad (12)$$

The same applies to each of the sensors (u_2, u_3).

9.2 Evaluation of spinner anemometer mounting

The three sonic sensors should be mounted on the spinner with the best possible rotational symmetry and equal distance from the spinner center of rotation. A visualization method for documentation of the sonic sensors installations was developed by Demurtas and Pedersen with the use of photography, Demurtas (2015). The initial mounting of the sensors was used for the first power curve measurements reported in Demurtas (2015). The accuracy of sensor mounting was then improved and the power curve measurement repeated and reported in this work. The mounting position was evaluated with photography method described in . Due to the challenge of photographing a feature of size in the order of centimeters (the sonic sensor) from a long distance (80 meters from ground to spinner) we used a 400 mm optic zoom and a high resolution digital camera (24 megapixel).

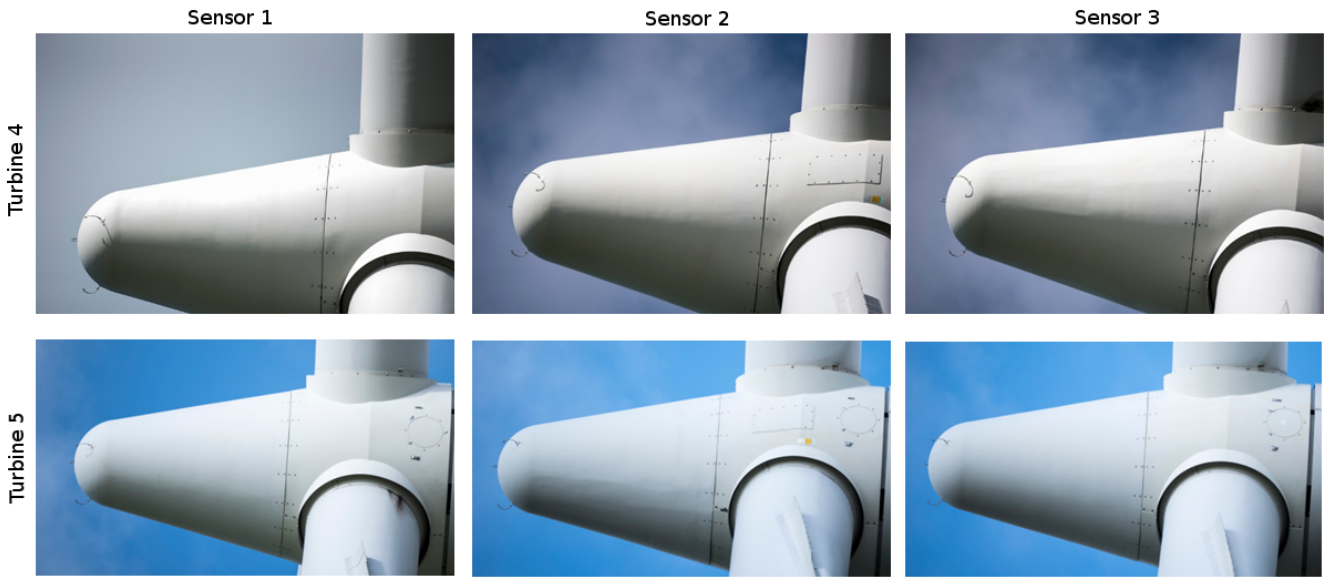


Figure 11. Photos of two spinner anemometers (turbine 4 above, turbine 5 below. Sensors 1, 2 and 3 from left to right.).

Several photos of the spinner were taken from the ground during rotation of the wind turbine and three photos selected each time a sonic sensor is visible on the side of the spinner, with the sky in the background.

Each of the six photos (three for each turbine, Fig. 11) was post processed making it semi-transparent. The photos were overlaid, scaled and rotated in order to make the spinner contour to match. The sky was made transparent and a contrasting red background added (Fig. 12).

The photo overlay was scaled to make the sonic sensor path 16.7 cm long, like it is in reality. The positions of the sonic sensors on the spinner were measured in the plane of the photos as the angle between a plane perpendicular to the spinner axis and the sensors of extreme forward and backwards positions. The position of the sensor paths were measured on the photo with a vector graphic software (inkscape).

The improved mounting of the sensors showed a mounting accuracy in the order of ± 2 cm. This was an improvement of the initial mounting whose accuracy was ± 6 cm. The sensors of the two turbines fell into a mounting angle interval $[a_-, a_+] = [31^\circ, 40^\circ]$ for the old mount, and $[48^\circ, 51^\circ]$ for the improved new mount. In the improved mount the sensors were also moved forward on the spinner, for practical reasons, not to interfere with the old mounting holes.

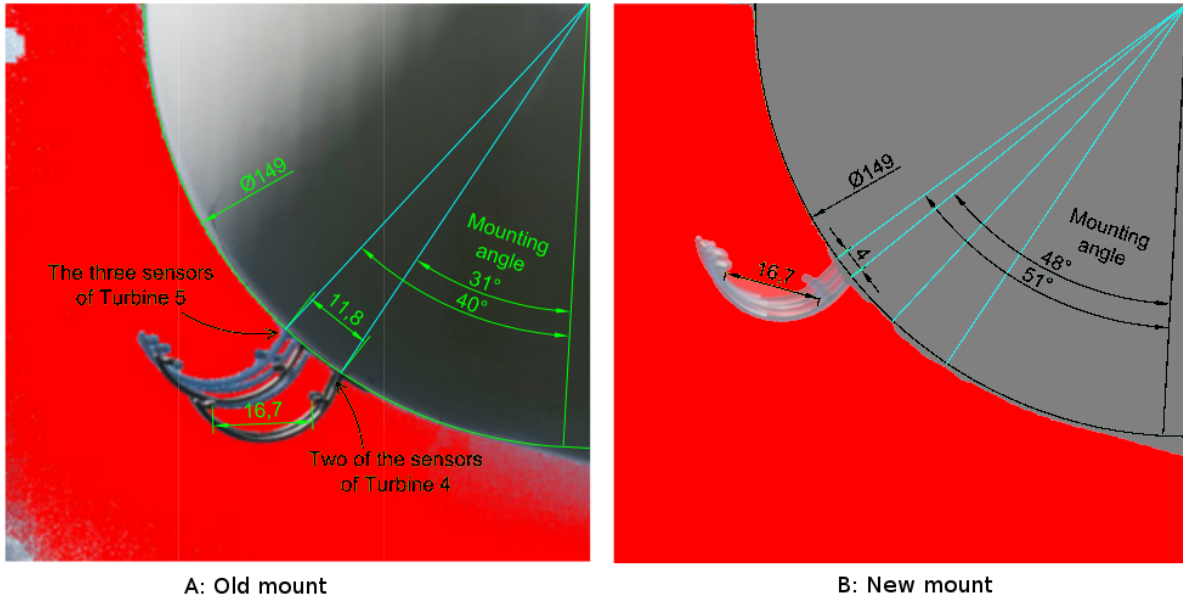


Figure 12. Sonic sensors relative mounting position between turbine 4 and turbine 5. Not to scale, dimensions are in centimeters.

Left: original mounting. Right: after improvement of the mounting accuracy. The blue lines connects the center of the spinner sphere with the extreme mounting position of the sensors. In the figure at the right hand side four blue lines show the position of the original and improved mounting.

9.3 Uncertainty in wind speed measurements due to mounting imperfections

The uncertainty connected to the error in mounting position of the sonic sensor was investigated approximating the spinner as a sphere and using potential flow theory to calculate the flow around a sphere. The mean air velocity along the sensor path was calculated averaging the wind velocity component along the sensor path in three points along the path (points shown with a black or red dots in Fig. 13).

The flow field was calculated for a mesh of 0.01 in x and y direction. The coordinates of each point were converted from cartesian coordinates (x_p, y_p) to polar coordinates (r, θ) with Eq. 13 and Eq. 14. An angle of $\pi/2$ was added to the θ_p coordinate (Eq. 14) to rotate the result in order to have the flow coming from the left parallel to the x axis. This also rotated the origin of the angles to the vertical axis, which is convenient to measure the position of the mounting angles of the sonic sensors.

$$r = \sqrt{(x_p^2 + y_p^2)} \quad (13)$$

$$\theta_p = \arctan(y_p/x_p) + \pi/2 \quad (14)$$

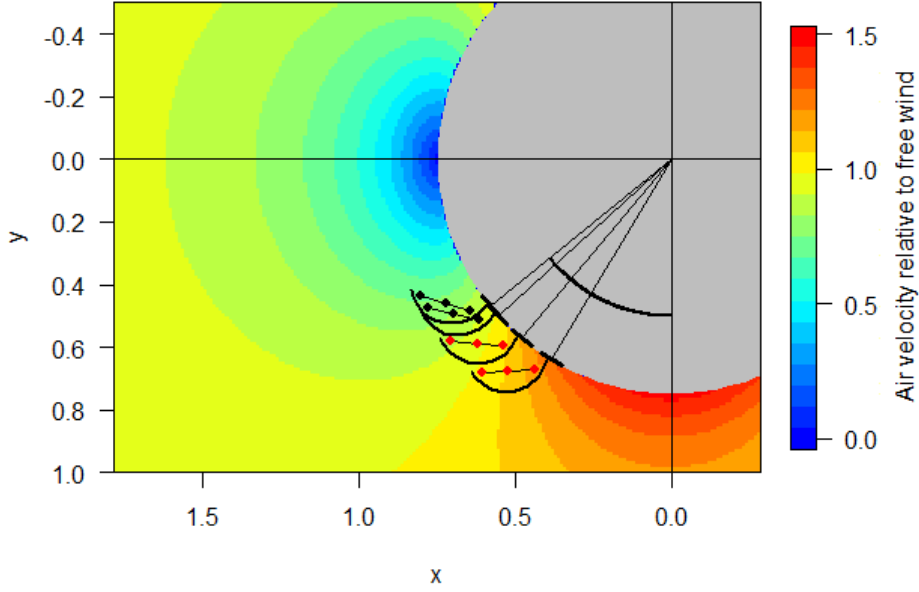


Figure 13. Simulation of the flow around the spinner, which was approximated to a sphere. The flow was calculated with the equations of the potential flow around a sphere. The sensor positions retrace the position of the sensors found in Fig. 12. The sensor paths with the red dots refer to the old mount (31° , 40°), while these with the black dots refer to the improved mounting (48° , 51°), where the sensors are more closely spaced.

The potential flow model is oriented such that the inflow is in axis with the pinner axis of rotation, therefore $U = U_{hor} = U_0$. The flow field was calculated in polar coordinates with Eq. 15 (along radius) and Eq. 16 (perpendicular to radius) with the equations by Faith and Morrison (2013).

$$v_r = U_0[1 - (R/r)^3] \cos(\theta_p) \quad (15)$$

5

$$v_t = -U_0[1 + 0.5 \cdot (R/r)^3] \sin(\theta_p) \quad (16)$$

The modulus of the wind speed was calculated with Eq. 17 and shown with the color scale in Fig. 13.

$$U = \sqrt{(v_r^2 + v_t^2)} \quad (17)$$

The air velocity along the sensor path at the point $p(r, \theta)$ was calculated with Eq. 18, where 35° is the default angle between
10 the sensor path and the sensor root (tangent to the spinner surface).

$$U_p = v_r \cdot \sin(35 \cdot \pi/180) - v_t \cdot \cos(35 \cdot \pi/180) \quad (18)$$

Equation 18 was used to calculate the wind velocity along the sensor path in each of the black points shown in Fig. 13. Then, the mean wind speed along each sensor path was calculated as average value of the velocity along the sensor path in the three points related to each sensor path (Eq. 19).

$$U_{path} = \frac{U_{p1} + U_{p2} + U_{p3}}{3} \quad (19)$$

5 The sensor path wind speed was calculated for each of the four sensor mounting positions measured with the photographic method of Fig. 12, and is presented in Tab. 3. The sensor path wind speed was normalized to the wind speed upstream of the spinner (U_0). The uncertainty due to mounting imperfections is a type B uncertainty ("Guide to the expression of uncertainty in measurements" (JCGM/WG1 (2008), chapters 4.3.1 and 4.3.7). The probability of the sonic sensor wind velocity to be within the interval a_- to a_+ calculated from the positions identified with the photographic method is equal to one and the probability
10 that it lies outside the interval is zero. There is no particular reason for the sensor path wind velocity to fall into the interval in a particular position. Therefore we can assume that the probability that the sensor path wind speed is within the interval is a rectangular distribution. This means that the standard uncertainty is:

$$u_m = (a_+ - a_-)/(2\sqrt{3}) \quad (20)$$

The uncertainty is a value relative to the wind speed upstream of the spinner anemometer (U_{hor}). This uncertainty does not
15 apply to the wind turbine 4 which was used to measure the NTF.

Table 3. Mounting angles, sensor path wind speed and uncertainty due to mounting accuracy.

	Initial mount		Improved mount	
Mounting angle	31°	40°	48°	51°
Sensor path relative speed (U_{path}/U_0)	$a_+ = 0.9864$	$a_- = 0.8940$	$a_+ = 0.7934$	$a_- = 0.7516$
Uncertainty of sensor path wind speed (u_m)	2.7% U_{hor}		1.2% U_{hor}	

9.4 Combination of uncertainties through the spinner anemometer conversion algorithm

This section will explain how to combine the uncertainty on the input quantities to obtain the uncertainty on the output of the spinner anemometer: the horizontal wind speed. The uncertainty on U_{hor} is the combination of the following uncertainty components:

20

- u_1 Sensor 1 wind tunnel calibration (which includes u_t and u_{ϕ_s}).
- u_2 Sensor 2 wind tunnel calibration (which includes u_t and u_{ϕ_s}).
- u_3 Sensor 3 wind tunnel calibration (which includes u_t and u_{ϕ_s}).
- u_m Sensors mounting.

– $u_{k\alpha}$ Angular calibration.

The uncertainty on k_1 is $u_{k_1} = 0$ because all the uncertainty related to wind speed is included in the uncertainty of the NTF (u_{NTF} , see section 9.7). The uncertainties on the sonic sensor speeds (u_1 , u_2 and u_3) are substantially equal but we keep them separated with different names for clarity. U is not measured directly, but is determined from the quantities V_{ave} and α through a functional relationship g :

$$U = g(V_{ave}, \alpha) = \frac{V_{ave}}{k_1 \cos \alpha} \quad (21)$$

α is also not measured directly but is determined from the quantities V_1 , V_2 , V_3 and k_α through a functional relationship f :

$$\begin{aligned} \alpha = f(V_1, V_2, V_3, k_\alpha) &= \arctan \left(\frac{k_1 \sqrt{3(V_1 - V_{ave})^2 + (V_2 - V_3)^2}}{\sqrt{3} k_2 V_{ave}} \right) = \\ &= \arctan \left(\frac{2}{k_\alpha} \frac{\sqrt{(V_1^2 + V_2^2 + V_3^2 - V_1 V_2 - V_1 V_3 - V_2 V_3)}}{V_1 + V_2 + V_3} \right) \end{aligned} \quad (22)$$

V_{ave} is the average between V_1 , V_2 , V_3 calculated with the relationship h :

$$V_{ave} = h(V_1, V_2, V_3) = \frac{1}{3}(V_1 + V_2 + V_3) \quad (23)$$

To calculate the uncertainty on U we need first to calculate the uncertainty on V_{ave} and on α .

The uncertainty on V_{ave} is calculated applying the rule for combination of uncertainties of uncorrelated input quantities (Eq. 10) to the function h (Eq. 23), resulting in Eq. 24 assuming that $u_1 = u_2 = u_3$.

$$u_{ave} = \sqrt{\left(\frac{1}{3}\right)^2 u_1^2 + \left(\frac{1}{3}\right)^2 u_2^2 + \left(\frac{1}{3}\right)^2 u_3^2} = \frac{u_1}{\sqrt{3}}. \quad (24)$$

The uncertainty on the inflow angle α can be calculated combining the uncertainty of V_1 , V_2 , V_3 , and k_α applying Eq. 10 to the function f (Eq. 22), resulting in Eq. 25.

$$u_\alpha = \sqrt{\frac{\partial f}{\partial V_1} u_1^2 + \frac{\partial f}{\partial V_2} u_2^2 + \frac{\partial f}{\partial V_3} u_3^2 + \frac{\partial f}{\partial k_\alpha} u_{k_\alpha}^2} = \sqrt{3 \frac{\partial f}{\partial V_1} u_1^2 + \frac{\partial f}{\partial k_\alpha} u_{k_\alpha}^2} \quad (25)$$

Given the complexity of the function f (Eq. 22) the derivative was computed numerically with the help of a computer.

V_1 , V_2 , V_3 were calculated for a wind speed U in a range 0-25 m/s with Eq. 27 to 29, for six arbitrary values of α , and used to compute the partial derivatives of Eq. 25. The uncertainty on k_α was set to $u_{k_\alpha} = 0.1 \cdot k_\alpha$ as found by Pedersen et al. (2015). In Fig. 14 one can see an uncertainty of about 1° for a inflow angle of 10° .

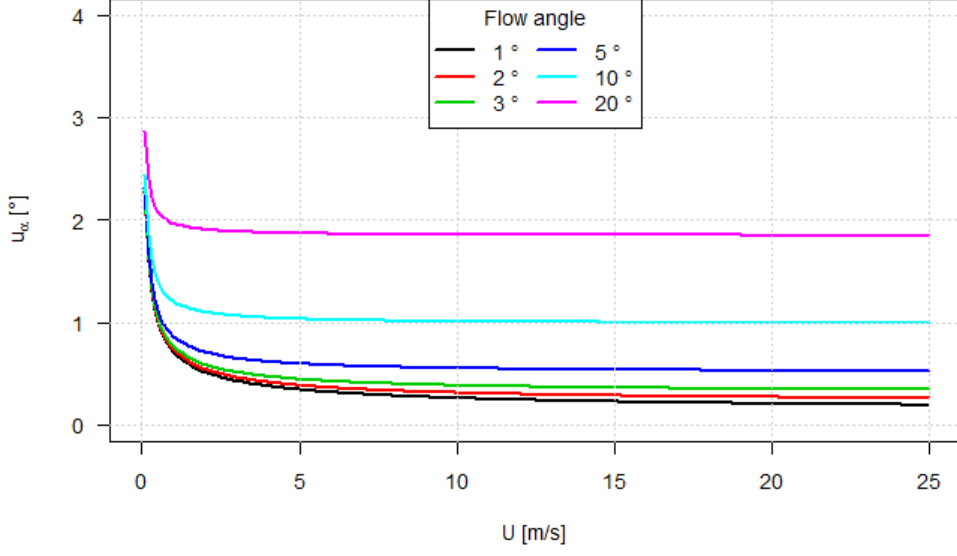


Figure 14. Uncertainty on the inflow angle α .

The uncertainty of the vector wind speed U can be calculated applying the method for combination of uncertainty of independent variables (GUM JCGM/WG1 (2008), Eq. 10) to the function $U = g(V_{ave}, \alpha)$ (Eq. 21), resulting in Eq. 26.

$$u_U = \sqrt{\left(\frac{\partial g}{\partial V_{ave}}\right)^2 u_{ave}^2 + \left(\frac{\partial g}{\partial \alpha}\right)^2 u_\alpha^2} = \sqrt{\left(\frac{1}{k_1 \cos \alpha}\right)^2 u_{ave}^2 + \left(\frac{V_{ave}}{k_1} \frac{\sin \alpha}{\sqrt{1 + \alpha^2}}\right)^2 u_\alpha^2} \quad (26)$$

The uncertainty on U calculated for six arbitrary values of α with Eq. 26. V_{ave} was calculated with Eq. 23 and V_1 , V_2 and V_3 with Eq. 27, 28 and 29. The results are shown in Fig. 15.

$$V_1 = U(k_1 \cos(\alpha) - k_2 \sin(\alpha) \cos(\theta)) \quad (27)$$

$$V_2 = U \left(k_1 \cos(\alpha) - k_2 \sin(\alpha) \cos\left(\theta - \frac{2\pi}{3}\right) \right) \quad (28)$$

$$10 \quad V_3 = U \left(k_1 \cos(\alpha) - k_2 \sin(\alpha) \cos\left(\theta - \frac{4\pi}{3}\right) \right) \quad (29)$$

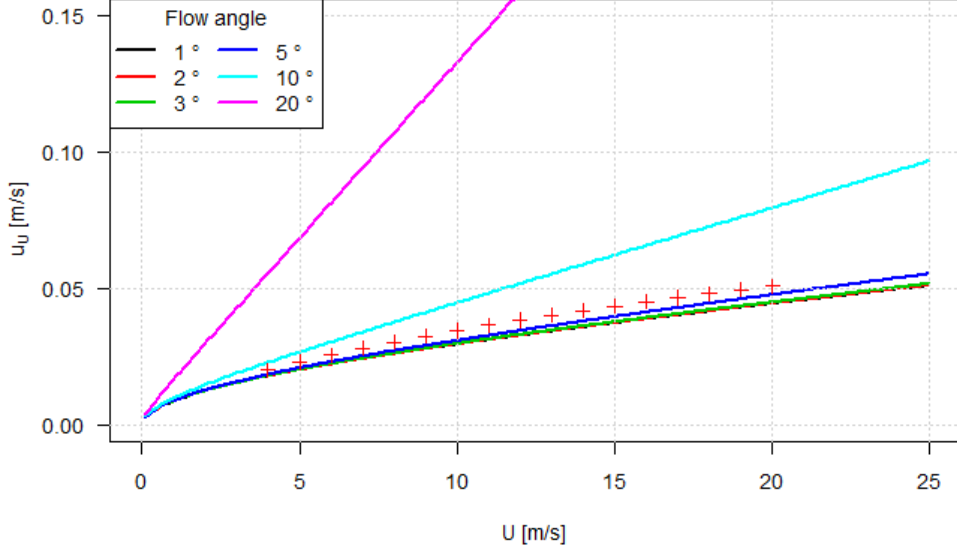


Figure 15. Uncertainty on wind speed (u_U) as a function of wind speed (U), for six possible values of inflow angle α . Red crosses shows the values of uncertainty as a function of wind speed for a common value of inflow angle of 6° .

As seen in Fig. 15, the uncertainty on U is function of the flow angle α . For inflow angles below 5° Fig. 15 shows that the u_U is basically only function of U . A typical average inflow angle to a wind turbine is smaller than 5° , as presented in Pedersen et al. (2014). The uncertainty of the wind speed is typically function of the wind speed only. In order to keep the calculation simple (especially in the calculation of power curve uncertainty), a simple model (Eq. 30, red crosses in Fig. 15) was fitted to the line corresponding to an inflow angle of 6° , which is unlikely to be exceeded on average during normal operation of most wind turbines in a range of wind speeds 4 to 20 m/s.

$$u_U = -0.005 + \frac{\sqrt{U}}{80}. \quad (30)$$

Now that the uncertainty on the wind speed modulus U is known, it is possible to calculate the uncertainty on its horizontal component U_{hor} . By combining the equations of the conversion algorithm (which can be found in Demurtas et al. (2016)), U_{hor} is expressed as:

$$U_{hor} = i(U, \delta, \phi, \theta, \alpha) = \sqrt{(U \cos \alpha \cos \delta - U \sin \alpha \sin(\phi + \theta) \sin \delta)^2 + (-U \sin \alpha \sin(\phi + \theta))^2} \quad (31)$$

The position of the flow stagnation point θ in Eq. 31 is a function of V_1, V_2, V_3 . The rotor position ϕ is calculated based on the accelerometers located in each sonic sensor root. To be absolutely correct, one should apply the method for combination of uncertainty to Eq. 31. However, it is reasonable to assume that $U_{hor} \sim U$ due to the small inflow angle α and that $u_{U_{hor}} \sim u_U$ because the uncertainty on the turbine tilt angle δ and rotor position ϕ is likely to be smaller than the other uncertainty

components. Moreover, the improved accuracy in the estimation of $u_{U_{hor}}$ would be wiped out by the simplification made with Eq. 30. Therefore, the uncertainty on the horizontal wind speed U_{hor} is reasonably equal to the uncertainty on U :

$$u_{U_{hor}} = u_U \quad (32)$$

9.5 Uncertainty of spinner anemometer output

- 5 The uncertainty of the spinner anemometer wind speed measurements of turbine 4 (Eq. 33) is the combination of the uncertainty on the spinner anemometer output ($u_{U_{hor}}$) with the uncertainty due to the discrepancies between different MEASNET wind tunnels ($U_{ME} = 1\%/\sqrt{3}$).

$$u_{s.a.4} = \sqrt{u_U^2 + u_{ME}^2} \quad (33)$$

- 10 The uncertainty on the measurements of the second spinner anemometer (on T5) shall also include the uncertainty due to mounting imperfections to account for the dissimilarity with the reference spinner anemometer (on T4):

$$u_{s.a.5} = \sqrt{u_U^2 + u_{ME}^2 + u_m^2} \quad (34)$$

Figure 16 shows the combination of each uncertainty term to the final uncertainty budgets. As it can be seen in Fig. 16, the uncertainty of the sensor path speed (pink crosses) is very close to the wind tunnel speed (black line), due to the small contribution to the uncertainty coming from the uncertainty of the sensor path angle ϕ_s .

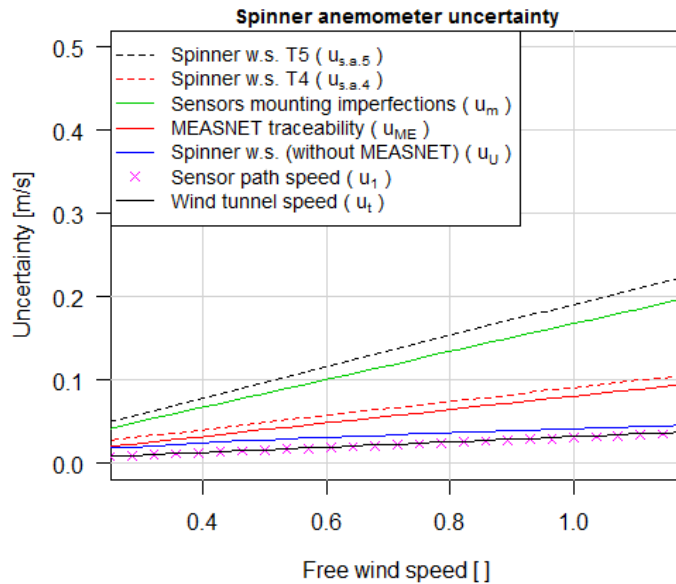


Figure 16. Overview of the size of the various uncertainty components and total uncertainty.

The spinner anemometer conversion algorithm combines the uncertainties of the spinner anemometer input quantities (V_1 , V_2 , V_3 , ϕ) resulting in the blue line of Fig. 16. Once combined with the MEASNET traceability uncertainty (red line) we arrive to the dashed red line. Once including the uncertainty of the mounting imperfection (green line) we arrive at the black dashed line. Among the uncertainty components ascribable to the spinner anemometer, the one due to mounting inaccuracy of the sensors is the largest one. Note that the mounting imperfections are null for the reference spinner anemometer, in fact what matters is that the mounting position of the sonic sensors and the shape of the other spinner anemometers (on T5 in this case) are similar to the reference one (on T4 in this case). All the sonic sensors were calibrated in the same wind tunnel. The MEASNET uncertainty was added to u_U instead of to u_1 , u_2 and u_3 to avoid counting it three times.

9.6 Uncertainty of met-mast measurements

The uncertainty of the met-mast wind speed measurement (Eq. 35, Fig. 17) is (according to IEC61400-12-2 (2013)) the combination of the wind tunnel uncertainty u_t , the MEASNET uncertainty to account the discrepancies between different wind tunnels u_{ME} , the uncertainty due to the cup anemometer class $u_{a.class}$ (that takes into account the response of the cup anemometer to turbulence and flow inclination), and $u_{s.cal.} = 2\%V_i$ because there was no site calibration.

$$u_{mm} = \sqrt{u_t^2 + u_{ME}^2 + u_{a.class}^2 + u_{s.cal.}^2} \quad (35)$$

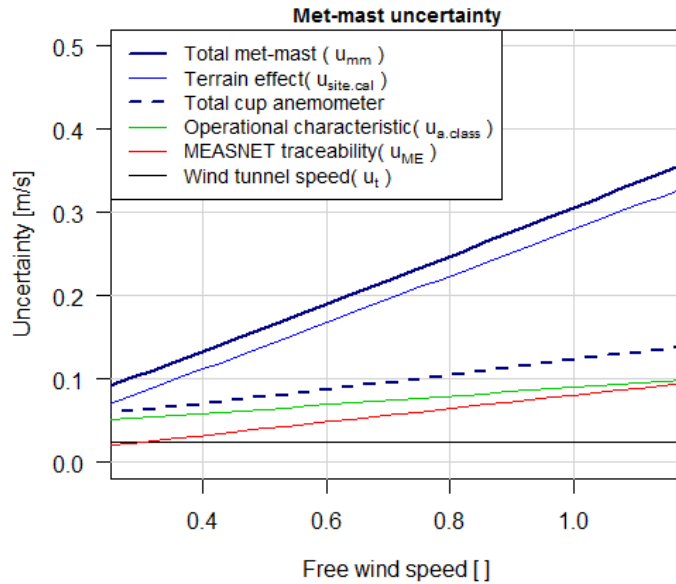


Figure 17. Overview of the size of the various uncertainty components and total uncertainty.

9.7 Uncertainty of NTF

The uncertainty on the NTF (u_{NTF}) is the combination of the various uncertainty components as:

$$u_{NTF} = \sqrt{u_{mm}^2 + u_{sa4}^2 + u_M^2 + s_{NTF}^2} \quad (36)$$

where

5 u_{mm} is the uncertainty on the measured free wind speed.

u_{sa} is the uncertainty of the spinner anemometer measurements.

u_M is the uncertainty due to the NTF method, considered 2% of the wind speed due to seasonal variations ($u_M = 0.02V_i$) in the standard IEC61400-12-2.

10 s_{NTF} is the statistical uncertainty of the captured data-set ($s_{NTF} = \frac{\sigma_{NTF}}{\sqrt{N_j}} U_{sa4}$). σ_{NTF} is dimensionless because it is the standard deviation of the ratio U_{free}/U_{sa4} .

9.8 Uncertainty on calculated free wind speed

To measure the absolute power curve of a wind turbine the spinner anemometer output must be corrected to free wind speed by use of the nacelle transfer function (NTF). The uncertainty on the free wind speed is therefore a combination of $u_{s.a.}$ with u_{NTF} .

$$15 \quad u_{free5} = \sqrt{u_{sa5}^2 + u_{NTF}^2} \quad (37)$$

For the case of the reference wind turbine (T4, used to measure the NTF) the uncertainty is calculated differently. u_{NTF} already contains the uncertainty of the reference spinner anemometer (T4) and the uncertainty of the met-mast measurements. Therefore the uncertainty of the free wind speed calculated with the NTF is just the uncertainty of the NTF (Eq. 38).

$$u_{free4} = u_{NTF} \quad (38)$$

10 Results of uncertainty analysis

The mounting accuracy was investigated by overlaying six photos of the spinner taken from ground level during rotation, each showing the corresponding sensor when it is at the side of the spinner. The photos unveil deviations in the order of ± 2 cm between some of the sensors. It was expected that the mounting imperfections played a major role in the total uncertainty of the second spinner anemometer. However, the contribution of other uncertainty sources combined (the $1/\sqrt{3}\%$ MEASNET traceability of wind tunnel calibrations for cup-anemometer on the met-mast and spinner anemometers sensors, the 2% for lack of site calibration) was much larger than the uncertainty due to the mounting of the sensors (which was 1.2%).

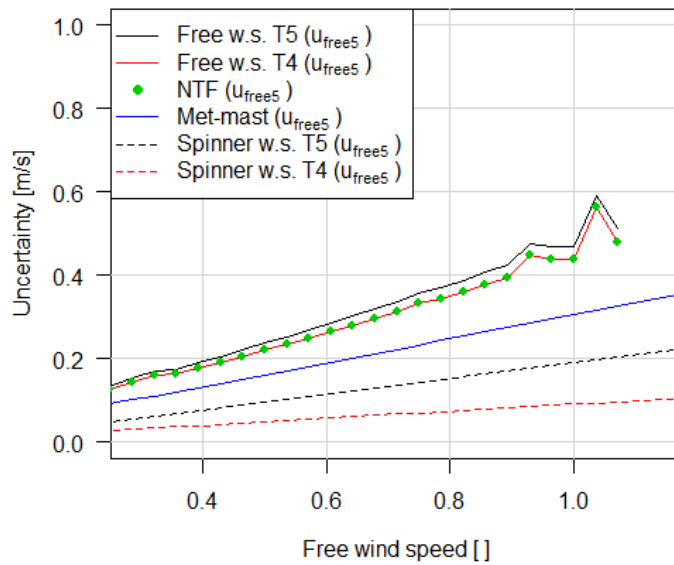


Figure 18. Uncertainty on wind speed. The met-mast wind speed includes 2% additional uncertainty due to lack of site calibration.

As shown in Fig. 18, the uncertainty of the NTF is larger than the met-mast uncertainty, as expected. The met-mast uncertainty is larger than the spinner anemometer uncertainties (dashed lines) because of the 2% added due to missing site calibration, which does not apply to the spinner anemometer output (but applies to the NTF later to calculate the free wind speed). The turbine T5 has a larger uncertainty than the reference turbine, as expected, due to the mounting imperfections. Note that the distance between the two dashed lines is due to the mounting imperfections, but the impact of such imperfections is significantly reduced once the uncertainties on the spinner anemometer output are combined with the NTF uncertainty.

11 Discussion

The main goal of this study was to measure the power performance of a wind turbine using a spinner anemometer which was calibrated with the calibration determined on a “reference” spinner anemometer on an identical wind turbine. The calibration (k_α and k_1 values) determined on the reference spinner anemometer can be moved to a second spinner anemometer estimating an additional uncertainty due to the mounting differences. This is only possible if the two spinners have the same outer shape. The mounting differences (and associated uncertainty) could be completely avoided if the positioning of the sonic sensors was exactly equal between the reference spinner, and another spinner. This geometric perfection could be achieved with the collaboration of the manufacturer of the spinner, by integrating the sensor mounting fittings in the mould, so that all the spinners comes out identical.

10 The spinner anemometer was calibrated for wind speed measurement, so that it reads the wind speed correctly in a condition of zero induction (stopped rotor, or operation at high wind speed). While this step is not essential because this correction can be included in the NTF, it is convenient to use the NTF to only correct the induction. When the spinner is calibrated for wind speed measurements, a change in the spinner anemometer configuration (for example move the sensors to another point on the spinner) can be accounted with a new k_1 , and the NTF stays unvaried.

15 Apply the same NTF on another turbine is reasonable only if the wind turbine control strategy and the rotor are identical to the reference turbine. This requirement however could be removed if further research can demonstrate that the induction at the rotor centre (what matters for the spinner anemometer) is unvaried for changing rotor diameter or control strategy.

The uncertainty due to discrepancies between MEASNET wind tunnels ($u_{ME} = 1\%/\sqrt{3}$) was combined with the uncertainty of the spinner anemometer output wind speed (u_U), while a more correct approach would have been to include u_{ME} in the wind tunnel uncertainty u_t . The first approach was used to keep the analysis of propagation of uncertainties (through the spinner anemometer conversion algorithm) free from contributions of constant terms (such as u_{ME}), which would otherwise have masked the contribution attributable to the sole spinner anemometer conversion algorithm.

25 Adding the MEASNET uncertainty to the spinner anemometer output instead of to the input does not lead to a significant error in the total uncertainty, since the effect of the conversion algorithm on the uncertainties is small (as shown in Fig. 16 by the small distance between the pink crosses and the blue line, which is basically all due to the 10% uncertainty on k_α).

If the spinner anemometer of the reference turbine (T4) is replaced, the uncertainty of the new spinner anemometer should be added to the NTF uncertainty ($u_{free4} = \sqrt{u_{NEWsa4}^2 + u_{NTF}^2}$). If the data set used to calculate NPC on T4 is different to the one used to measure the NTF, the type A uncertainty of the new data set shall be added to the NTF uncertainty ($u_{free4} = \sqrt{u_{NTF}^2 + s_{NEWsa4}^2}$).

30 Each sonic sensor (three for each spinner anemometer) should be calibrated in the wind tunnel and the results of the calibration set in the spinner anemometer conversion box (the procedure is explained in Demurtas (2014)). If a sensor fails and is replaced, the new wind tunnel calibration values should be set in the conversion box. If the sensors are not calibrated, a new (more difficult) calibration of k_1 should be made every time a sonic sensor is replaced.

The reference spinner anemometer should be calibrated in flat terrain. The calibration of the spinner anemometer for wind speed measurements and the measurement of the NTF can, in practice, be done with any free wind speed measurement device (met-mast, nacelle lidar or ground based lidar). In complex terrain, a spinner anemometer should be assigned the calibration and NTF measured on an identical wind turbine in a flat terrain. The free wind speed calculated applying the NTF to the spinner anemometer measurements in complex terrain will provide a free wind equivalent to the one of a flat site, with no need for site calibration.

A large flow inclination can also be expected in a wind farm environment. The spinner anemometer is well suited to measure in the wake of other turbines (turbulent flow with large flow inclination angles). However it has to be kept in mind that the spinner anemometer is a point measurement, compared to the rotor swept area. If the rotor is partially operating in the wake of another turbine there will be a reduced power output, but the spinner anemometer measurement (which is not interested by the wake) would not be representative of the average wind condition over the swept area.

12 Conclusions

The study investigated the methods to evaluate the power performance of two wind turbines using spinner anemometers.

The power curves of two adjacent wind turbines (T4, T5) were measured by means of a common traceable calibrated met-mast and spinner anemometers on each turbine. All sonic sensors were calibrated in a traceable wind tunnel. T4 was the reference turbine. The reference spinner anemometer installed on T4 was calibrated with respect to angular and wind speed measurements to take into account the shape of the spinner and the mounting position of the sensors. The spinner anemometer on T5 instead, was assigned the calibration constants of the reference spinner anemometer. Similarly, the NTF (Nacelle Transfer Function) was measured on the reference turbine T4 and applied to both turbines. The four power curves of the two turbines (two met-mast power curves and two spinner anemometer power curves) were compared in terms of AEP (Annual Energy Production). The nacelle power curves compared very well with the met-mast power curves for a range of annual average wind speeds. The uncertainty of the spinner anemometer wind speed measurements was analyzed in detail, taking account of the propagation of the uncertainty through the spinner anemometer conversion algorithm. Some small approximations were made.

The sonic sensor mountings were verified with photos taken from the ground and a method for estimation of uncertainty related to mounting imperfections was proposed. The uncertainty on the free wind speed calculated with the NTF was mostly due to the uncertainty of MEASNET traceability and lack of site calibration. In less significant part the uncertainty was due to the spinner anemometer sensor calibration and mounting imperfections.

In summary, under the condition that the mounting of the sonic sensors are very similar to the reference mounting, power performance measurements with use of spinner anemometer can be made within 0.38% difference in AEP for an annual average wind speed of 8 m/s.

Appendix A: List of symbols

- α Wind inflow angle relative to the shaft axis.
- β Flow inclination.
- δ Wind turbine tilt angle.
- 5 F_1 Calibration factor mainly related to wind speed calibration.
- F_α Calibration factor related to angle calibration.
- γ Yaw misalignment.
- ϕ Rotor azimuth position (equal to zero when sonic sensor 1 is at top position, positive clockwise seen from the front of the wind turbine).
- 10 ϕ_s Angle of the sensor path respect to the mounting plate.
- k_1 Calibration constant mainly related to wind speed calibration.
- k_α Calibration constant related to angle calibration.
- k_2 Calibration constant (equal to $k_\alpha \cdot k_1$).
- m Slope coefficient of the wind tunnel calibration equation (generic).
- 15 q Offset of the wind tunnel calibration equation (generic).
- R Radius of the sphere approximating the pinner.
- r Radial coordinate in a polar coordinate system.
- θ Azimuth position of the flow stagnation point on the spinner measured clockwise from sensor 1.
- U Wind speed vector modulus ($U = \sqrt{U_{hor}^2 + w^2}$).
- 20 U_{hor} Horizontal wind speed (calibrated).
- $U_{hor,d}$ Horizontal wind speed (measured with default values $k_{1,d}$ and $k_{2,d}$).
- $U_{hor,d,c}$ Horizontal wind speed (calibrated with correct k_α but not correct k_1).
- U_{mm} Horizontal wind speed measured by the met-mast at hub height.
- $U_{mm,n}$ Horizontal wind speed measured by the met-mast at hub height, corrected to standard air density.

- U_{free4} Free wind speed calculated with the nacelle transfer function from spinner anemometer measurements (turbine 4).
- U_{free5} Free wind speed calculated with the nacelle transfer function from spinner anemometer measurements (turbine 5).
- U_0 Free stream inlet wind speed used in the potential flow analysis.
- u_1 Uncertainty on V_1 .
- 5 u_t Uncertainty on V_t .
- u_m Uncertainty on wind speed due to mounting imperfections.
- u_M Uncertainty due to the NTF method (seasonal variations equal to $0.02 V_i$).
- u_{ME} Uncertainty to account for the discrepancies between different MEASNET wind tunnels.
- u_{mm} Uncertainty on U_{mm} .
- 10 u_{sa4} Uncertainty on wind speed measurements of the spinner anemometer mounted on turbine T4.
- u_{sa5} Uncertainty on wind speed measurements of the spinner anemometer mounted on turbine T5.
- V_1 is the wind speed in the sensor path 1.
- V_2 is the wind speed in the sensor path 2.
- V_3 is the wind speed in the sensor path 3.
- 15 V_{ave} Average wind speed of sonic sensors.
- V_{avg} Annual average wind speed used to calculate the wind speed probability distribution.
- V_i Center wind speed of bin i .
- v_r Velocity component along radius in a polar coordinate system.
- v_t Velocity component perpendicular to radius in a polar coordinate system.
- 20 V_t Wind tunnel air speed.
- w Vertical wind component.

Appendix B: List of abbreviations

C _p	Power coefficient of a wind turbine	s. a.	Spinner anemometer
IEC	International Electrotechnical Commission	SN	Serial Number
NPC	Nacelle power curve	T4	Turbine 4
5 NTF	Nacelle transfer function	T5	Turbine 5
PC	Power curve	10	

Acknowledgements. Romo wind A/S is acknowledged for the good collaboration along the project and for the help to provide the spinner anemometer and power data of the Nørrekær Enge wind farm. Vattenfall A/S is acknowledged for providing access to the wind turbines used in the test and the help for installation of the met-mast. This work was performed under the EUDP-2012-I project: iSpin (J.nr 64012-0107).

Chapter 6

Power curve with Dynamic Data Analysis

Chapter 5 demonstrated how to measure the power curve of a wind turbine by using the spinner anemometer and the method of bins applied to 10 minute averages. The collection of a sufficient amount of 10 minute measurements requires typically few weeks of good wind conditions. The possibility of the spinner anemometer to sample the wind at high frequency (up to 20 Hz) and the good correlation with the wind turbine power opens the possibility for determining the power curve of a wind turbine in a shorter time.

The content of this chapter was developed and written as part of the Fastwind project, which results are available in [12]. The experimental set-up used to collect the measurements was the same as the one described in chapter 5, with the sole difference that the met-mast was not used in the analysis and the spinner anemometer was not calibrated for simplicity (as the primary focus of this chapter is on the level of agreement between different methods of analysis more than the absolute values of the power curve).

A reference power curve was determined with the method of bins applied to 126 hours of 10 minute averages. Then, three different methods were applied to 4 hours of 10 Hz measurements:

1. Method of bins applied to 4 hours of 10 Hz measurements.
2. Method of bins applied to 4 hours of 10 Hz measurements averaged to 1 Hz.
3. Langevin method [17–21] applied to 4 hours of 10 Hz measurements averaged to 1 Hz.

The resulting three power curves were compared to the reference power curve.

6.1 Introduction

The wind turbine was part of the same wind farm described in Chapter 5. The turbine under consideration was the 4th counting from west. The rotor diameter was 90 m and the hub height 80 m. The wind turbine was equipped with a spinner anemometer. At a direction of 215 degrees from the wind turbine there was an IEC61400-12-1 compliant met-mast instrumented with cup anemometer at hub height and wind vane on a boom at 78 m height. The sampling frequency was 10 Hz for both the spinner anemometer and the electric power output

6.2 Reference power curve from 126 h of measurements and the method of bins

The wind speed was simultaneously measured by the met-mast and by the spinner anemometer installed on the turbine. The selected valid wind direction sector as calculated from the IEC standard was 101-229 degrees. However we only used 120 to 210 degrees (according to the 10 Hz wind turbine yaw position), which is 90 degrees wide and is centered onto the direction 165 degrees to have some safety margins to avoid wind turbine wakes. A narrower sector should increase further the correlation between mast wind speed and turbine power. The spinner anemometer was calibrated for yaw misalignment measurements [15], but the wind speed calibration and the nacelle transfer function were not determined. As a consequence, the power curve by the spinner anemometer differs significantly from the one by the met-mast (Figure 6.1).

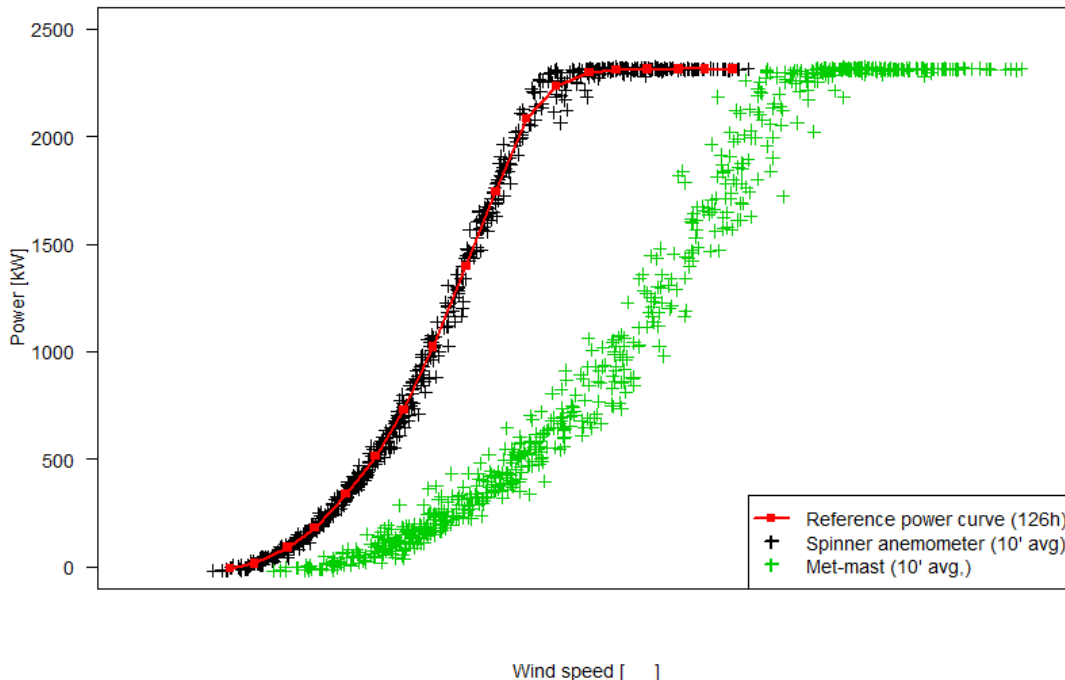


Figure 6.1: Power curve by met-mast (green) and spinner anemometer (red) without a calibration factor. Scatter plot showing 126 hours of simultaneous measurements. The x scale was suppressed for confidentiality of the measurements.

This discrepancy is not an issue for the present analysis, which aims at comparing relative power curves calculated with different methods of analysis. Therefore, the power curve shown in red in Figure 6.1 (obtained by binning the spinner anemometer 10 min measurements) is used as the reference power curve and other power curves (presented in section 6.3 and 6.5) are related to it. The data from the met-mast (green crosses in Figure 6.1) are not used.

The correlation between power and wind speed is much better for the spinner anemometer than for the met-mast, as seen by the low scatter of the black crosses as compared with the green crosses in Figure 6.1. This is a result of the reduced distance between the wind speed sensor and the turbine rotor.

6.3 Method of bins applied to 4 hours of spinner anemometer measurements

The periods of measurements were selected in order to cover the whole wind speed range. Four periods of one hour were identified, as shown in the (not continuous) time series of Figure 6.2. The periods are (UTC+1 time, or Danish normal time) : 2014-09-15 h 06-07; 2014-12-08 h 09-10; 2014-12-08 h 15-16; 2014-12-02 h 08-09

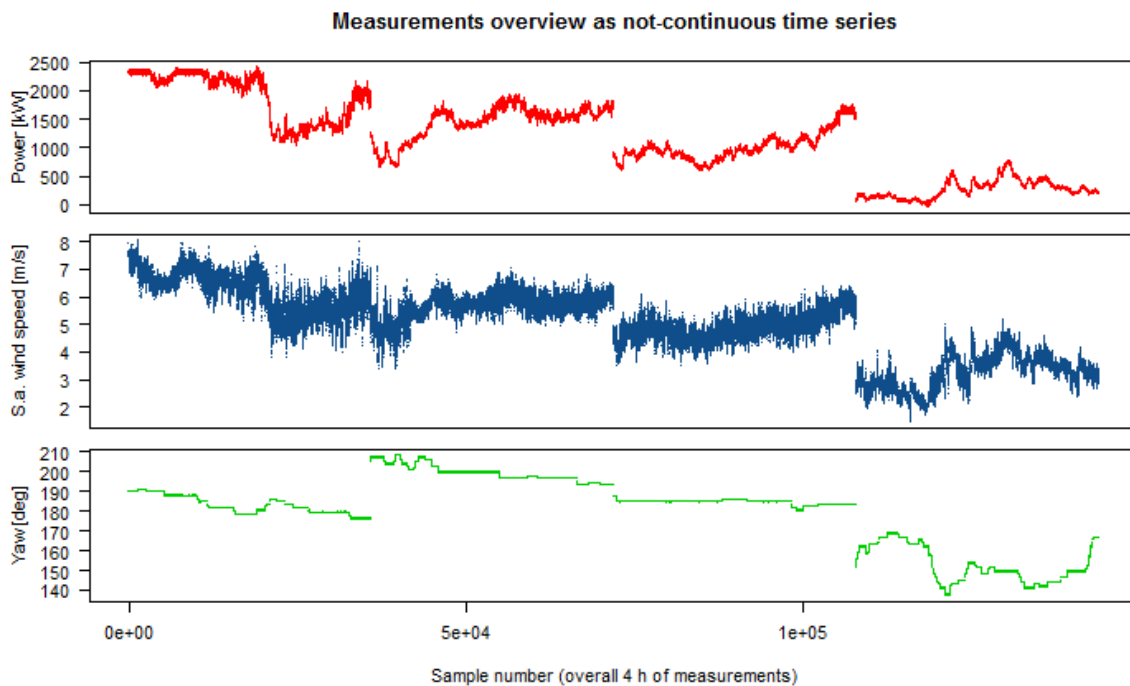


Figure 6.2: Not continuous time series of the four hours of measurements of 10 Hz data used for the DDA. Red is the power output, blue is the horizontal wind speed by the spinner anemometer (not calibrated values). Green is yaw position of the wind turbine (approximating the wind direction).

A scatter plot of 10 Hz data between wind speed and power is shown in Figure 6.3. The same data averaged to 1 Hz are shown in Figure 6.4. The scatter is seen to be reduced significantly, as well as the amount of data is reduced ten times.

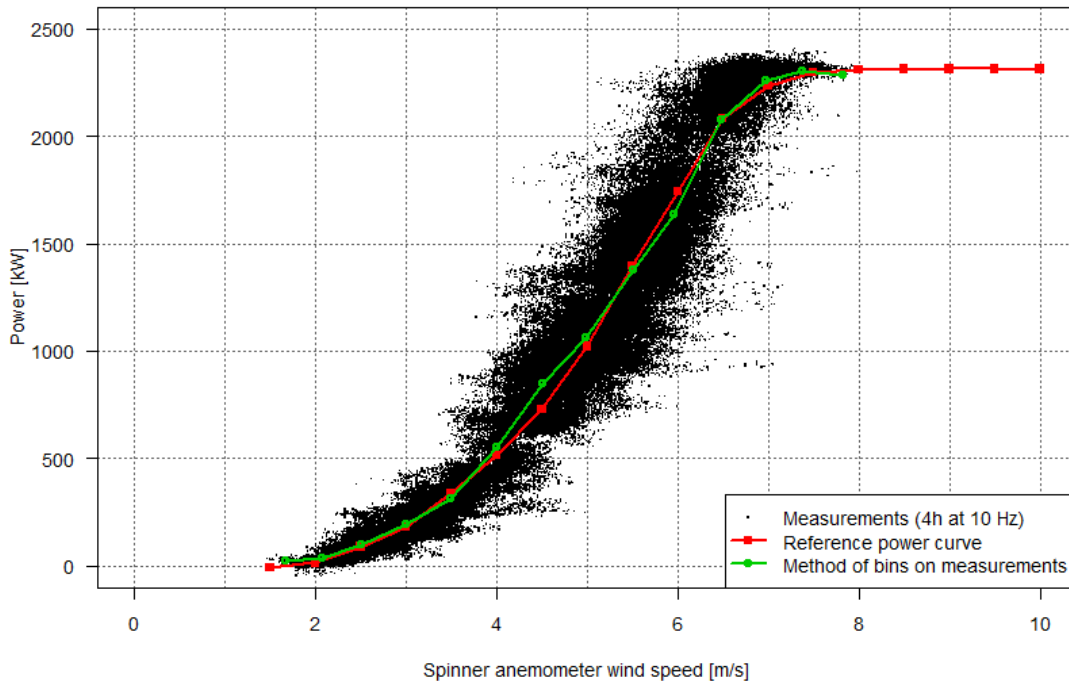


Figure 6.3: Fast power curve data. In black 10 Hz sampled data, 4 hours in total. In red binned reference power curve with IEC standard 10min averaging. In green binned power curve with 10Hz data

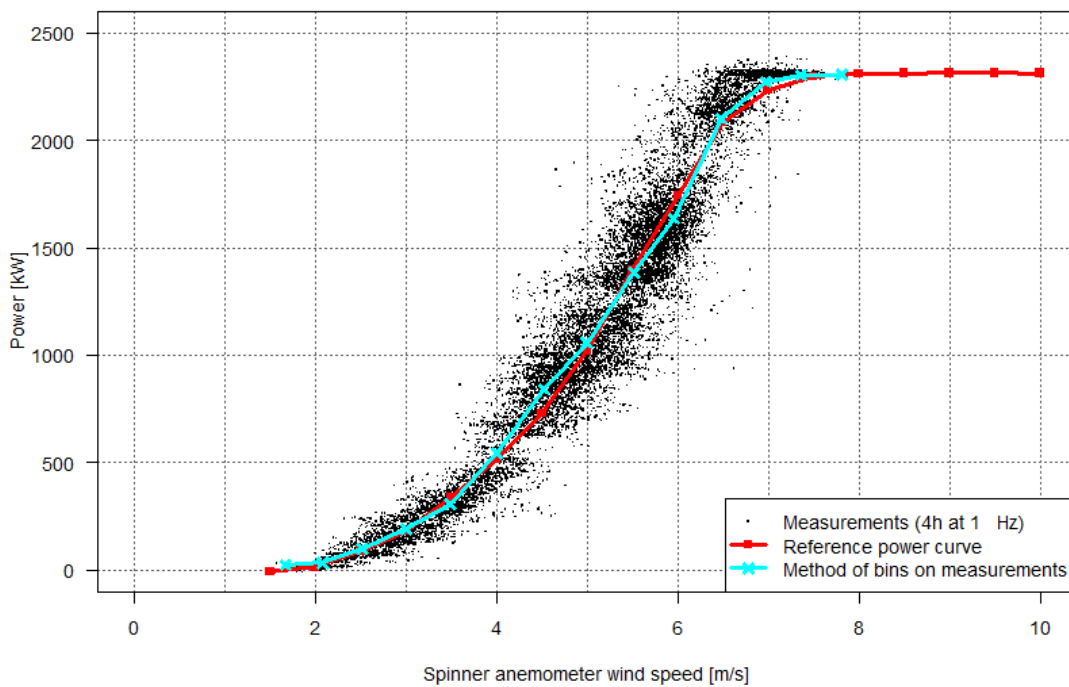


Figure 6.4: Fast power curve data. In black 10 Hz measurements averaged to 1 s, , 4 hours in total. In blue binned power curve with 10 Hz measurements averaged to 1s.

The deviations between the reference power curve (red curve in Figure 6.4) and the fast power curve (blue curve in Figure 6.4) seems to be due to the uneven distribution of measurements along the power values. This is more visible in Figure 6.5.

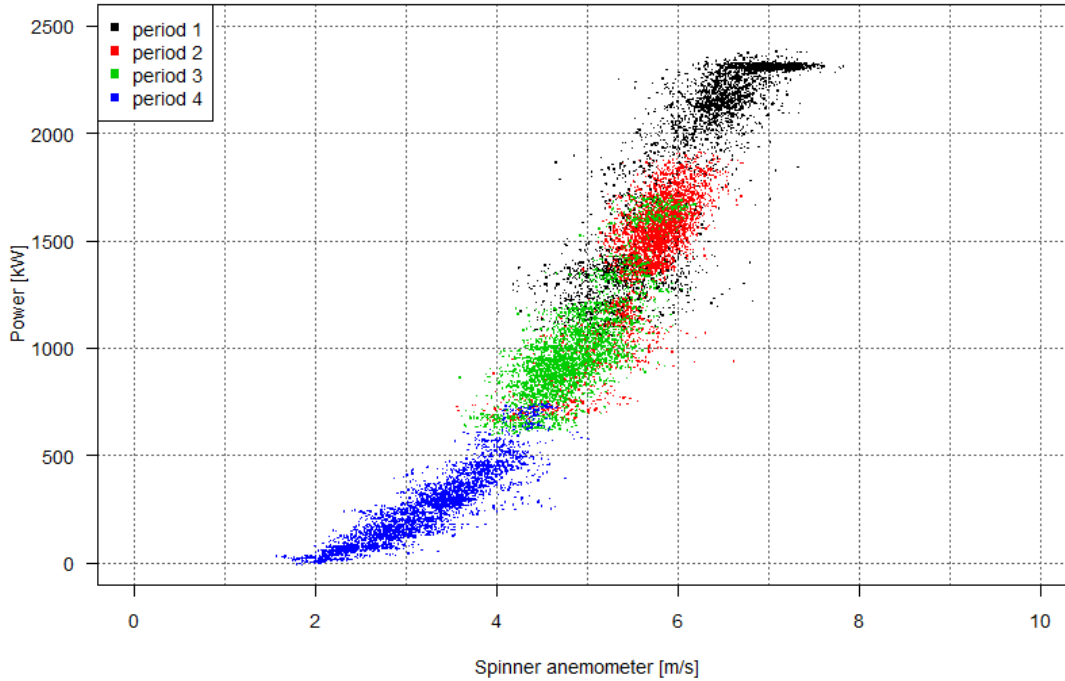


Figure 6.5: 10 Hz measurements averaged to 1 s, 4 hours in total, shown with a colour for each hour of the data-set.

Few measurements in a certain power bin will increase the uncertainty of the average bin power (and speed). Missing values of power (due to insufficient amount of data, or an uneven distribution along the power curve) will result in a deformed average value. As seen in Figure 6.5, there is a gap in power between the four data sets. This is clearly visible also in the count of the measurements binned according to the power (Figure 6.6).

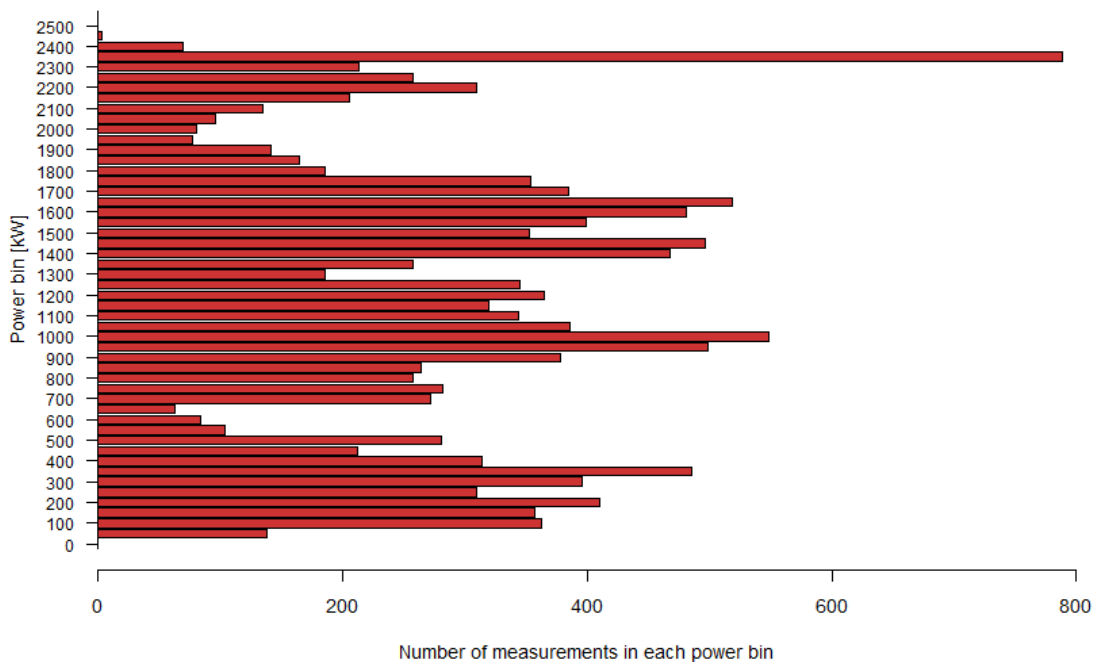


Figure 6.6: Number of measurements in each power bin

6.4 The Langevin method

The Langevin power curve method which was proposed by researchers at Oldenburg University [17–21] uses measurements sampled at high sampling frequency. From the Nyquist-Shannon sampling theorem, for a correct reconstruction of the signal the sampling frequency should be at least twice higher than the maximum frequency present in the signals for power and wind. Due to the nature of wind and electric power of a wind turbine, where signal frequencies may reach a few Hz a practical sampling frequency of at least 10 Hz should be used. As a result of this short period between measurements, the correlation between the wind speed and the power is much lower compared to a standard IEC power curve made with 10 min averaged measurements. The scatter is therefore higher than what is normally seen for an IEC power curve made with 10 min averaged values.

The concept behind the Langevin method lays in the model of the dynamics of the power curve where the power output is considered as a set of univariate Langevin processes which lead to definition of the drift and of the fixed points [22]. The drift is a measure of the tendency of the power to increase in time (positive drift) or to decrease (negative drift) in time. The fixed points identify the power curve, through a value of power and a value of wind speed. There is one fixed point for each wind speed bin. The scatter in the measurements cause some measurements to be located above the power curve (hence above a specific fixed point of power), while others are located below. Points above the power curve will generally tend to have a decreasing power (negative drift), since the power tend to go towards the fixed point. However, the average drift must be based on a high variety of drift values for each wind speed bin. In [17] it was found that the influence of the wind direction on the correlation between wind speed and power was important, and for the analysis a wind sector of 25° was

used, centred on the direction between met-mast and wind turbine.

6.4.1 Drift field reconstruction

The objective of this step of the calculation is to determine, for each wind-power bin the value of the drift. The drift is found for the time step τ going towards zero:

$$D_i^1(P) = \lim_{\tau \rightarrow 0} \frac{1}{\tau} \langle P(t + \tau) - P(t) | u_i \rangle \quad (6.1)$$

For each specific wind and power bin, the drift is calculated as follows:

- Investigate the change of power in the original time series for a time step τ .
- From each time series, find $\Delta P = P(t + \tau) - P(t)$ and let τ be going towards zero (eventually make a linear regression through origin) for several τ values, i.e. 1 to 10).
- Average the power differences $\langle \Delta P \rangle$ for each time step. At this point, averaged time series should show a tendency to increase for the power bins below the power curve, and a tendency to decrease for the bins above the power curve.
- Find the drift from the average power difference divided by the time step $\langle \Delta P \rangle / \tau$ find the drift by making a linear fit of ΔP function of τ forced through the origin. The procedure is repeated for each wind speed and power bin, so that a complete drift field is obtained.

At present the Langevin method as described in [18–21, 23–26] sets no requirement regarding the amount of measurements in each power bin, as absolute value as well as difference to neighboring bins.

6.4.2 Simplified drift field reconstruction

The drift is defined for $\tau \rightarrow 0$. However, the simplest way to calculate the drift on the basis of discretized data is to simply calculate the difference between two consecutive values of power. $\Delta P = P(t + 1) - P(t)$. This can easily be made on the original time series, obtaining a drift time series. The drift is not calculated where the time series is not continuous. The drift should for the turbine sizes examined in the project be within a range of about ± 100 kW/s. Higher rate of change of the power is likely to be the result of some problem in the analysis or in the measurements rather than a real (extreme) variation of power. However, it might be observed in some cases. A condition of a minimum number of measurements might be used prior to calculation of the mean drift in a wind and power bin, to avoid excessive variability.

6.4.3 Fixed points determination

The fixed points are determined from the drift field. The objective is for a specific wind speed bin to find the zero drift. The drift coefficient of a specific bin is plotted as function of power. The drift graphs should show a decreasing drift for increasing power. A linear fitting might be applied, and the value of the fixed point (in kW) be found for drift equal to zero. For some bins there might be several crossings, however, of the zero. In [17] it is suggested to do an integration of the drift over the power variation and take the absolute minimum of the integral plotted as a function of power. In [22] it is suggested to interpolate the drift values with a cubic spline.

6.4.4 Application summary of the Langevin method

The Langevin method was summarized in the following steps:

1. Load the time series measurements of u_i (horizontal wind speed), P_i (power output), ρ_i (air density).
2. Normalize power (stall regulated rotor) or wind speed (actively controlled rotor) of time series data to standard air density with the method described in the standard IEC61400-12-1 [1] to find u_{in} and P_{in} .
3. Calculate $P_{in}(t + \tau) - P_{in}(t)$ of the normalized power data from the time series data using the smallest appropriate τ where the time series is continuous in time. Filter out measurements where it was not possible to calculate ΔP_n .
4. Make a binning of wind speeds of 0.5 m/s bin size centered on full and half wind speeds.
5. Make a binning of power into an appropriate amount of bins, for example about 50 bins.
6. Average all wind speeds in each wind speed bin to obtain the wind speed fixed point $u_{fixed} = \langle u_{in} \rangle$
7. Average all ΔP_n 's for each power bin to find $\langle \Delta P_{i,j} \rangle$
8. Find the drift coefficient $D_{i,j} = \langle \Delta P_{i,j} \rangle / \tau$ to obtain the drift for each power bin
9. For each wind speed bin make a plot of the drift as a function of power bin and determine the fixed point as $P_{fixed} = P | D_{i,j} = 0$
10. Table and plot the power curve P_{fixed} as a function of u_{fixed}

6.5 Langevin method applied to 4 hours of spinner anemometer measurements

The data-set analyzed by use of the Langevin method is the same described in section 6.2 (4 hours of 10 Hz spinner anemometer and power measurements, which were averaged down to 1 Hz). The major difficulties encountered were the determination of a robust value of the power fixed point. In fact, while the drift was expected to be decreasing in a wind speed bin for increasing power, we observed a not clear tendency. See for example the positive drift near a negative drift in bin corresponding to 5 m/s. in Figure 6.7.

The same data showed with colors in Figure 6.7 are shown as drift as a function of power in Appendix D. Each plot corresponds to a column of Figure 6.7. In each figure of the Appendix, the vertical segment shows the value of power of the reference power curve. The drift curves (red) are crossing the zero drift (horizontal black line) in correspondence of the vertical blue mark. This value of power was obtained simply fitting a linear regression (blue line) to the drift curve. Due to the unclear shape of the drift curve, it was impossible to identify a better fitting method.

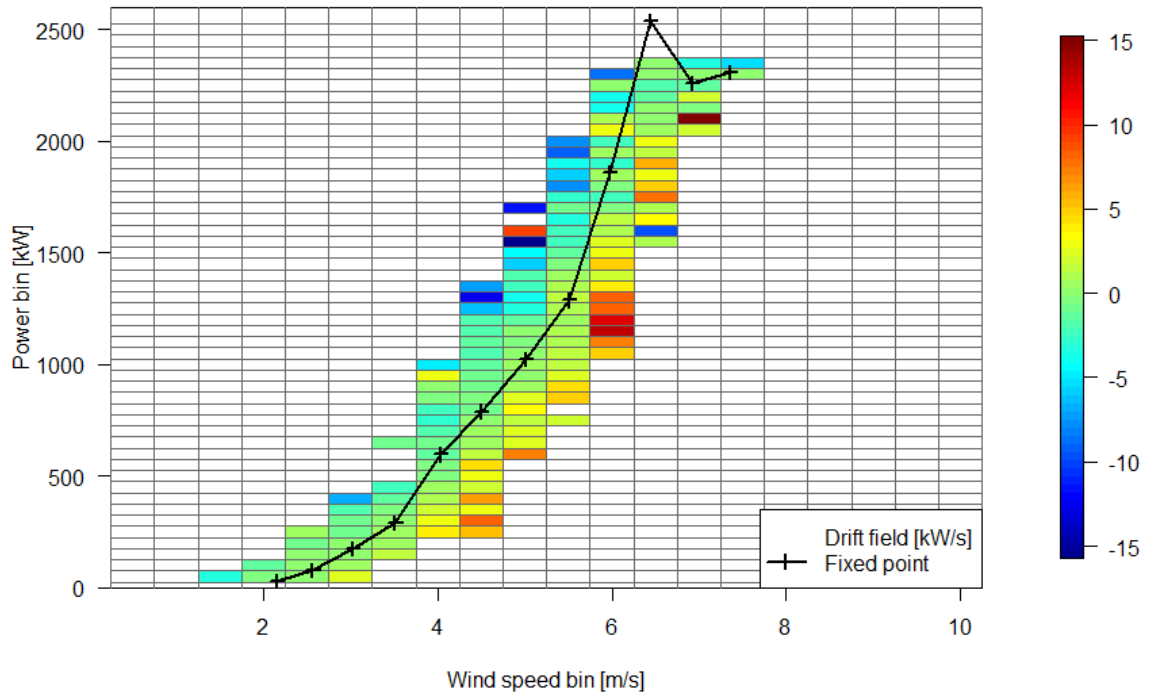


Figure 6.7: Drift field and Langevin power curve (power bin is 50 kW)

6.6 Comparison of DDA methods

The power curve used as reference for comparing the methods was made on the basis of 126 hours of spinner anemometer measurements and the method of bins. The deviations from the reference power curve shown in Figure 6.8 are better represented in Figure 6.9, where the vertical scale shows the difference between each of the three methods and the reference power curve. The deviation between use of the method of bins or use of the Langevin method seems comparable.

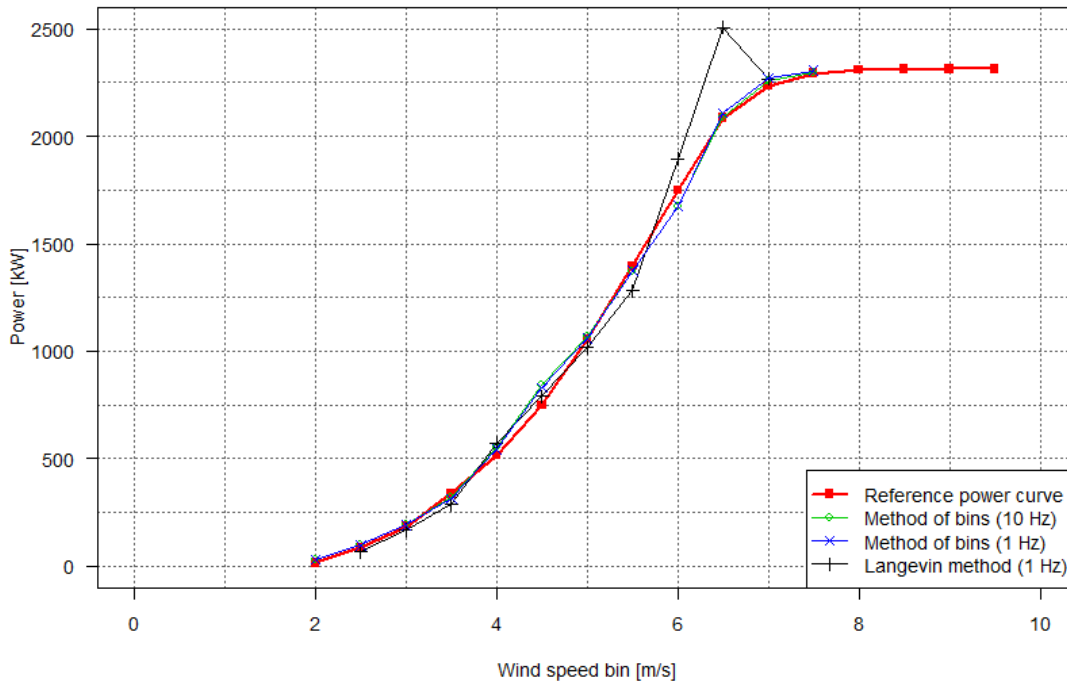


Figure 6.8: Figure 10 Comparison of power curves made with different methods.

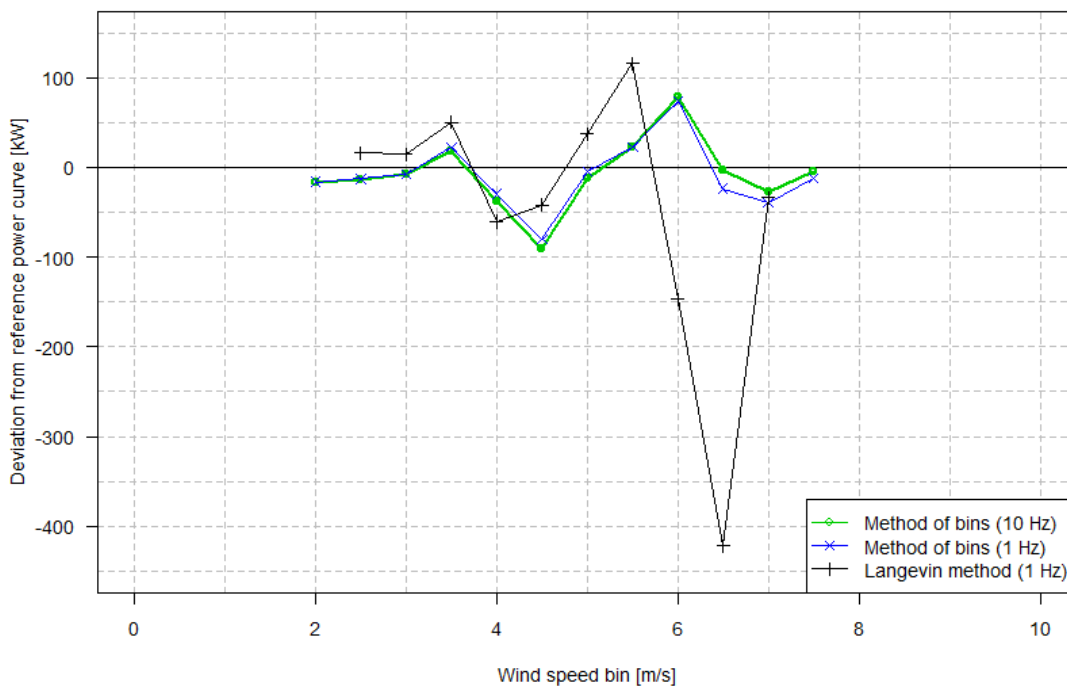


Figure 6.9: Drift field and Langevin power curve (power bin is 50 kW)

6.7 Conclusion on DDA methods

In the Fastwind project the Langevin power curve measurement method was used on real power curve measurement data sets. The purpose was to evaluate methods for making faster power curves. The Langevin method was developed by several authors in the past by applying the method to a theoretical power curve where noise was added. Several authors concluded that the method worked well and that it had potential for making faster power curves, which means a power curve of comparable uncertainty by use of a reduced observation time.

Analysis of the Langevin method with spinner anemometer data showed that the fixed points were very sensitive to bin size and also to the requirement of minimum amount of data in each bin. For the spinner anemometer measurements the Langevin method failed to produce acceptable power curves that were comparable to the IEC measured power curve with 10min data. Simple binned averaging of data with shorter time averages gave significantly better results than the Langevin power curve method. With 1 second averages the power curve was very similar to the IEC measured power curve with 10min averages. For determination of fast power curves or dynamic data analysis the preferred method seems to be the simple binned averaging of short time averages. Especially for measurements with spinner anemometry this method seems to have good potential thanks to the high cross correlation between wind speed and power measurements.

Chapter 7

Conclusions

The main goal of this PhD was to investigate the use of spinner anemometer for power performance measurements. Traceability, calibration and uncertainty analysis are central topics to evaluate the power performance of a wind turbine in an accurate, and traceable way. The PhD study developed a new method for the calibration of a spinner anemometer compared to the past. Calibration requirements were defined in relation to the specific use of the sinner anemometer:

1. Yaw misalignment (and flow inclination) sensor for wind turbine operation.
2. Wind speed sensor for wind turbine operation.
3. Wind speed sensor for power performance measurements according to IE61400-12-2.

The conclusions are here organized by answering one by one the research questions proposed in chapter 1.

7.1 Specific conclusion

1. How to calibrate a spinner anemometer?

Remove a spinner from an erected wind turbine to place it into a (large) wind tunnel is not a feasible solution. Therefore the calibration should follow a different approach. Several methods were investigated, where the spinner anemometer is calibrated using the natural wind. Most of the methods investigated are based on postprocessing of non calibrated spinner anemometer measurements. Besides the basic calibrations (zero wind calibration, wind tunnel calibration of individual sonic sensors, internal calibration of spinner anemometer to account for mounting imperfections), the spinner anemometer should undergo two calibrations: the first one is for flow angle measurements (yaw misalignment and flow inclination), while the second one is for wind speed measurements.

Several methods for calibration of angular measurements were proposed during the PhD. The most recent and robust one is the WSR (wind speed response) method. This method consist in yawing the stopped wind turbine several times in and out of the wind while recording at high sampling frequency (10 Hz) the yaw misalignment and wind speed measured by the spinner anemometer. Once the test is complete, the data are calibrated iteratively to find a value of F_α that minimizes the dependency of wind speed to the yaw misalignment. The F_α values found for 4 tests for the exact same rotor position were within $\pm 2.7\%$ of the mean

value. A yawing span of $\pm 60^\circ$ was recommended for the analysis, however the turbine shall be yawed further than this angle ($\pm 90^\circ$ recommended, reading in the wind turbine controller display) to compensate for initial offset error in the yaw position and wind speed direction change during the test.

Regarding the calibration for wind measurements, it is important that the spinner anemometer is calibrated for flow angle measurements before undertaking the wind speed calibration, as it will notably simplify the equation needed to calculate F_1 . Several methods were developed, two of which were based on comparison with a met-mast wind speed measurement during operation or stopped condition of the wind turbine. According to the calibration correction factor F_1 (F_1 is the ratio between spinner anemometer horizontal wind speed and free horizontal wind speed in a condition of zero induction), the correct method to determine F_1 is by using a stopped turbine. However stopping the wind turbine for a long period is unwanted due to the consequent energy loss. Therefore the calibration was performed with the wind turbine in operation at high wind speed (low rotor induction effect). The calibration correction factor F_1 was then the mean ratio between the spinner anemometer horizontal wind speed and free horizontal wind speed. The method was found to be applicable for a pitch regulated turbine. For a calibration on a stall regulated turbine the condition of having F_1 to stabilize to an asymptotic value was not met (the wind speed was not high enough and the induction was still significant and decreasing).

2. How to ensure traceability?

The traceability of measurements is ensured through the individual calibration of 1D sonic sensors in a wind tunnel. The sensor calibration values are set into the spinner anemometer settings. In this way, if a sensor is replaced, the new values are set into the spinner anemometer conversion box and there is no need to repeat any other calibration.

3. How to use a spinner anemometer for power performance measurements?

Once the spinner anemometer is calibrated, it will measure correctly the wind when the turbine is stopped. The NTF will then correct the rotor induction when the turbine is in operation. The NTF was binned according to the met-mast wind speed (which differs from IEC61400-12-2 which requires to bin according to the spinner anemometer wind speed). The NTF self consistency check with this method was still not zero, and the check is still necessary.

The calibration values k_α , k_1 , and the NTF measured in a flat site on a reference turbine (T4, which spinner anemometer was calibrated comparing with a met-mast) were used on a second turbine (T5) of exact same model. Over all, use of the spinner anemometer was demonstrated to be able to measure the power performance of both wind turbines very well, within 0.1% of AEP of met-mast measurements on T4 or within 0.38% AEP on T5. The uncertainty on wind speed measurements due to spinner anemometer mounting imperfections and uncertainty on k_α was very small compared to the contribution due to NTF, met-mast, site effects, and MEASNET wind tunnel variations. If the spinner anemometer is used for relative power performance measurements (which compare the turbine performance to itself or to other identical turbines over time) there is no need for wind speed calibration and NTF, and the total uncertainty may be significantly be reduced.

4. How is the uncertainty of spinner anemometer measurements evaluated?

The uncertainty on the spinner anemometer output values (such as yaw misalignment and horizontal wind speed) is evaluated through combination of the uncertainty of the input values

(the three velocities measured by the 1D sonic sensors). The uncertainty on the input values comes from the wind tunnel calibration certificates. There is no uncertainty associated to the k_1 calibration because it is included in the NTF. The uncertainty on k_α was assumed 10% (the repeatability of the result was found within $\pm 8.5\%$ in a series of eight repeated calibration tests performed on the same turbine). The combination of uncertainty involved an extensive use of partial derivatives, which were computed numerically due to their complexity. The uncertainty was not only depending on the wind speed, but also on the flow angle. At the end, the result presented in chapter 5 was simplified to the following expression of the uncertainty on horizontal wind speed in m/s, as a function of horizontal wind speed:

$$u_{U_{hor}} = -0.005 + \frac{\sqrt{U_{hor}}}{80} \quad (7.1)$$

The equation is valid for spinner anemometers similar to the one used for the uncertainty analysis in chapter 5. Specifically, the uncertainty due to mounting and wind tunnel calibration should be equal or lower, and the calibration constants should be similar to $k_\alpha = 1.4$ and $k_1 = 0.6$.

5. Is it possible to avoid individual calibration of spinner anemometers?

Yes, as long as the mounting position of the sonic sensors and the spinner outer shape are identical. An additional uncertainty must be introduced due to the mounting differences between the reference spinner anemometer (on which the calibration values were measured) and the other spinner anemometer. The mounting position of the individual sonic sensors could be measured by means of photos of the spinner taken from ground level during operation of the wind turbine, as it was presented in chapter 5. The sonic sensors should be calibrated in the wind tunnel, unless the uncertainty of a non calibrated sensor is acceptable.

6. What are the impacts of mounting imperfections of the sonic sensors?

The uncertainty for sensor mounting imperfections shall not be considered on the reference wind turbine (the one used for the wind speed calibration and NTF measurement). The other turbines will have an uncertainty due to the dissimilarity with the reference wind turbine.

A geometric difference of 4 cm lead to a wind speed uncertainty of 1.2%, which is a minor contributor to the total uncertainty of the free wind speed calculated with the NTF. This was an improvement of an initial mounting whose uncertainty was 2.7% for a tolerance of 12 cm.

The major contributors are the NTF uncertainty, the met-mast uncertainty, the 2% due to lack of site calibration, and the MEASNET variability $1/\sqrt{3}\%$. The uncertainty due to mounting could be easily reduced further by reducing the mounting tolerances.

7. Is there any advantage in using short time averages to measure a power curve?

The spinner anemometer wind speed measurements correlate with the wind turbine power, better than the met-mast (which is at a considerable distance from the turbine) and better than a nacelle anemometer (where flow is disturbed by the blade roots and nacelle body). This allows for use of shorter time averages. 10 min. measurements were used to determine a reference power curve with the method of bins. Fast sampled measurements were analyzed with the Langevin method and with regular binning of 1s averages. The simple binning (as of IE61400-12-2) gave a power curve close to the reference power curve. The Langevin method gave a similar result with exception of some bins, which failed completely to estimate the correct power. A number of parameters had to be chosen to apply the Langevin method,

such as the width of the power bins, and the method to calculate the fixed point from the drift curve. Because of the better result, the lack of arbitrary parameters and its simplicity, the method of bins is still the most appropriate to analyze fast sampled measurements, with the advantage of broadening the wind speed distribution.

8. What minimum time is required to measure a power curve?

Wind speed is always sampled at high frequency (typically 10-20 Hz for sonic anemometers and 1-5 Hz for cup anemometers) and the measurements averaged to 10 minute averages. A shorter averaging time (or no averaging) can help to broaden the wind speed range covered by the measurements. It was found that the wind speed and power probability distribution plays a major role in providing a good power curve. A power curve was made with 4 hours of high frequency measurements which were selected to cover as best as possible the power interval from zero to nominal power. The four hours were selected over a period of measurements of 2.5 months. So, the answer to this question is related to the wind conditions more than to the instrumentation or method of analysis.

7.2 Recommendations for future work

The spinner anemometer has proven to be suitable to measure yaw misalignment and power performance of wind turbines. However, very few wind turbines in the world are equipped with this instrument. As of the current state of development, the areas in which there are possible improvements to do are:

1. **Calibration methods.** The existing methods for calibration of flow angle measurements should be validated in a flow with no turbulence. Practically this could be done in a large wind tunnel.
2. **Mounting accuracy.** The procedures to mount the sonic sensors on the spinner of a wind turbine which is already erected shall be improved to reduce the mounting accuracy. The mold used to cast the spinners shall be modified to mark with absolute accuracy the position for sonic sensors, or even embed the sensor fittings in the fiberglass infusion. This is to ensure the best geometric accuracy and make sure that all the spinner anemometers are identical, for a certain spinner model.
3. **Spinner anemometer classification.** The evaluation of uncertainties shall be simplified further. The uncertainty related to wind tunnel calibration is typically the same for different 1D (one dimensional) sonic sensors. The uncertainty due to mounting can also be considered constant if the tolerance of the mounting is constant. An expression of the uncertainty as a function of wind speed and calibration constants could be developed. The simplification could follow the approach that was used for the classification of cup anemometers.
4. **Yaw control.** Up until now the spinner anemometer has been used for correction of static yaw misalignment, by correcting the mounting offset of the wind direction sensor on the roof of wind turbines. A dedicated collaboration with a wind turbine manufacturer could integrate the spinner anemometer signals in the wind turbine control system.

5. **Condition monitoring.** Method of data analysis to detect power performance changes of a wind turbine should be developed and tested. For this, it is not necessary to calibrate the spinner anemometer. Initial recordings must define what is the normal behaviour of the wind turbine, and some boundaries set at a certain distance would trigger an alarm when exceeded.
6. **Generalized NTF,** investigation of the rotor center induction. It could be that the rotor center induction is very similar among different wind turbine control strategies, or different rotors, or even different wind turbine models. If so, it would be possible to define a generalized NTF to use with spinner anemometers to calculate free wind speed.
7. **New IEC requirements to wind and power database.** The DDA (Dynamic Data Analysis) has shown that the shape of the probability distribution of the power can affect the shape of the power curve made with binning as a function of wind speed. This was evident when analysing 4 hours of 1 Hz data, but it would also affect a power curve made with many hours of measurements (the IEC requirements are 180 h of measurements and at least 30 minute of measurements in each bin). Would it be more appropriate in the IEC method to insert a limit on the difference in number of measurements between adjacent bins? or, would it be better to have the same amount of measurements in each bin?
8. **NPC in complex terrain.** The spinner anemometer could give much better insight of the wind conditions inside a wind farm as well as in complex terrain, that is in all those situations of turbulent and not horizontal wind. The spinner anemometer should be installed in all the wind turbines of a large offshore wind farm.
9. **NPC in wind farm environment.** The spinner anemometer can not detect if a part of the rotor disc is operating in the wake of a wind turbine. However, thanks to the ability to well measure the flow inclination can detect very well the wake swirl at the sides of the wake. This information could be used to identify the wind direction sectors to exclude to perform a NPC measurement.

Chapter 8

Appendix

8.1 Appendix A - Wind speed measurement by sonic means

The sound waves propagate in air with a speed c related to the absolute air temperature T in Kelvin, absolute pressure p and the water vapour pressure e according to [27]

$$c = 20.067 \sqrt{T \left(1 - 0.319 \frac{e}{p} \right)} \quad (8.1)$$

Sound waves are a compressional phenomenon which propagates in air thanks to its elastic properties. The air velocity v is superimposed to the velocity of the sound waves c . The sonic anemometer is based on the measurement of the time of travel of a sound wave between two transducers (Figure 8.1) spaced of a distance L . The time of travel from sensor A to sensor B is

$$t_1 = \frac{L}{c + v}. \quad (8.2)$$

Both transducers can be used as transmitter as well as receiver. The time of travel in the opposite direction (from B to A) is

$$t_2 = \frac{L}{c - v}. \quad (8.3)$$

By combining equations 8.2 and 8.3 the air velocity can be calculated as a function of the time of travel and path length only as

$$v = \frac{L}{2} \left(\frac{1}{t_1} - \frac{1}{t_2} \right) \quad (8.4)$$

with the advantage of eliminating the dependency from temperature, pressure and humidity.



Figure 8.1: Wind speed sonic sensor (from Romo Wind A/S brochure). The nominal sensor path length is $L = 167$ mm.

8.2 Appendix B - Calibration of a spinner anemometer for angular measurements on a Siemens 2.3 MW wind turbine

As described in chapter 2, the methods for calibration of a spinner anemometer are based on a test where the wind turbine is stopped with one blade pointing downwards and yawed six times in and out of the wind. During the test, the signals of yaw misalignment, yaw position (if measured), horizontal wind speed and flow inclination are recorded at high sampling frequency (10 Hz). The time series of a yaw misalignment test performed on turbine 4 are shown in Figure 8.2. Black points are showing non calibrated yaw misalignment measurements, while the red points are showing the reference yaw misalignment (which is calculated as the difference between the average yaw position during the test minus the measured yaw position).

In this specific case we observe that the yaw misalignment is overestimated by the spinner anemometer (black points spanning more than red points), which suggest that the default k_α is too small (need an $F_\alpha > 1$ to correct $k_{\alpha,d}$ to k_α). The default settings of the spinner anemometer was $k_{\alpha,d} = 1$, therefore k_α and F_α are numerically equal.

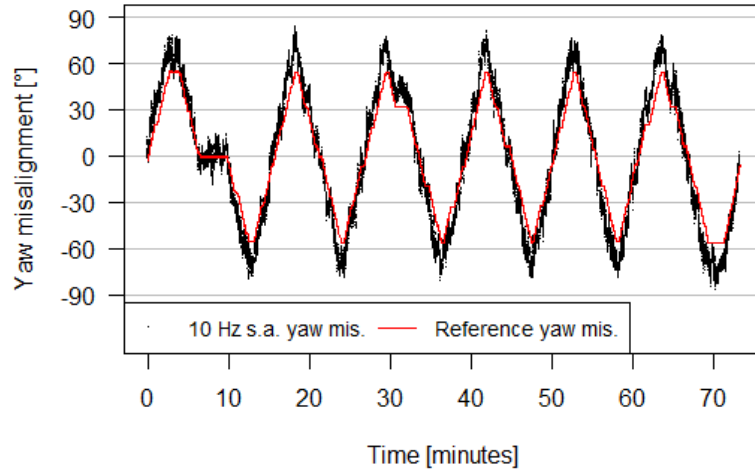


Figure 8.2: Time series of yaw misalignment during a calibration test, as measured by the spinner anemometer with default k_1 and k_2 constants. Black: yaw misalignment measured by the spinner anemometer. Red: yaw misalignment as measured by the yaw scale.

The measurements shown in Figure 8.2 were analyzed with the following methods:

- GGref: γ as a function of γ_{ref} . (Section 8.2.1)
- TanTan: $\tan(\gamma)$ as a function of $\tan(\gamma_{ref})$. (Section 8.2.2)
- WSR: wind speed response. (Section 8.2.3)

8.2.1 GGref calibration method (γ vs γ_{ref})

This method of determining F_α is based on optimizing F_α so that the linear fitting of γ as a function of γ_{ref} has slope equal to one. γ_{ref} is the reference yaw misalignment, calculated as the mean wind direction during the test minus the yaw position.

$$\gamma_{ref} = \overline{\theta_{dir}} - \theta_{yaw} \quad (8.5)$$

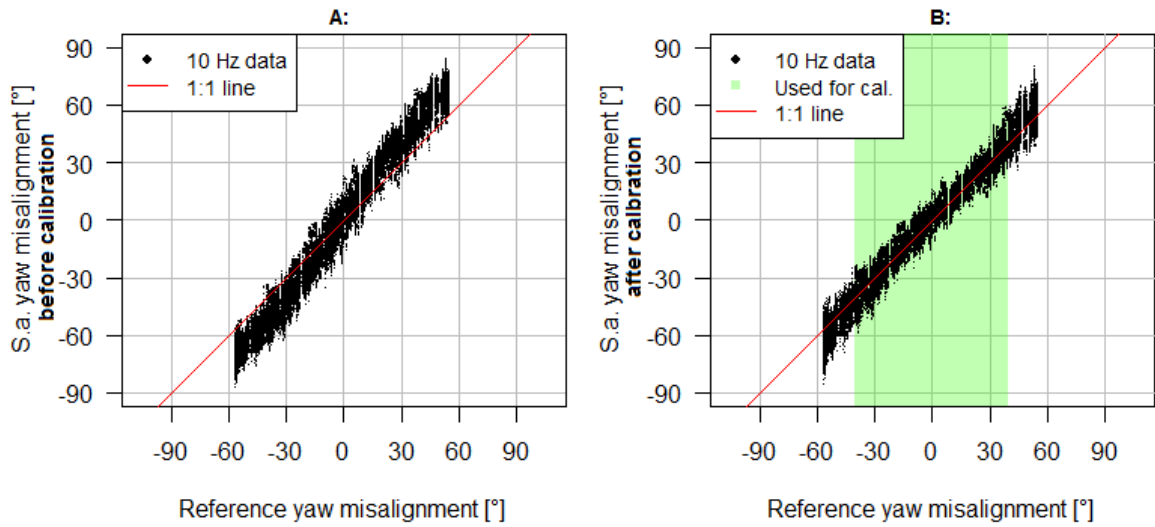


Figure 8.3: Yaw misalignment as a function of reference yaw misalignment measured with the yaw position sensor. Left: before calibration. Right: after calibration with $F_\alpha=1.49838$.

8.2.2 TanTan calibration method ($\tan(\gamma)$ vs $\tan(\gamma_{ref})$)

In this method, F_α is the slope of the linear fit made to a plot of $\tan(\gamma_d)$ as a function of $\tan(\gamma_{ref})$.

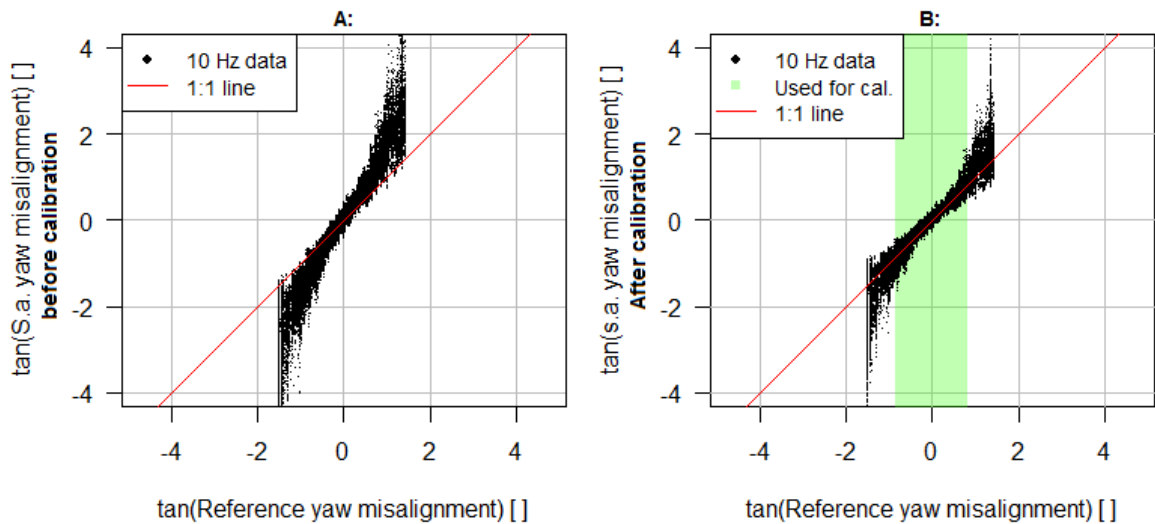


Figure 8.4: Linear fit to $\tan(\gamma_d)$ as a function of $\tan(\gamma_{ref})$. Left: before calibration. Right: after calibration with $F_\alpha=1.524033$.

8.2.3 WSR calibration method

Figures 8.5 and 8.6 show the 10 Hz data recorded during the calibration procedure. Figure 8.5A, B and C show non calibrated measurements, while Fig. 8.6A, B and C show calibrated measurements. In both figures 8.5 and 8.6, sub-figure A shows the time series of the yaw

misalignment and yaw misalignment reference (measured with a yaw position sensor). Sub-Figure B shows the time series of the wind speed. Sub-Figure C shows the wind speed response as a function of yaw misalignment. Figure 8.5D shows the value of F_α calculated with the three different methods (GGref, TanTan, WSR), for varying range of yawing the wind turbine out of the wind (data were filtered according to γ_{ref} in steps of 5° span per side).

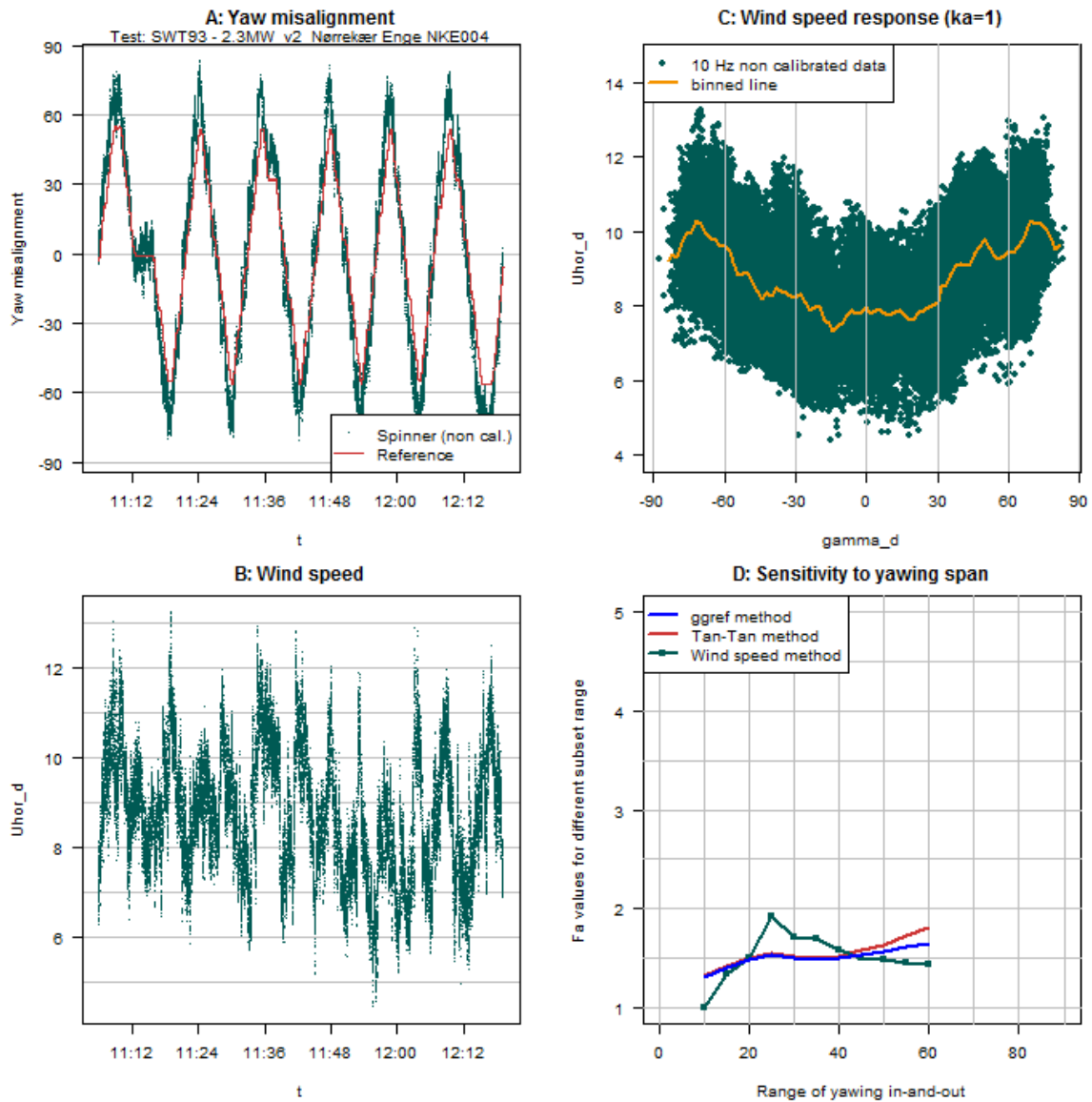


Figure 8.5: Before calibration. A: Time series of yaw misalignment as measured by the spinner anemometer and by the yaw position sensor. B: wind speed time series as measured by the spinner anemometer before F1 calibration. C: Wind speed as a function of yaw misalignment both measured by spinner anemometer. D: Calibration correction factor F_α calculated with three different methods, as a function of yawing span ranging from $\pm 10^\circ$ to $\pm 90^\circ$ in steps of $\pm 5^\circ$.

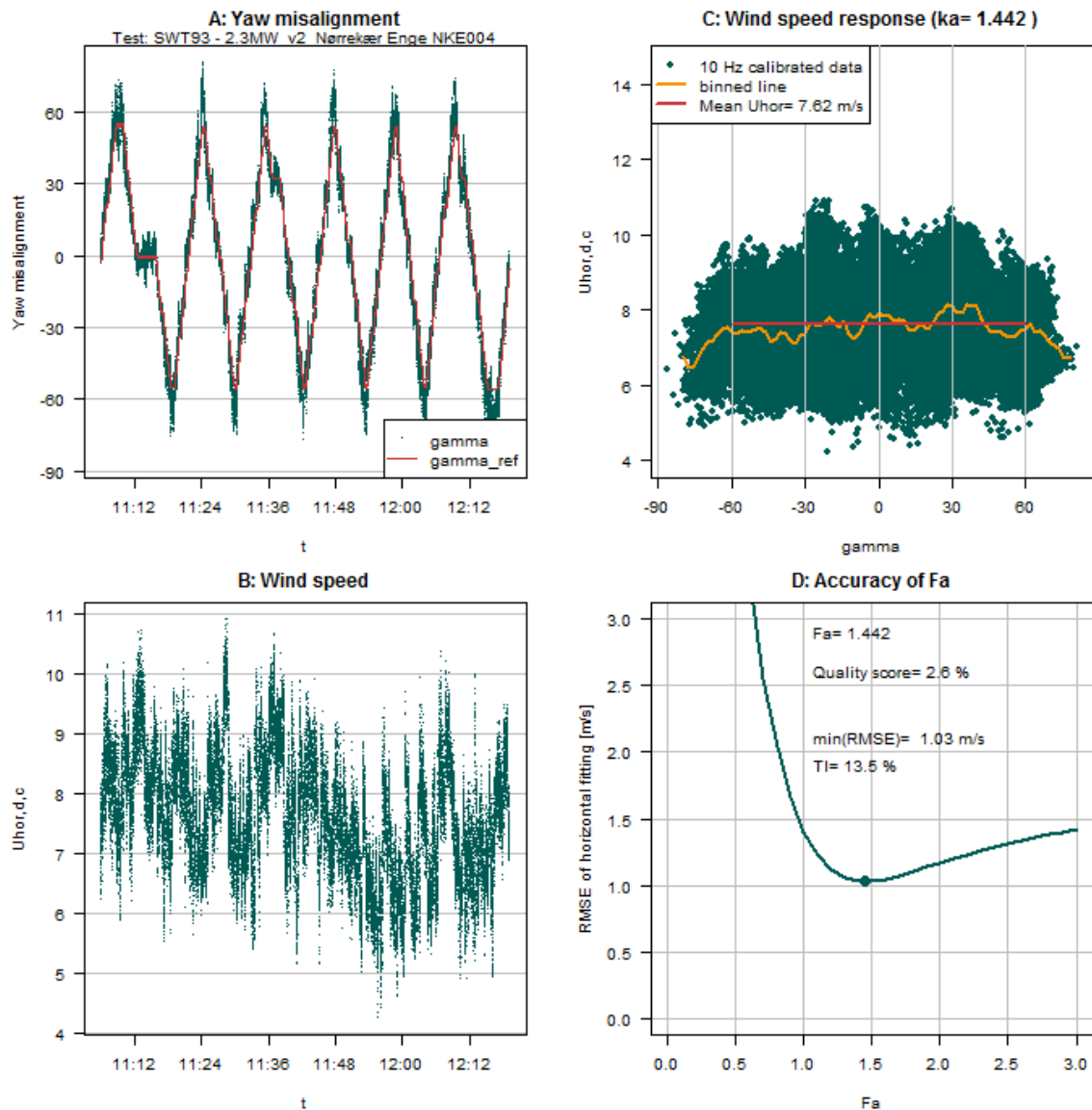


Figure 8.6: After calibration of k_α value. A: Time series of yaw misalignment as measured by the spinner anemometer and by the yaw position sensor. B: wind speed time series as measured by the spinner anemometer before F_1 calibration, after F_α calibration. C: Wind speed as a function of yaw misalignment both measured by spinner anemometer and calibrated with F_α . D: Root mean square error of the horizontal fit (red line in sub-figure C) as a function of F_α .

The WSR gave a $F_\alpha = 1.442$ for a yawing span of $\pm 60^\circ$.

8.2.4 Discussion regarding k_α calibration

The three k_α calibration methods presented in sections 8.2.1, 8.2.2 and 8.2.3 gave the following F_α values:

Method:	GGref	TanTan	WSR
F_α :	1.498	1.524	1.442

Table 8.1: Summary of F_α values calculated with three different methods for a Siemens 2.3 MW wind turbine.

Note that the calibration examples presented in chapter 2 were based on measurements made on wind turbine with different spinner shape (a Nordtank 500 kW or a Neg-Micon NM80 2 MW) therefore the F_α values presented in Table 8.1 shall not be compared with the values presented in the article.

A sensitivity analysis to the span of yawing the wind turbine in and out of the wind made in chapter 2 unveiled limitations related to the first two methods. For this reason, the value used to calibrate the spinner anemometer measurements of this wind turbine is the one calculated with the WSR method ($F_\alpha=1.442$).

8.3 Appendix C - Calibration of a spinner anemometer for wind speed measurements on a Siemens 2.3 MW wind turbine

The objective of the spinner anemometer calibration for wind speed measurements is to find the k_1 calibration constant that makes U_{hor} to match the free wind speed U_{mm} when the turbine is stopped and is facing the wind. During operation of the wind turbine the rotor induction is accounted for with the nacelle transfer function described in the IEC61400-12-2 standard. The calibration procedure was based on measurements acquired with a spinner anemometer where k_1 was set to default value $k_{1,d}$. The correction factor F_1 was calculated as the ratio

$$F_1 = \frac{U_{hor,d,c}}{U_{mm}} \quad (8.6)$$

where $U_{hor,d,c}$ is the horizontal wind speed measured with default $k_{1,d}$ and correct k_α . The data-set used to find the F_1 value is show in Figure 8.7.

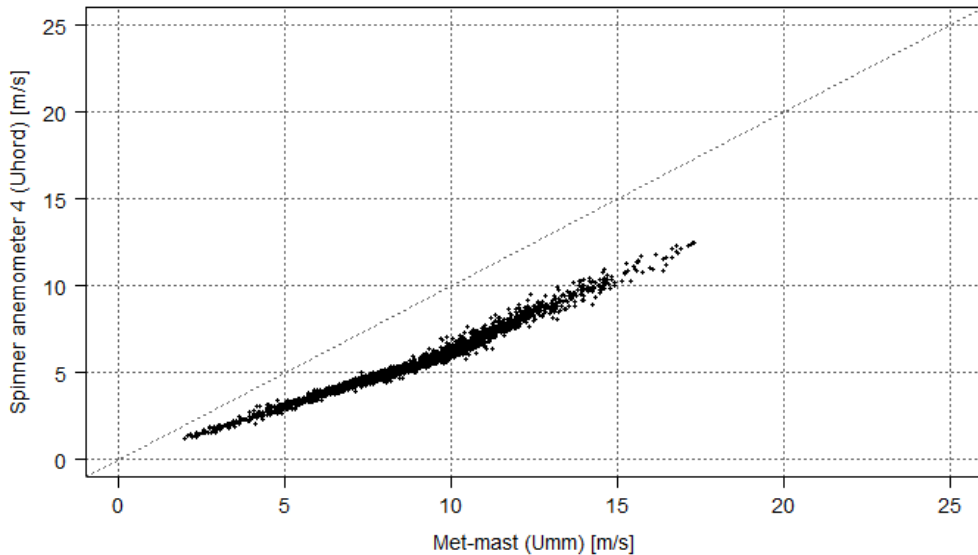


Figure 8.7: Horizontal wind speed of the spinner anemometer (prior to calibration) as a function of the met-mast horizontal wind speed. Turbine 4.

To acquire the measurements needed for the calibration the wind turbine shall ideally be stopped. However, this is not desirable due to power production losses, therefore the calibration was performed with the wind turbine in operation, as proposed in [28] for a stall regulated turbine. In the case shown in Figure 8.8 the wind turbine is pitch regulated and the F_1 as a function of free wind speed shows a clear asymptote as the induction decreases. The value of $F_1 = 0.7101$ was calculated as average of the values for free wind speed greater than 15 m/s. Note that the article is based on measurements acquired after the sensor mounting position on the spinner was improved. The sensors were moved forward in the new mounting, determining a lower F_1 . In Figure 8.9, the good agreement between met-mast wind speed and spinner anemometer wind speed confirm that the calibration is correct.

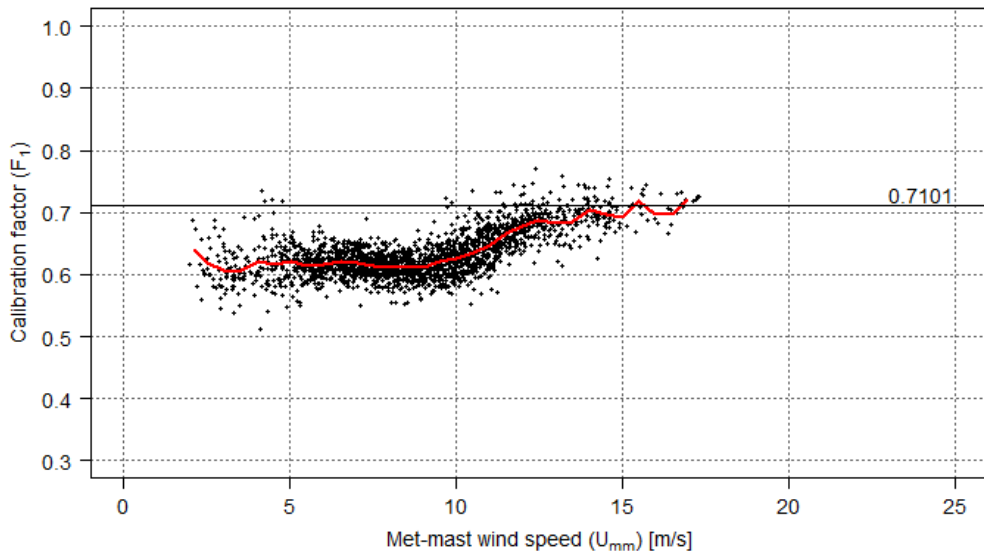


Figure 8.8: F_1 correction factor as a function of met-mast wind speed, disturbed by the rotor induction during operation of the wind turbine. The horizontal black line shows the value of F_1 chosen to calibrate the measurements. Turbine 4 (initial mounting position of sonic sensors).

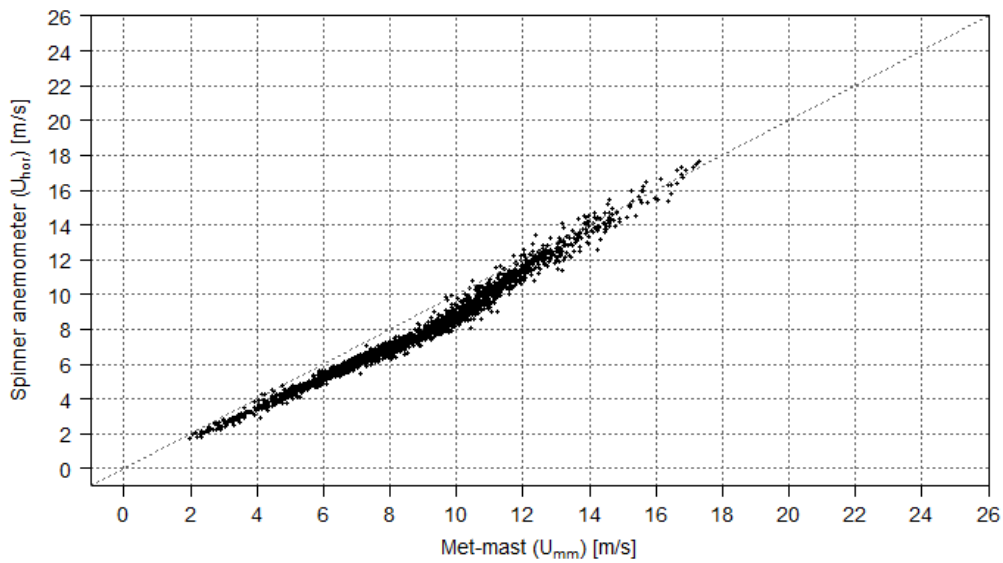
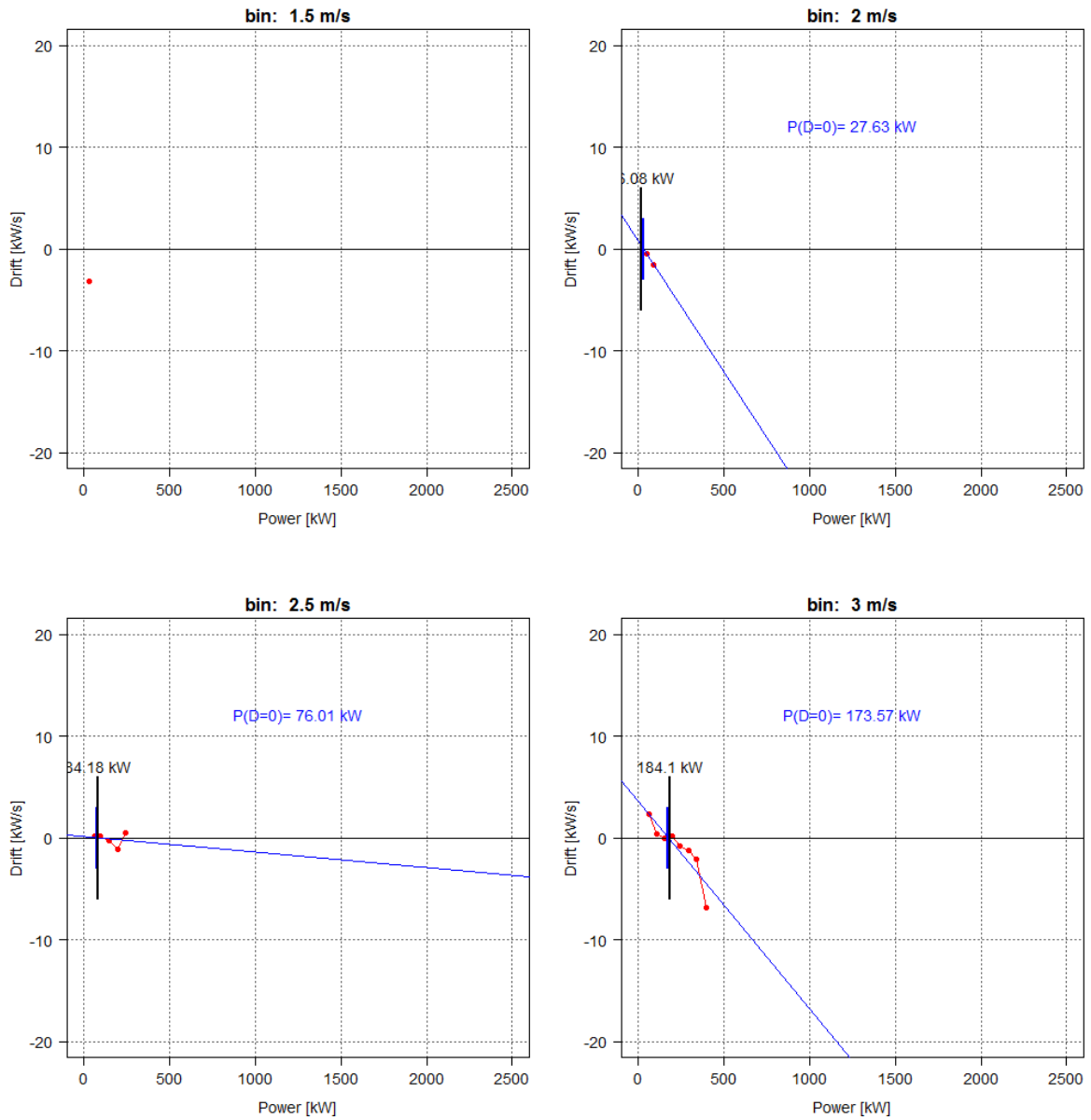
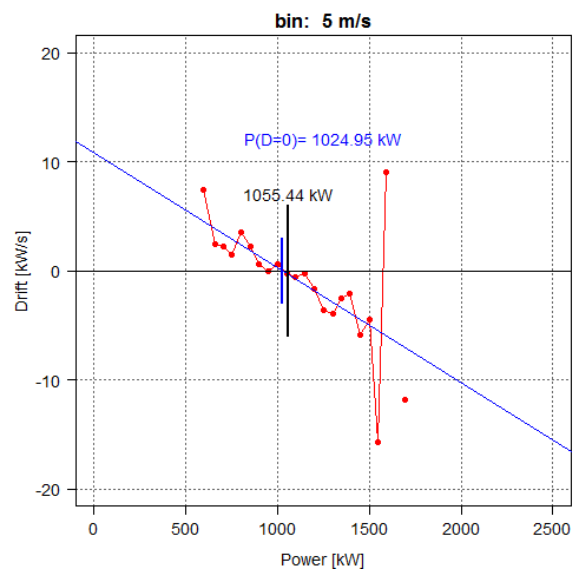
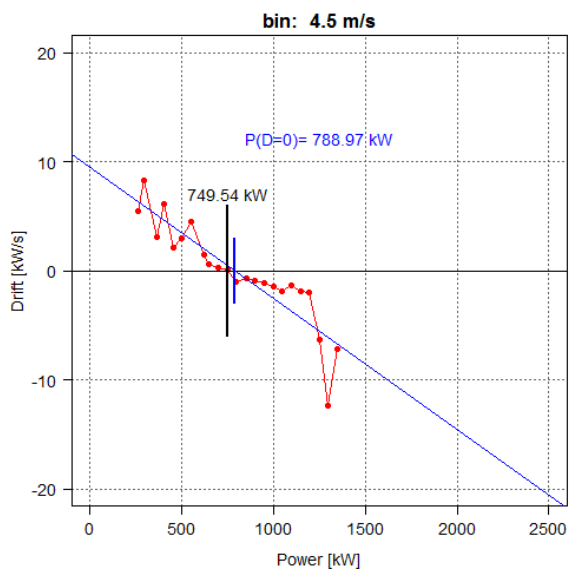
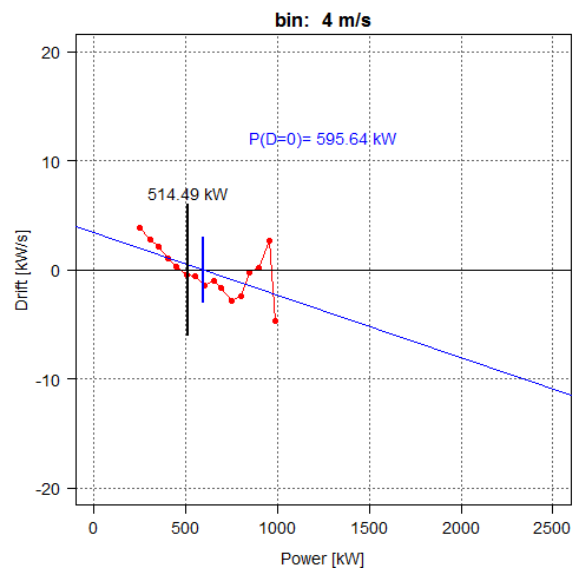
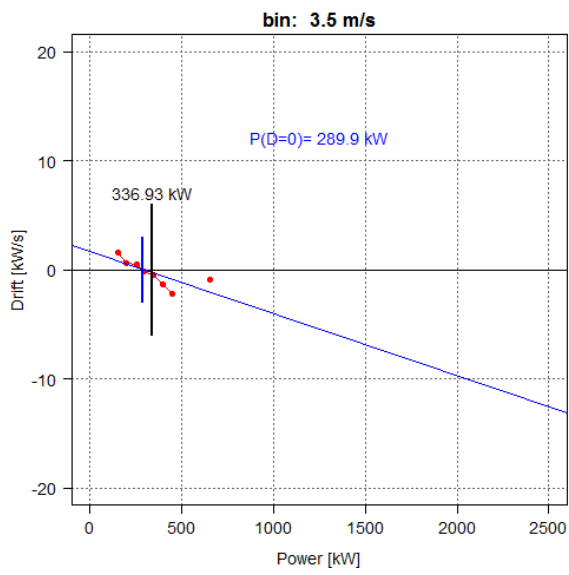


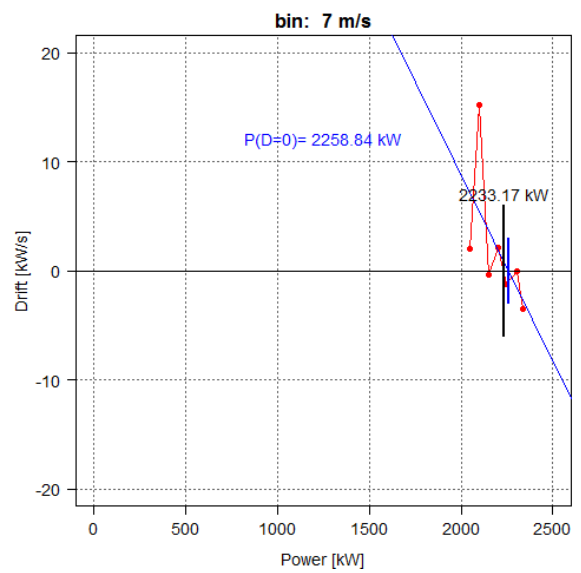
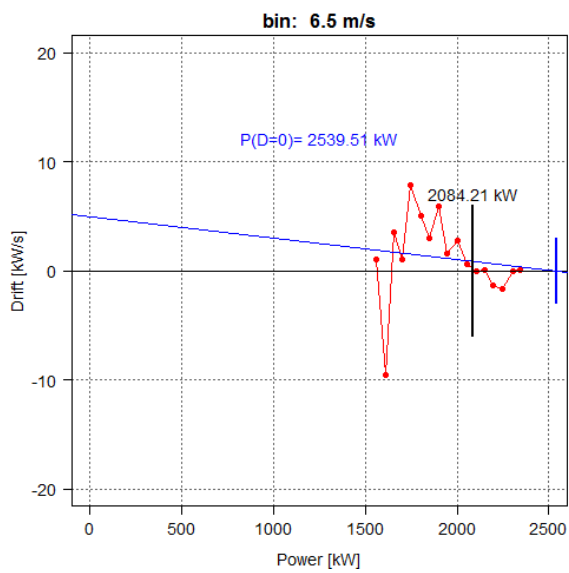
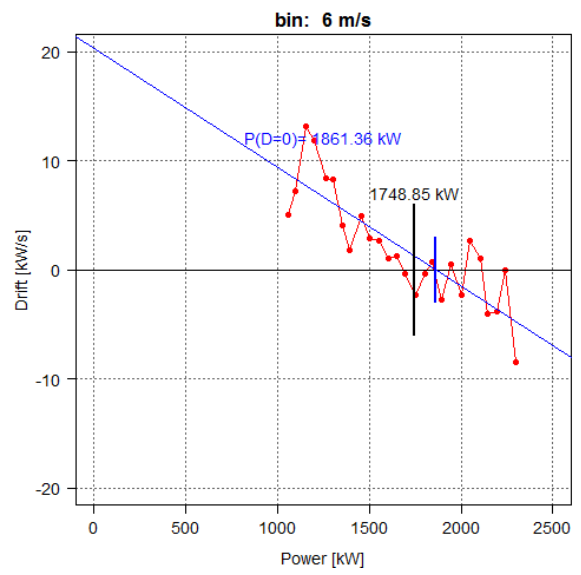
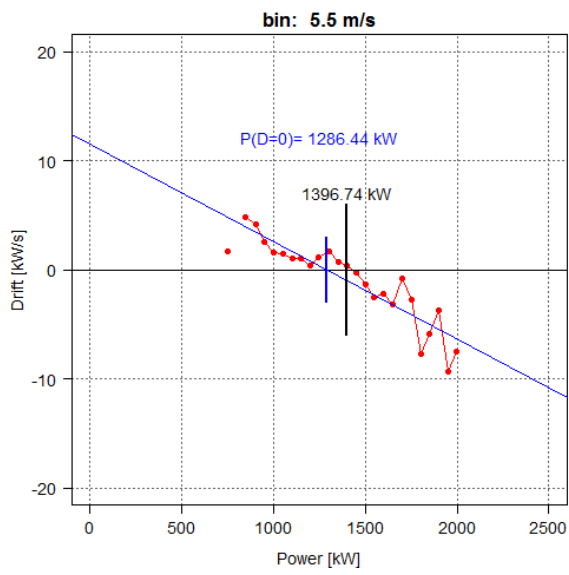
Figure 8.9: Horizontal wind speed (calibrated with $F_1 = 0.7101$) of the spinner anemometer as a function of the met-mast horizontal wind speed. Turbine 4.

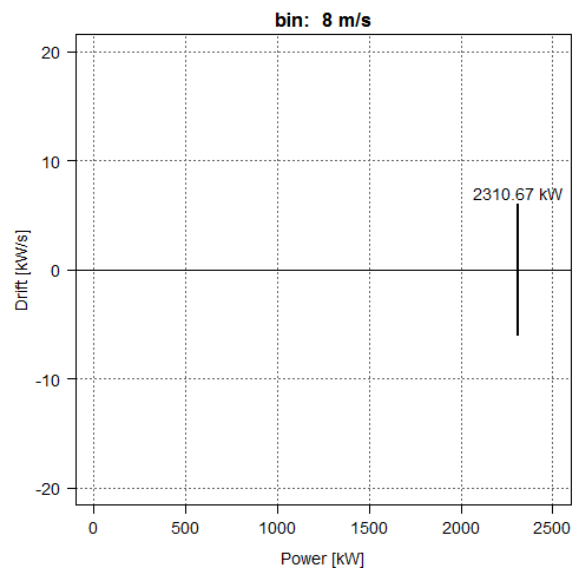
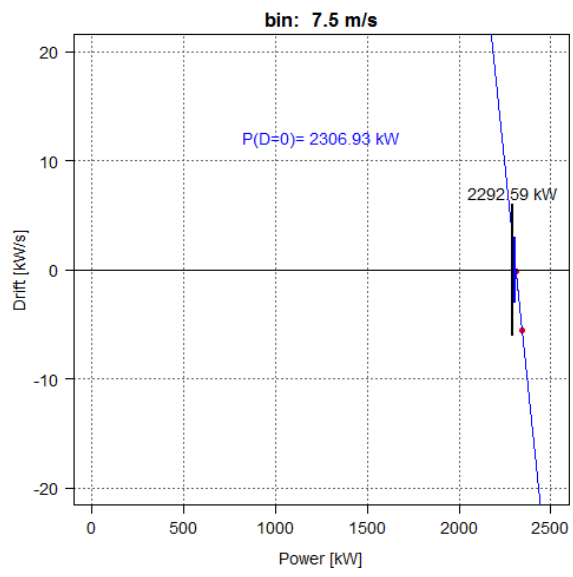
8.4 Appendix D - Drift curves for a Siemens 2.3 MW wind turbine

See chapter 6 for description.









Bibliography

- [1] “Iec61400-12-1 wind turbines part 12-1: Power performance measurements of electricity producing wind turbines,” 2008.
- [2] “Iec61400-12-2 wind turbines part 12-2: Power performance of electricity producing wind turbines based on nacelle anemometry,” 2012.
- [3] F. Zahle and N. N. Sørensen, “Characterization of the unsteady flow in the nacelle region of a modern wind turbine,” *Wind Energy*, vol. 14, no. 2, pp. 271–283, 2011.
- [4] “Apparatus for adjusting the yaw of a wind turbine. WO2013117470A1.”
- [5] T. F. Pedersen, N. Sørensen, and P. Enevoldsen, “Aerodynamics and Characteristics of a Spinner Anemometer,” *Journal of Physics: Conference Series*, vol. 75, p. 012018, 2007.
- [6] EWEC 2008 Brussels, *Theoretical model of spinner anemometry based on ultrasonic paths*, 2008.
- [7] T. F. Pedersen, G. Demurtas, J. Gottschall, J. Højstrup, J. D. Nielsen, G. Weich, A. Sommer, and R. Kristoffersen, “E-0040 Improvement of Wind Farm Performance by Means of Spinner Anemometry,” Tech. Rep. E-0040, DTU Wind Energy, December 2013.
- [8] Metek, “Spinner anemometer user manual 05-01-2009.”
- [9] T. F. Pedersen, U. S. Paulsen, S. M. Pedersen, and P. Enevoldsen, “Operational Experience and Analysis of a Spinner Anemometer on a MW Size Wind Turbine,” *Wind Energy*, no. 1, pp. 356–356, 2007.
- [10] T. F. Pedersen, N. Sørensen, L. Vita, and P. Enevoldsen, “Optimization of Wind Turbine Operation by Use of Spinner Anemometer,” Tech. Rep. R-1654, DTU Wind Energy, August 2008.
- [11] P. Troels Friis, “Risø spinner anemometer, prototype 2, installation and calibration and quality of signal output.,” Tech. Rep. Risø-I-2779, DTU Wind Energy, October 2008.
- [12] T. F. Pedersen, R. Wagner, and G. Demurtas, “Wind Turbine Performance Measurements by Means of Dynamic Data Analysis,” 2015.
- [13] EWEC 2007 Milan, *Spinner Anemometry - An Innovative Wind Measurement Concept*, 2007.
- [14] G. Demurtas and T. F. Pedersen, “Summary of the steps involved in the calibration of a spinner anemometer,” Tech. Rep. I-0364, DTU Wind Energy, November 2014.

- [15] T. F. Pedersen, G. Demurtas, and F. Zahle, “Calibration of a spinner anemometer for yaw misalignment measurements,” *Wind Energy Wiley*, vol. 18, no. 11, pp. 1933–1952, 2015.
- [16] G. Demurtas, “Power curve measurement with spinner anemometer according to iec 61400-12-2,” Tech. Rep. I-0440, DTU Wind Energy, December 2015.
- [17] C. Brown, “Fast Verification of Wind Turbine Power Curves : Summary of Project Results (MSc Thesis - Tec. Uni of Denmark),” *Thesis*, 2012.
- [18] J. Gottschall and J. Peinke, “How to improve the estimation of power curves for wind turbines,” *Environmental Research Letters*, 2008.
- [19] P. Milan, T. Mücke, A. Morales, M. Wächter, and J. Peinke, “Applications of the langevin power curve,” in *Proceedings of the EWEC 2010*, (Warsaw, Poland), EWEA, 2010.
- [20] M. Wächter, P. Milan, T. Mücke, and J. Peinke, “Power performance of wind energy converters characterized as stochastic process: applications of the langevin power curve,” *Wind Energy*, vol. 14, pp. 711–717, 2011.
- [21] E. Anahua, S. Barth, and J. Peinke, “Markovian power curves for wind turbines,” *Wind Energy*, vol. 11(3), p. 219–232, 2008.
- [22] J. Gottshall and M. Courtney, “On the robustness of the fixed points for a dynamical performance characteristic \hat{U} or: a closer look at the langevin power curve,” *Wind Energy*, no. we1718, 2014.
- [23] A. Rauh and J. Peinke, “A phenomenological model for the dynamic response of wind turbines to turbulent wind,” *Journal of Wind Eng. Ind. and Aerody*, no. 92, pp. 159–183, 2004.
- [24] E. Anahua, S. Barth, and J. Peinke, “Characterization of the wind turbine power performance curve by,” *EWEC*, 2006.
- [25] J. Gottschall and J. Peinke, “Stochastic modelling of a wind turbine’s power output with special respect to turbulent dynamics,” *Journal of Physics: Conference Series*, no. 75: 012045 (8pp) DOI: 10.1088/1742-6596/75/1/012045, 2007.
- [26] J. Gottschall and J. Peinke, “On the definition and handling of different drift and diffusion estimates,” *New Journal of Physics*, 2008.
- [27] R. M. Schotland, “The Measurement of Wind Velocity by Sonic Means,” 1955.
- [28] G. Demurtas, T. F. Pedersen, and F. Zahle, “Calibration of a spinner anemometer for wind speed measurements,” *Wind Energy*, 2016.

Curriculum vitae

Giorgio Demurtas was born on 14th March 1986 in Cagliari, Italy.

He received the high school diploma in Electrotechnics and Automation in 2005 from the G. Marconi technical school in Cagliari, Italy. He completed the Bachelor in Electrical Engineering at the University of Cagliari in 2009. Soon after, he funded the company Piccolecentrali, which designed and installed approximately 140 kW of photovoltaic solar plants.

In August 2010 he started the Master of Science in wind Energy at the Technical University of Denmark. In August 2012 he completed the Master of Science with a thesis written in collaboration with Alsom Wind in Barcelona.

He then worked in the Test and Measurements section of DTU Wind Energy as research assistant and later as PhD student. During the second year of PhD he registered the company Startak IVS, in Denmark, to produce and sell control systems for solar trackers.

In 2015, during a two months leave from the PhD he worked as consultant for Aentula Srl, developing the control system for a 30 kW pitch regulated direct drive wind turbine.

For the future, he wants to free the world from fossil fuels in favour of renewable energies.

DTU Wind Energy is a department of the Technical University of Denmark with a unique integration of research, education, innovation and public/private sector consulting in the field of wind energy. Our activities develop new opportunities and technology for the global and Danish exploitation of wind energy. Research focuses on key technical-scientific fields, which are central for the development, innovation and use of wind energy and provides the basis for advanced education at the education.

We have more than 240 staff members of which approximately 60 are PhD students. Research is conducted within nine research programmes organized into three main topics: Wind energy systems, Wind turbine technology and Basics for wind energy.

Danmarks Tekniske Universitet

DTU Vindenergi
Nils Koppels Allé
Bygning 403
2800 Kgs. Lyngby
Telephone 45 25 25 25

info@vindenergi.dtu.dk
www.vindenergi.dtu.dk